Factors controlling the formation of a very large maar volcano and the fragmentation process in phreatomagmatic eruptions: Lake Purrumbete Maar, southeastern Australia

by
Simone C. Jordan

PhD thesis
Submitted in fulfillment of the Requirement for the Degree of
Doctor of Philosophy

Supervisor: Emeritus Professor Ray Cas
Associate supervisor (20 %): Dr. Patrick Hayman

School of Geosciences
Monash University, Clayton, Victoria, Australia

February 2013

Contents

List of Figures

ADDENDUM: Reply to questions from Dr. Gerardo Carrasco-Nunez

The reason why sample material from Mount Rouse was used for the experiments instead of sample material from Lake Purrumbete Maar, is explained in the thesis on page 81 and 98. The major problem with sample material from Lake Purrumbete is that it is a little weathered, whereas I was able to find generally compositionally and texturally similar fresh material from Mount Rouse. Mount Rouse is a volcanic complex which was formed by predominantly dry magmatic, Strombolian eruptions from multiple vents. Although Mount Rouse is located 90 km to the west of Lake Purrumbete, it is still part of the Newer Volcanics Province (NVP), with a similar geological setting as Lake Purrumbete. Both volcanoes are located at the northern edge of the underlying Otway Basin and belong to the same sub-province of the NVP. The experiments are generic. The idea was to determine in general the influence of vesicles or bubbles within the melt on the fragmentation behavior of the melt and to clarify processes during magmatic and phreatomagmatic fragmentation. Therefore using sample material from Lake Purrumbete, if fresh material could be found, would produce similar results.

In chapter 5 the experiments were used to investigate in general 'the possibility of a different mechanism of microlite formation' and to 'evaluate the influence of the fragmentation process on microlite formation' (page 80 of the thesis). Both 'dry and wet blow-out experiments showed that microlites can also form in an extremely short time frame of seconds and during the fragmentation process (page 92 of the thesis), indicating that this process is independent of the eruption style. However, this is a general result and therefore it has been stated in the conclusion of this chapter that 'study of the morphology and textures of microlites related to fragmentation mechanisms of host pyroclasts from different types of pyroclastic and autoclastic deposits should be undertaken to develop a better understanding of the conditions of microlite formation and pyroclast formation' (page 93 of the thesis).

In chapter 6 the influence of vesicles in the melt in general on the fragmentation process and the resulting clast morphology was determined using these experiments. The findings and conclusion can be applied to the phreatomagmatic eruption process and are

not dependent on the volcano type.

'The analysis of the particle shape follows the method of image particle analysis (IPA) proposed by Dellino and LA Volpe (1996) and used by Zimanowski et al. (2003) and Durig et al. (2012b) for comparison of natural and experimental derived ash particles' (page 102 of the thesis). Durig et al. (2012b) showed that in the case of experimental derived clasts the material properties play an important role in the formation of the fragments. These properties are predominantly controlled by the chemistry of the melt. By using material with the same geochemical composition this problem should be eliminated. This approach can be used, as only experimental derived particles were compared to natural particles from Lake Purrumbete, not natural particles from Mount Rouse. The eruption style and conditions of Mount Rouse are therefore not important for the analysis and the results.

Acknowledgements

I would like to thank my supervisor Prof. Ray Cas for his advice, supervision and funding of this project. Thank you for giving me the opportunity to do this project on the other side of the world and for guiding me through this long journey.

I also would like to thank Robert Oakley for his patience and help with various forms and administration matters during all these years. Without his help I would not even have managed to start this journey.

I want to thank the Monash Research Graduate School and the Faculty of Science for their financial support of this project in form of two scholarships, which allowed me to undertake my research at the School of Geosciences.

Many thanks also go to Harald Hofmann for being an awesome officemate for three years and for so many helpful conversations. He helped me so much especially in the first year, when everything was still very foreign to me.

Special thanks go also to Janine Kavanagh for all the discussions and for all the encouragements. She made me believe that I can actually make it.

I also want to thank Patrick Hayman for his supervision and proof reading and Bernd Zimanowski and the team of the Physikalisch, Vulkanologisches Labor Würzburg, for the possiblity of undertaking experiments at their laboratory, the advice and many discussions. Special thanks go to Tobi Dürig, who helped me to understand the physics behind everything, and to Simon Jowitt, for all the feedback on geochemical questions.

I want to thank everyone in the School of Geosciences who helped me and supported me throughout the years, it has not always been easy and I appreciate a lot that you have been there for me.

Special thanks go to two very close friends who have nothing to do with Geology, Alexander Radi and Martina Sanchez. Alexander has been an awesome friend throughout all these years, joint in the same journey of doing a PhD abroad. Martina has given me an amazing friendship, a place to live and a family when I needed it most.

Last I want to thank my parents for their support and to say sorry for moving to the other side of the world. And a huge 'thank you' goes to my sister for all those long talks on Skype at any time, the support, the advice and the encouragement. I would not have made it without her.

Abstract

The Pleistocene Lake Purrumbete Maar is one of the largest maar volcanoes world wide, with a complex pyroclastic sequence that reflects variations in the eruption style, ranging from magmatic influenced dry phreatomagmatic to wet phreatomagmatic. The country rock xenoliths within the pyroclastic deposits originate from very shallow stratigraphic layers indicating a very shallow bowl shaped maar diatreme, that is difficult to explain by the traditional model of downwards growth of a singular explosion point. The detailed field studies, presented here, including mapping, stratigraphic logging, measurements of base surge transport directions and ballistic impact structures, led to the reconstruction of at least three major vent locations, suggesting that the large size is the result of multiple coalesced craters. Vent migration occurred along basement structures and was probably caused by the collapse of the crater walls and clogging of the vent. In addition, a complex eruption history was determined with three eruption phases and at least one significant volcanic hiatus. This is supported by the geochemical data of the Lake Purrumbete pyroclastic sequence, which shows distinct trace element trends that correlate with the stratigraphic height and the three determined eruption phases, indicating that the maar activity was controlled by deep processes within the feeding system. The trace element trends cannot be explained by crystal fractionation or crustal contamination and are best explained by melt differentiation caused by melt transport through highly porous mantle channels. Tapping these melt channels may have controlled the release of single magma pulses and therefore the activity of the Lake Purrumbete Maar. Analysis of the bubble number densities and the bubble size distribution of vesicles preserved in ash sized juvenile clasts of the pyroclastic sequence show that vesicle nucleation appeared in different phases within the conduit, with an early phase deeper in the conduit and a late phase of vesicle nucleation near the fragmentation level, caused by the exsolution of H_2O and acceleration of the magma. Strain within the magma caused by the acceleration of the melt is also indicated by micro-textures, including stretched vesicles and aligned microlites, whereby the difference in the microlite abundances and the microlite shape, observed in ash particles are difficult to explain with the traditional models of decompression and cooling induced microlite formation. The results of fragmentation experiments conducted in this project show that microlites can form on extremely small time scales. Furthermore

the exclusive occurrence of microlites in particles that experienced mechanical stress during brittle fragmentation, suggests that microlite formation may be the result of mechanical stress. The differences in the microlite populations observed in the Lake Purrumbete ash particles are therefore best explained by modification of the microlite population due to stress induced microlite formation caused by the strain of the magma during acceleration near the fragmentation level. In addition, high strain rates may also cause deformation of the magma and the formation of fractures. The fragmentation experiments have also shown that vesiculated magma can react with water in the way of molten fuel coolant interaction, if the magma/water interface is enhanced by fractures, suggesting that the phreatomagmatic eruption style at Lake Purrumbete was supported by fracturing of the magma due to acceleration near the fragmentation level. Furthermore, the results show that pre-stress of the magma, that is most likely caused by strain, has a major influence on the shape of the produced pyroclasts.

This research project shows that the formation of a very large maar system is controlled by many factors starting at the source of the melt and magma ascent dynamics to subsurface processes, whereby the formation of a specific volcano form is predominantly controlled by subsurface and surface processes including the availability of water and the surrounding stratigraphy. The results, presented here show that the combination of hard and soft rock substrate together with fractures within the country rock and the location on fault structures led to the formation of this very large maar structure. Aquifer sourced water supply, mass flow of the Black Rock Sandstone and water, together with changing magma ascent rates influenced the explosive eruption dynamics.

This research projected has touched on many different aspects of the eruption of very large maar systems and raised new questions which should be addressed in future work. In addition, it has shown the importance of detailed stratigraphic work on this volcano type as the basis of many other studies, such as geochemistry and pyroclast textures. The geochemical variations detected within the Lake Purrumbete pyroclastic sequence suggest, that this volcano type is perfect for studies of mantle processes, as the magma rises very fast to the surface leaving no time for crustal contamination and magma differentiation. Furthermore, highly porous melt channels within the mantle may be the explanation and reason for the activity of intra-plate volcanic provinces and should be further investigated in the future. In addition, strain within the magma seems to have a major influence on the eruption type and the resulting pyroclast shape, the results presented here suggesting that the strain may be linked to the acceleration of the melt near the fragmentation level and to the exsolution of H_2O. This connection should be further addressed in future work.

1 Introduction

The eruption of the Eyjafjallajökull volcano in Iceland 2010 has brought new focus on the vulnerability of modern society to volcanic eruptions, especially those producing large volumes of fine ash. Fine ash is the product of the most intensive fragmentation of magma occurring during the most violent and explosive eruptions (Zimanowski et al., 2003), which are typically caused by magmas of a more felsic composition. In basaltic systems, however, phreatomagmatic eruptions, caused by magma/water interaction, are the most violent eruptions (Houghton et al., 2004) and are able to produce significant amounts of fine ash.

Phreatomagmatism is the characteristic eruption style of maar volcanoes (Vespermann and Schmincke, 2000, Büttner et al., 2002). These relatively small volcanoes are one type of basaltic monogenetic volcano (Vespermann and Schmincke, 2000, Valentine and Gregg, 2008) and are the most dangerous volcanoes in monogenetic volcanic fields (White and Ross, 2011) such as the Eifel (Germany), Auckland volcanic field (New Zealand) and the Newer Volcanics Province (Australia). Many of the known basaltic monogenetic volcanic fields are still active and are located in the direct vicinity of densely populated areas. This vicinity makes it so important to have a good understanding of the eruption processes of these monogenetic volcanoes and the controlling factors to be able to make correct hazard predictions. Eruptions of maar volcanoes are rare and have been observed in modern history only a few times during the eruptions of Ukinrek 1977 (Self et al., 1980), Nilahue (Chile) 1956, Rotomahana (New Zealand) 1886 and Lake Taal (Phillipines) 1965 (White and Ross, 2011). These have been eruptions of relatively small maars and research has been done so far mostly on maars in the typical size range of 100 to 1000 m in diameter. However, only little work has been done on very larger maars up to and more than 3000 m in diameter. For very large maars there is a question about the evolution of the maar diatreme and the eruption process, including eruption style and duration, eruption volume and melt source.

Lorenz (1986) established a model for the formation of maar volcanoes, in which the deepening of the fragmentation level is caused by the lowering of the groundwater table, causing the maar diatreme to grow deeper and wider. The formation of very large maars, however, is difficult to explain with this model, as these maars would have a few kilometre deep diatreme. At a depth of a few kilometres, the lithostatic pressure of the

overlying diatreme infill may be higher than 20 to 30 bar, which is a threshold above which phreatomagmatic explosions cannot occur (Lorenz, 1986). Later it has been shown by many authors (Auer et al., 2007, Lorenz, 2007, Németh et al., 2001, Ross et al., 2011) that the subsurface diatreme structure of the maar is influenced by the substrate the maar formed in. In addition, vent migration has been found to be common in maar volcanoes, caused by processes including clogging of the vent by crater wall collapse and changes in the feeder dyke system due to tectonic activity (Sohn and Park, 2005, Carrasco-Núñez et al., 2007, Son et al., 2012). These processes may play an important role in the formation of a large maar volcano.

Maar volcanoes are often considered to be monogenetic and therefore formed during a single eruptive event. However, research has shown that they can be active multiple times (Freda et al., 2006, White and Ross, 2011), raising the question if very large maars form during a single eruptive event or over multiple events and a long period of time. The activity of a maar volcano is most likely controlled by processes in the mantle and during magma ascent, but it is not clear which processes in particular control the recurrence of maar eruptions. However, Németh (2010, and references therein) suggested that the reactivation of small volcanoes, such as maars, may be controlled by the tapping of melt channels within the mantle.

The main process during phreatomagmatic explosions is the dynamic interaction between magma and water, known as molten fuel coolant interaction (MFCI). The magma is fragmented by rapid quenching and the simultaneous explosive expansion of the steam trapped within the melt, into fine ash particles (Wohletz, 1983, Zimanowski et al., 1997a, Büttner et al., 2002). During this process the efficiency of the fragmentation is controlled by the availability of water. Wohletz (1983) and Kokelaar (1986) determined that the most intense fragmentation is caused by a magma to water mass ratio of 1:3, whereas other ratios would result in less fragmented deposits. In very large maar volcanoes phreatomagmatic eruptions occurred over a long time frame, therefore these systems must have either a sustained water supply or phreatomagmatic activity is supported by other processes. White (1996) suggested that the mixing process of magma and water is influenced by the density of the coolant. For so-called impure coolant, such as sediment laden water, the mixing of magma and the coolant is more efficient, which enhances the efficiency of the magma water interaction. White (1996) further suggested that water may be recycled in maar diatremes due to fall back of pyroclastic material into the crater. The mixing process of magma and water, however, is the most important process in phreatomagmatic explosions and is mainly controlled by the density contrast of the two liquids and their viscosity. As a result the properties of the magma such as viscosity, vesicularity and crystal content, may also play an important role.

Lake Purrumbete Maar volcano in the late Cainozoic Newer Volcanics Province of southeast Australia is the perfect field area to investigate the eruptive history and the factors influencing evolution of a very large maar system, due to the great preservation of the maar rim deposits and the continuous outcrop of the whole crater rim. The

Lake Purrumbete Maar has a diameter of over 3 km, and is one of the largest maar volcanoes on Earth. The occurrence of another large maar volcano, the Tower Hill maar in the Newer Volcanics Province shows that the formation of these unusual large maars is relatively common in this province. Therefore it is important to reconstruct their eruption behaviour and understand the causes of the formation of such large maars, for future hazard implications. Research has been carried out in the past at Lake Purrumbete by Slots (1999) and Edmonds (2008) as part of honours projects at Monash University, which concentrate on the formation of the maar rim deposits. The research of the project presented here uses detailed analysis of the maar rim to reconstruct the eruption history of Lake Purrumbete Maar and how it formed. This will form the basis for further analysis of possible internal and external factors, which may have influenced the formation of this unusually large maar.

The aims of this project are to:

- determine the process of the formation of a large maar system, such as Lake Purrumbete, and the controlling factors
- determine the source and the mantle processes supplying the magma to the large system
- understand the melt transport and conduit processes
- determine the influence of microlites and vesicles on the process of phreatomagmatic explosions

1.1 Thesis structure

This thesis is structured into an introduction chapter, 5 research chapters and a conclusions and discussion chapter at the end. Each research chapter is structured as a scientific journal article on its own, as Monash University accepts the thesis to be structured as a collection of submitted papers. Although this produces some repetition in the introductory background material in each chapter, this is an accepted format at Monash University.

The evolution of a large maar system and the controlling factors are the subject of Chapter 2, with the title "*The origin of a large (>3 km) maar volcano by coalescence of multiple shallow craters: the Lake Purrumbete Maar, southeastern Australia*". It describes the lithofacies types, the stratigraphic architecture and the eruption history of Lake Purrumbete Maar and discusses possible processes that may have caused the unusually large size of the maar including aquifer dynamics, vent migration and crustal structure controls. A slightly different version of the chapter has been published in the Journal of Volcanology and Geothermal Research, (Jordan et al., 2013a).

The melt source and mantle processes supplying the large maar system are described in Chapter 3. The title of this paper is: "'*Partial melting and channelised melt transport in the mantle underneath the Newer Volcanics Province, southeastern Australia: Geochemical*

evidence from the Lake Purrumbete Maar"'. The Lake Purrumbete pyroclastic sequence shows geochemical variations which can be related to mantle processes including partial melting and magma differentiation by transport through highly porous channels within the mantle. This work has been submitted as a paper to the Bulletin of Volcanology.

Conduit processes indicated by vesicle microtextures in pyroclasts are described in Chapter 4, including bubble size distributions and bubble number densities. This work is described in the paper: "*Multi stage vesicle nucleation in the conduit system of a large maar volcano, Lake Purrumbete Maar, southeastern Australia*", which was submitted to the Journal of Volcanology and Geothermal Research.

The origin of microlites in juvenile pyroclasts is discussed in Chapter 5, raising the general question of when microlites form during an eruption. The chapter deals with the differences in microlite abundances and textures observed in the Lake Purrumbete juvenile clasts. Taking a new approach of using explosive fragmentation experiments to investigate microlite formation, this chapter gives a new insight into the process of microlite formation and will be submitted as a research paper with the title: "*New perspective of microlite formation*" to Geology (in prep.).

Chapter 6 concentrates on the results of dry and wet explosive fragmentation experiments, used as laboratory analogues of magmatic and phreatomagmatic explosions. Comparison of natural and experimental derived particles using image parameter analysis gives insight into fragmentation processes during the Lake Purrumbete eruption. This work is described in the paper "*Experimental study of the fragmentation behaviour of vesiculated basaltic melt in dry and wet explosive fragmentation experiments as analogues to magmatic and phreatomagmatic explosions*". This will be submitted to the Journal of Volcanology and Geothermal Research (in prep.).

The results of the five research chapters are linked together in Chapter 7: Conclusions and Discussion to answer the research questions of this project. The results are discussed in detail in a broader context than they were discussed in each chapter to consider the wider implications of the research beyond developing a better understanding the Lake Purrumbete Maar volcano. In addition, future perspectives of further research work are given at the end of this chapter.

1.2 Methods

The methods used for the research of this project are listed below and are described in detail in the relevant chapters of the thesis.

- Fieldwork: including detailed mapping and logging of stratigraphically important sections, collecting structural data and measurements of ballistic bombs and blocks and their impact structures, and sampling for petrography and geochemistry (Described in chapter 2).

- Grain size analysis: Including sieving and image analysis (Described in chapter 2).

- Componentry analysis: including field descriptions, point counting and petrography (Described in chapter 2).
- Geochemistry: including XRF analysed at the Advanced Analytical Centre of the James Cook University and trace elements conducted at Monash University (Described in chapter 3).
- Vesicularity analysis: including SEM/BSE imaging at the Monash Centre of Electron microscopy, image analysis with Gimp2 and ImageJ and 3D corrections with the computer program CSDcorrection (Described in chapter 4).
- Explosive fragmentation experiments: including dry and wet blow out experiments at the Physikalisch Vulkanologisches Labor at the University of Würzburg, Germany (Described in chapter 5 and 6).
- Image particle analysis (IPA): including SEM imaging at the Monash Centre of electron microscopy, image analysis using Gimp2 and ImageJ and statistical equivalents tests (Described in chapter 6).

1.3 Geological framework

The Late Cainozoic Newer Volcanics Province onlaps the Jurassic-Holocene Otway Basin in the south, and the Palaeozoic metasedimentary and granite basement to the north. Lake Purrumbete Maar is located above the southern Otway Basin sedimentary succession which contains several prominent aquifers.

1.3.1 Otway Basin

The Otway Basin is part of a Mesozoic-Tertiary basin system which forms the southwestern margin of Victoria and formed as a result of the break-up of Gondwana, and the separation of Australia from Antarctica, with the Bass and Gippsland basins lying further to the east (Edwards et al., 1996).

Stratigraphy of the sedimentary Otway Basin succession

The stratigraphy of the Otway Basin is summarised in Table 1.1. Deposition of the thick sequence of clastic non marine and marine sediments of the Otway Basin began in the Late Jurassic with the break up of Gondwana and lasted into the Cainozoic. Sedimentation started with the deposition of the carbonaceous shales of the volcanogenic Casterton Formation in the early half graben structures (Boult et al., 2002, Jensen-Schmidt et al., 2002), while the following period of active rifting with rapid sedimentaiton and subsidence of the rift basin is reflected by the overlying fluviolacustrine volcanogenic sediments of the Crayfish Group (Perincek and Cockshell, 1995, Edwards et al., 1996, Jensen-Schmidt et al., 2002, Miller et al., 2002). The later transition from an active rift basin to a sag

basin in the Early Cretaceous (133-125 Ma) is recorded by thick lacustrine shales and fluviatile siltstones and sandstones of the Eumeralla Formation (Perincek and Cockshell, 1995, Boult et al., 2002, Miller et al., 2002).

The second rifting stage of the Otway Basin began in the Late Cretaceous and is recorded in the sandstones of the Sherbrook Group which were deposited in a fluviatile and/or deltaic environment on a subsiding continental margin (Perincek and Cockshell, 1995, Boult et al., 2002, Miller et al., 2002). The end of this rifting stage is marked by the deposition of the sand, silt and clay sediments of the Wangerrip Group in a shallow marine to continental environment during Palaeocene-Eocene times. This sequence comprises the sandstones and conglomerates of the Pebble Point Formation, the Pember Mudstone and various sandstone and mudstone lithologies of the Dilwyn Formation. The latter forms a regional aquifer within the Otway Basin (Love et al., 1994). The following major transgression event is reflected in the Eocene sand, mud and limestones of the Nirranda Group and the Eocene - Oligocene marine limestones and marls of the Heytesbury Group (Edwards et al., 1996). The Heytesbury Group comprises limonitic sandstones and sandy limonitic bryozoan-coral calcarenite of the Clifton Formation, the Gellibrand Marl, and the limestones of the Port Campbell Limestone (Edwards et al., 1996). The Port Campbell Limestone forms the second major aquifer in the region and may play an important roll for the phreatomagmatic volcanism in the NVP (Cas et al., 1993, Love et al., 1994). The youngest unit in the sedimentary record is the partly lateritic Black Rock Sandstone of Pliocene age, (former known as Hanson Plain Sand Geoscience Australia (2012)) consisting of predominantly quartz grains in a clay matrix and forming a local aquifer in the Lake Purrumbete area (Edwards et al., 1996, Jensen-Schmidt et al., 2002, Tweed et al., 2009).

The sedimentary succession varies within the Otway Basin, in particular towards the basin edge, where stratigraphic units are thinning out. Therefore the stratigraphy underneath Lake Purrumbete is slightly different to the main stratigraphy of the basin, which is shown in Table 1.1.

Structural trends within the Otway Basin

Different structural trends occur within the Otway Basin as the result of various tectonic events. The oldest structures are N-S strinking trends from the underlying Palaeozoic basement of the Lachlan and Delamerian fold belts. The boundary of these two fold belts is marked by the Moyston Fault, one of the major fault lines within the Palaeozoic basement. NW-SE to E-W striking troughs, half graben and accomodation zones originate from the early rifting stages of the Otway Basin in the Late Jurassic-Early Cretaceous (Hill et al., 1995, Perincek and Cockshell, 1995, Jensen-Schmidt et al., 2002, Miller et al., 2002). These structural elements form two different trends within the Otway Basin. The predominant structure in the eastern part of the Otway Basin are ENE striking normal faults with a NNW dip direction (Figure 1.1), while in the western part the major structural trend are WNW striking faults with wide accommodation zones in between (Perincek and Cockshell, 1995, Miller et al., 2002). The orientation of faults in these accommodation zones can

Table 1.1: Stratigraphic table of the Otway Basin sequence and the thickness of the formations underneath Purrumbete (after Edwards et al. (1996), Boult et al. (2002)). The main tectonic events are shown in column 4 (adopted from Perincek and Cockshell (1995)).

Otway basin		thickness (m) at Purrumbete	lithology	Tectonic event
Black Rock Sandstone(5-2 Ma)		0-10	various clay and sand lithologies	
Heytesbury Group	Port Campbell limestone	0	calcarenite	Tasman Sea and Southern
(29-5 Ma)	Gellibrand Marl	300-400	marl	Ocean spreading Otway
	Clifton Formation	0-25	bryozoal calcarenite	Basin under compression
Nirranda Group	Narrawaturk Marl	100-200	marl and mudstones	Tasman Sea and Southern
(45-29 Ma)	Mepunga Formation		mud and sandstones	Ocean spreading
Wangerrip Group	Dilwyn Formation	0 - a few m	mud and sandstones	Tasman Sea and Southern
(65-45 Ma)	Pember Mudstone	0	carbonaceous mudstone	Ocean spreading
	Pebble Point Formation	0	sandstones and conglomerates	
Sherbrook Group	Paaratte Formation	0	carbonaceous silt and sandstones	Tasman Sea rifting
(97-65 Ma)	Belfast Mudstone	0	carbonaceous mudstone	Southern ocean spreading
	Waarre Formation	0	carbonaceous mud and sandstones	
Otway Supergroup	Eumeralla Formation	400	fluviolacustrine shales and volcanoclastic sandstones	sagging
(140-97 Ma)	Crayfish Group	60	fluviolacustine silt and sandstones	rifting
Casterton Formation (157-140 Ma)		0	carbonaceous shales	rifting

vary strongly. The Moyston Fault in the underlying Palaeozoic basement rocks, coincides with the boundary zone between these two structural trends. The change between the two trends is not sharp but appears in a zone of ca. 30 km to the east of the Moyston Fault, known as the Sorell-Purrumbete Trend (Miller et al., 2002). In the area south of Camperdown to Colac (see Figure 1.2 for location) several half graben structures occur which are oriented in E-W direction. Amongst these, the Elingamite Graben (Figure 1.1) is the largest structure (Perincek and Cockshell, 1995). Since the Miocene compression of the area caused right-lateral wrenching, inversion of previous faults and regional uplift of the basin generated further faulting, folding and was accompanied by volcanic activity, which began in the Pliocene (Perincek and Cockshell, 1995).

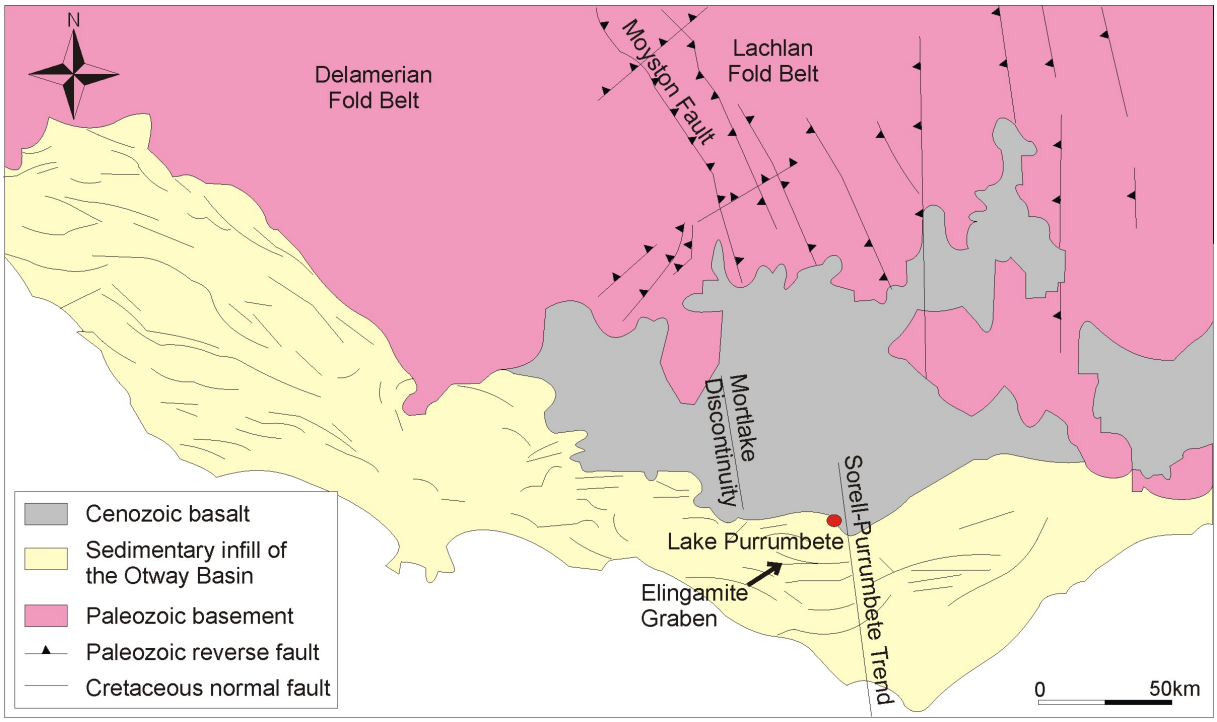

Figure 1.1: Simplified tectonic map of the NVP and the Otway Basin. The Paleozoic N-S trending fault structures occur in the North, whereas the Otway Basin is characterised by the two younger structural trends of WNW trending faults in the western part and ENE trending faults in the eastern part (modified after Miller et al. (2002))

.

1.3.2 Newer Volcanics Province

Lake Purrumbete Maar is part of the Late Pliocene-Quarternary intra-plate, monogenetic, basaltic Newer Volcanics Province (NVP) of southeastern Australia. The province extends over an area of 23000 km^2 from the western part of Melbourne to the Mt Gambier area of South Australia (Figure 1.2).

Volcanism in southeastern Australia is recorded over the last 190 Myr. Poorly known Jurassic volcanics occur in western Victoria. Then, activity was concentrated in the Palaeocene/Eocene forming the Older Volcanics, which occur mostly in eastern Victoria, and again in the Plio-Pleistocene generating the Newer Volcanics, with little or no activity

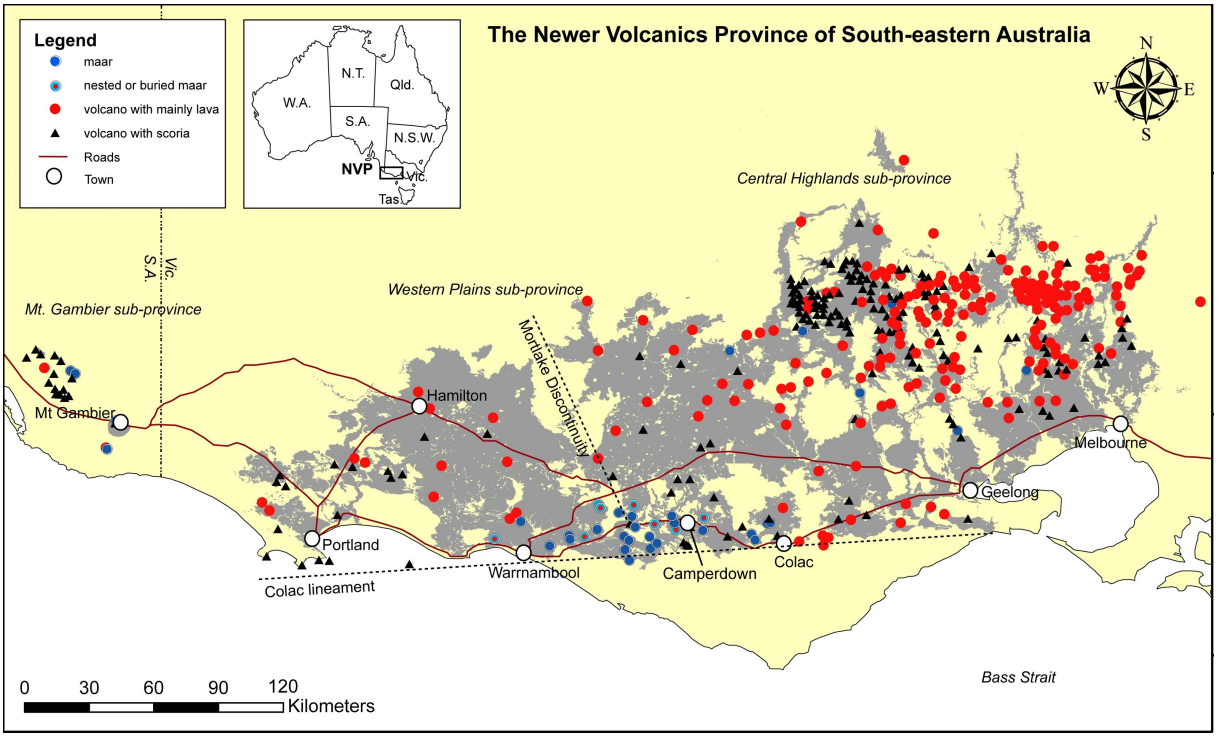

Figure 1.2: Overview over the Newer Volcanics Province (in grey), with over 450 eruption points (after Cas and van Otterloo (2011)).

occurring in the early Eocene and middle Miocene (Hare and Cas, 2005). Volcanic activity in the NVP occurred first in the late Pliocene at about 4.6 Ma and lasted throughout the Quaternary with the latest eruption of Mt Gambier, 5000 years ago. In recent times, natural springs with mantle derived CO_2 emission are the only indications of a likely still active volcanic system. Since the beginning of the activity a total volume of 1300 km^3 of volcanic products has been erupted throughout the province (Joyce, 1975, Cas et al., 1993).

The volcanoes in the NVP comprise approximately 200 scoria cones, 200 lava volcanoes and 40 maars of basaltic composition (Joyce, 1975). The lava flows of the early phase were erupted onto the erosional surface developed on the underlying limestones and marl of the Heytesbury Group, burying the former drainage system, and forming extensive lava plains. Explosive activity became more prominent in the final phase, generating scoria cones and maar volcanoes (Cupper et al., 2003, Price et al., 2003).

The NVP can be divided into three morphologically distinct subprovinces. The Central Highland Subprovince in the north contains about 250 eruption centres and valley fill lava flows. The scoria cones and maars of the Mt Gambier Subprovince are located in the west, and are separated from the Western Plains Subprovince in the east by Holocene sediments. The flat lava plains of the Western Plains Subprovince are the dominant feature of the NVP (Hare and Cas, 2005). The sequence of multiple lava flows can be up to 100 m thick. The volcanic rocks of the NVP range in their geochemistry from tholeiitic to alkalic and can be divided in three different compositional suites with two end-members and a transitional suite (Vogel and Keays, 1997). Highly fractionated and sulphur saturated

rocks of the tholeiitic plains suite form one end-member and contain more than 50 % SiO_2. SiO_2 undersaturated rocks of the alkalic cones suite form the other endmember. They can locally contain abundant upper-mantle xenoliths. Rocks of the transitional suite contain less than 50 % SiO_2.

According to Vogel and Keays (1997) the origin of these different melts is that the magma derived from partial melting of eclogitized oceanic crust, which was subducted in a previous event and that the spectrum of magma compositions observed in the NVP is caused by melting of different compositional parts of the oceanic slab. Further differentiation of the melts was caused by crystal fractionation (Vogel and Keays, 1997).

The basement of the Newer Volcanics Province is formed by Mesozoic to Tertiary sediments of the Otway and Port Phillip basins underlain by Palaeozoic rocks of the Lachlan and Delamerian fold belts (Hare and Cas, 2005). According to Lister and Etheridge (1989) and Price et al. (1997), the rifting processes along the Australian southern margin during the break up of Gondwana is the cause of the volcanism in the Newer Volcanics Province produced by mantle upwelling and decompressional melting. However, volcanism occurred 50 Myr after break-up, and the regional tectonic stress field changed to a compressional one about 10 million years ago (Sandiford, 2003, Sandiford et al., 2004, Hare and Cas, 2005). Many of the volcanic centres are aligned along NW-SE Mesocoic-Cenozoic, N-S Paleozoic and E-W Cretaceous structures, indicating that magma ascent and dyke propagation was influenced by tectonic structures (Lesti et al., 2008). Lesti et al. (2008) suggested volcanism could have been triggered in transtensional windows along these structures caused by NW-SE orientated compressional stress field, leading to decompressional melting.

2

The origin of a large (>3 km) maar volcano by coalescence of multiple shallow craters: Lake Purrumbete maar, southeastern Australia

S.C. Jordan, R.A.F. Cas and P.C. Hayman

Abstract

Lake Purrumbete Maar is located in the intraplate, monogenetic Newer Volcanics Province in southeastern Australia. The extremely large crater of 3000 m in diameter formed on an intersection of two fault lines and comprises at least three coalesced vents. The evolution of these vents is controlled by the interaction of the tectonic setting and the properties of both hard and soft rock aquifers. Lithics in the maar deposits originate from country rock formations less than 300 m deep, indicating that the large size of the crater cannot only be the result of the downwards migration of the explosion foci in a single vent. Vertical crater walls and primary inward dipping beds evidence that the original size of the crater has been largely preserved. Detailed mapping of the facies distributions, the direction of transport of base surges and pyroclastic flows, and the distribution of ballistic block fields, form the basis for the reconstruction of the complex eruption history, which is characterised by alternations of the eruption style between relatively dry and wet phreatomagmatic conditions, and migration of the vent location along tectonic structures. Three temporally separated eruption phases are recognised, each starting at the same crater located directly at the intersection of two local fault lines. Activity then moved quickly to different locations. A significant volcanic hiatus between two of the three phases shows that the magmatic system was reactivated. The enlargement of especially the main crater by both lateral and vertical growth led to the interception of the individual craters and the formation of the large circular crater. Lake Purrumbete Maar is an excellent example of how complicated the evolution of large, seemingly simple, circular maar volcanoes can

be, and raises the question if these systems are actually monogenetic.

2.1 Introduction

The size of maar volcanoes ranges from 100 m to over 3000 m (Cas and Wright, 1987, Németh et al., 2001). A model for the formation of maar volcanoes was first established by Lorenz (1986) for smaller maar volcanoes in the range of less then 100 m to 1500 m, where the maar crater is widened by the downwards excavation of the underlying diatreme. The deepening of the explosion focus is caused by the depression of the groundwater table. Lorenz (1986) suggested in his figures that this process results in a crater diameter to diatreme depth ratio of 1:1, implying that large maar volcanoes would have an enormous subsurface structure. Other authors (Carn, 2000, Gençalioğlu-Kuşcu et al., 2007) suggested that widening of the crater by crater rim erosion will change this ratio and can be used as a measure of the age and maturity of the maar crater. However, vent migration during the eruption is reported from many large maar volcanoes such as the Tihany Maar Volcanic Complex, Hungary (Németh et al., 2001), Fekete-hegy volcanic complex, Hungary (Auer et al., 2007) and the Coombs Hills, Antarctica (White and McClintock, 2001), as indicated by their characteristic elongated and lobate shapes.

This paper aims to determine the processes leading to the formation of large, circular maar structures. Lake Purrumbete Maar is the perfect maar for these investigations, due to the continuous outcrop of the crater wall succession. From the preserved stratigraphy, the eruption chronology and location of vents can be assessed to produce a reconstruction of the evolution and formation of Lake Purrumbete Maar.

2.2 Geological setting

The Lake Purrumbete Maar lies in the late Cenozoic, continental, intraplate basaltic Newer Volcanics Province (NVP) of southeastern Australia. The NVP is underlain by the metasedimentary, volcanic and granitic rocks of the Palaeozoic Delamerian and Lachlan fold belts in the north, and the sedimentary succession of the Mesozoic - Cenozoic Otway Basin in the south (Graeber et al., 2002). The Otway Basin overlies the Palaeozoic basement and was formed by rifting between Australia and Antarctica throughout the Cretaceous. Structural trends within the Otway Basin are north trending Palaeozoic faults and Cretaceous normal faults both ENE striking in the western Otway Basin and WNW striking in the eastern part (Figure 2.1). The change from ENE striking faults to WNW striking faults takes place in a ca. 30 km wide zone to the east of the Moyston Fault, which is called the Sorell-Purrumbete Trend (Miller et al., 2002). The syn- and post-rift sedimentary infill of the Otway Basin consists of sandstones, marls and limestones. The succession varies within the Otway Basin and some members pinch out towards the basin margin.

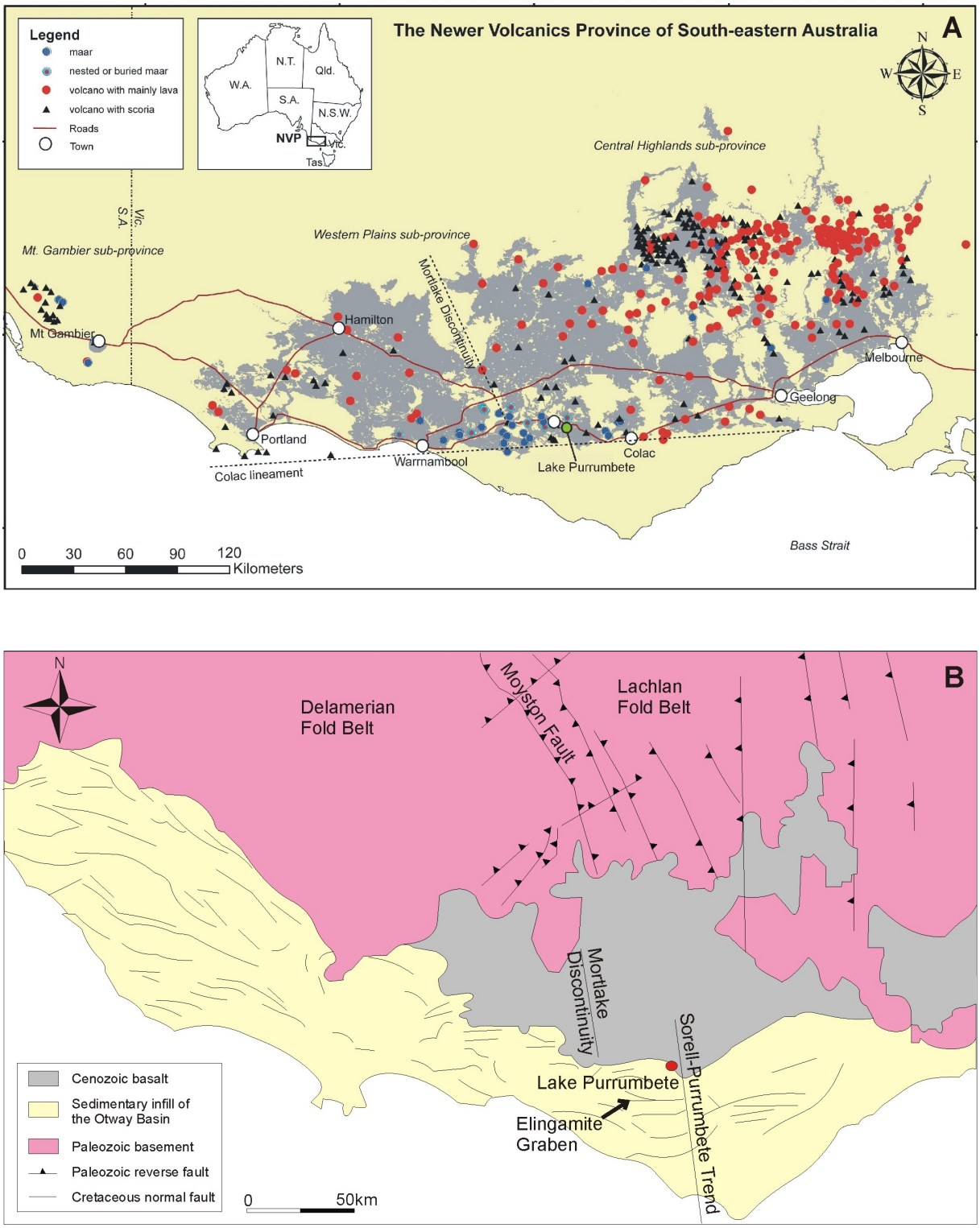

Figure 2.1: A: Distribution of eruption centres in the NVP with the location of Lake Purrumbete marked in green. B: Structural map of the NVP region. The change of NW striking normal faults in the western part to NE striking normal faults in the eastern part occurs along the Sorell-Purrumbete Trend (modified after Miller et al. (2002)).

Volcanism in the NVP started in the early Pliocene and continued into the Holocene, with ongoing activity of natural hot springs and mantle derived CO_2 emission (Lesti et al., 2008). The province has an area of over 25000 km^2 and comprises 440 eruption points (Figure 2.1), including 40 maar volcanoes (Joyce, 1975). The NVP can be divided into three morphologically distinct subprovinces: the Mt Gambier subprovince to the west, the Central Highland subprovince to the north and the Western Plains subprovince, which comprises Lake Purrumbete. Flat, widespread lava sheets are characteristic for the Western Plains subprovince, but small volcanic edifices, such as scoria cones, maars and lava shields, exist as well (Hare and Cas, 2005, Lesti et al., 2008).

Lake Purrumbete, with a 3 km diameter, is one of the largest maar volcanoes within the NVP and worldwide. The maar is located within the Palaeozoic Sorell-Purrumbete Trend (Miller et al., 2002) at the northern edge of the Otway Basin (Figure 2.1), where Cretaceous sedimentary cover is relatively thin (Edwards et al., 1996). Deep seismic data show half graben structures and normal faults steeply dipping to the north (Hill et al., 1994, Finlayson et al., 1996) and that the Moho underneath Lake Purrumbete is at 30 km depth (Finlayson et al., 1996).

The main aquifers in western Victoria are the sandstones of the Dilwyn Formation and the Port Campbell Limestone. However, the latter is missing at Lake Purrumbete and the existence of the Dilwyn Formation underneath Purrumbete is not certain (Figure 2.2). Water boreholes in the area intersect the Black Rock Sandstone and the basaltic lava flows of the NVP, both are local aquifers close to the surface. Some boreholes reach the top part of the Gellibrand Marl, where the sandy beds act as a minor aquifer (Edwards et al., 1996), while the Gellibrand Marl itself is an aquitard (Jones et al., 2001, Tweed et al., 2009).

2.3 General architecture of the Lake Purrumbete Maar

Figure 2.3A and B show that Lake Purrumbete is circular, with the western part transected by a N-S trending linear structure, coinciding with two depressions, in the crater walls roughly on opposite sides lake side, and subaqueous channels, described by Timms (1976). This lineament is parallel to N-S trending Paleozoic basement structures (Lesti et al., 2008) and is considered to be the surface expression of a Paleozoic fault. A topographical lower area along the fault is further indicated by swampy areas to the north and south of Lake Purrumbete. The subaqueous channels indicate that the fault has been active to recent times. A second NW-SE trending tectonic structure is indicated by magnetic measurements (Edmonds, 2008). The bathymetry of the maar lake reflects a bowl-shaped sub-surface structure.

A minimum volume of 0.25 km^3 has been calculated for the pyroclastic material from a 3-D model of the maar rim, using the log data of water boreholes in the area around Lake Purrumbete (Figure 2.4). The model does not take into account the erosion of the maar rim, material carried away by wind during the eruption and the pyroclastic material in the

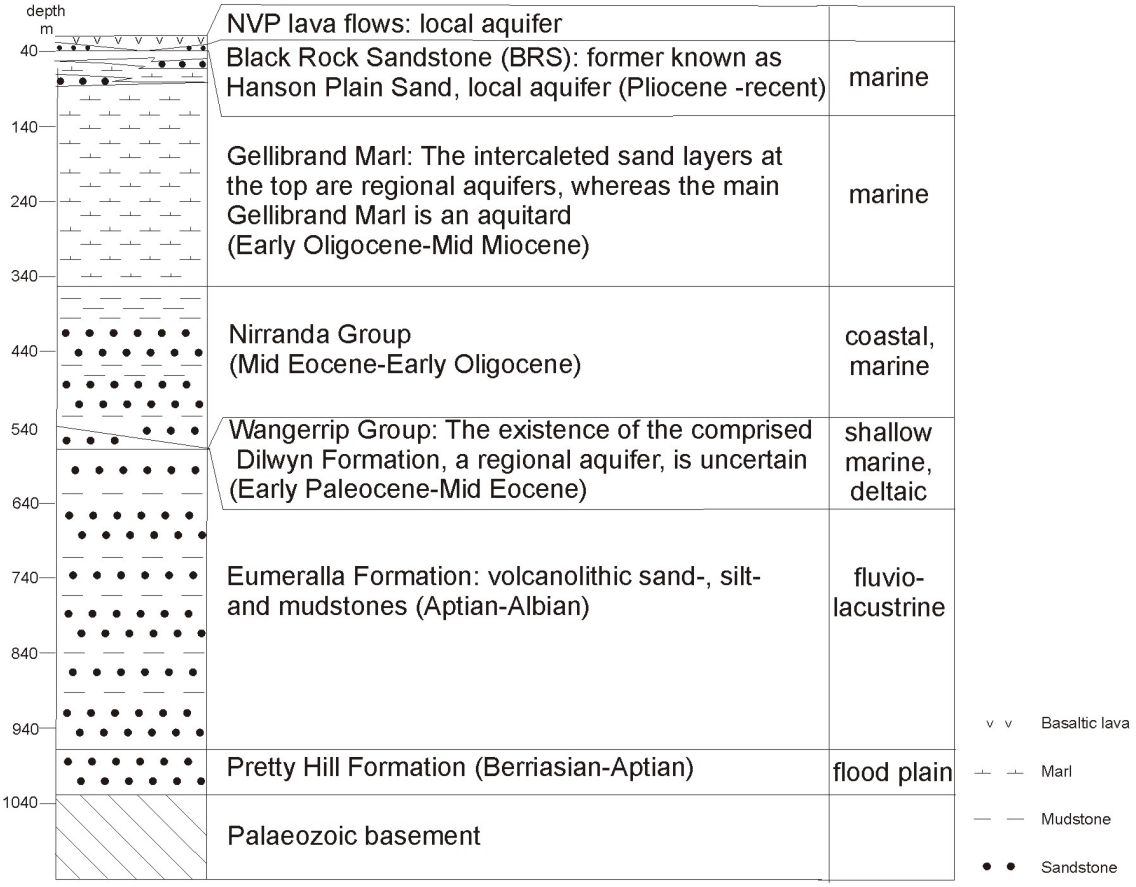

Figure 2.2: Stratigraphic log of the Otway Basin stratigraphy underlying Lake Purrumbete at the basin margin (data used from Edwards et al. (1996)).

diatreme, as these factors are unknown. The model shows that the deposits are distributed unevenly around the crater and differ in thickness on either side of the lineament, with a maximum thickness of 8 m on the western side, compared to a maximum thickness of 40 m on the eastern side. Furthermore, the stratigraphical architecture of the eastern maar rim is very complex with a large variety of lithofacies, in contrast to only 5 lithofacies in the western rim.

The Lake Purrumbete Maar rim deposits consist predominantly of phreatomagmatic base surge deposits, indicated by cross stratification. The succession generally dips gently away from the crater, except for a few locations where surge deposits discordantly mantle the older maar rim deposits and dips towards the crater. In the eastern maar sector, the succession includes many normal faults, that are bounded by two larger normal faults, which are interpreted to form one large ring fault structure. Five lithofacies sequences were identified, based on changes in the lithofacies distribution and field relationships. Each sequence contains several lithofacies forming a unique pattern of lithofacies variations. The geochemistry of the juvenile material generally ranges from trachybasaltic to basanitic.

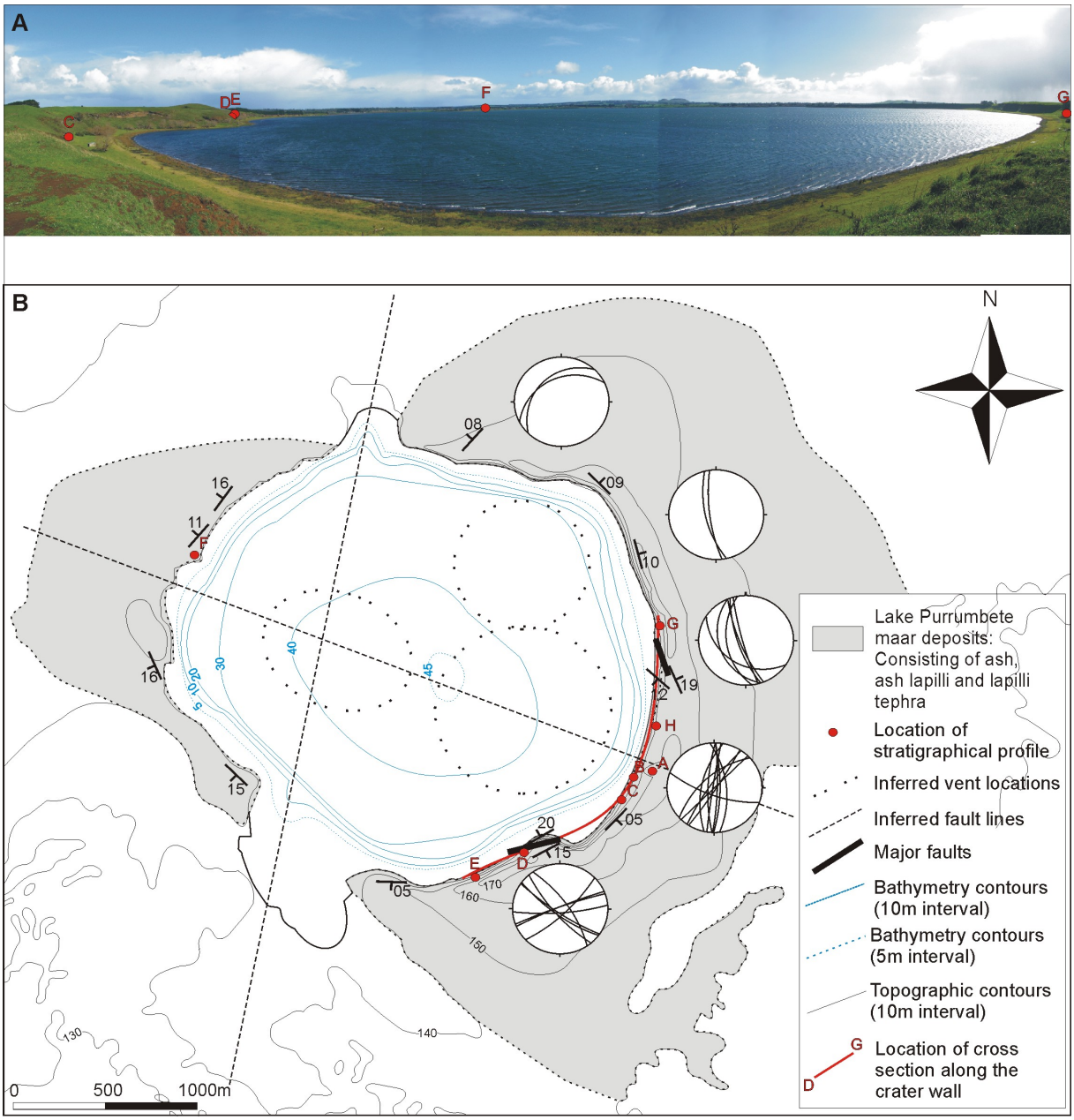

Figure 2.3: A) View of Lake Purrumbete from the eastern maar sector, with the visible locations of profiles marked in red. B) Geological map of the Lake Purrumbete Maar volcano. The stereonets show the trend of the fault lines along the crater walls. The tectonic basement structures are marked in dashed lines, while the suggested vent locations are shown by dotted circles, with the location of the cross section (Figure 2.12) marked as a red line along the eastern margin.

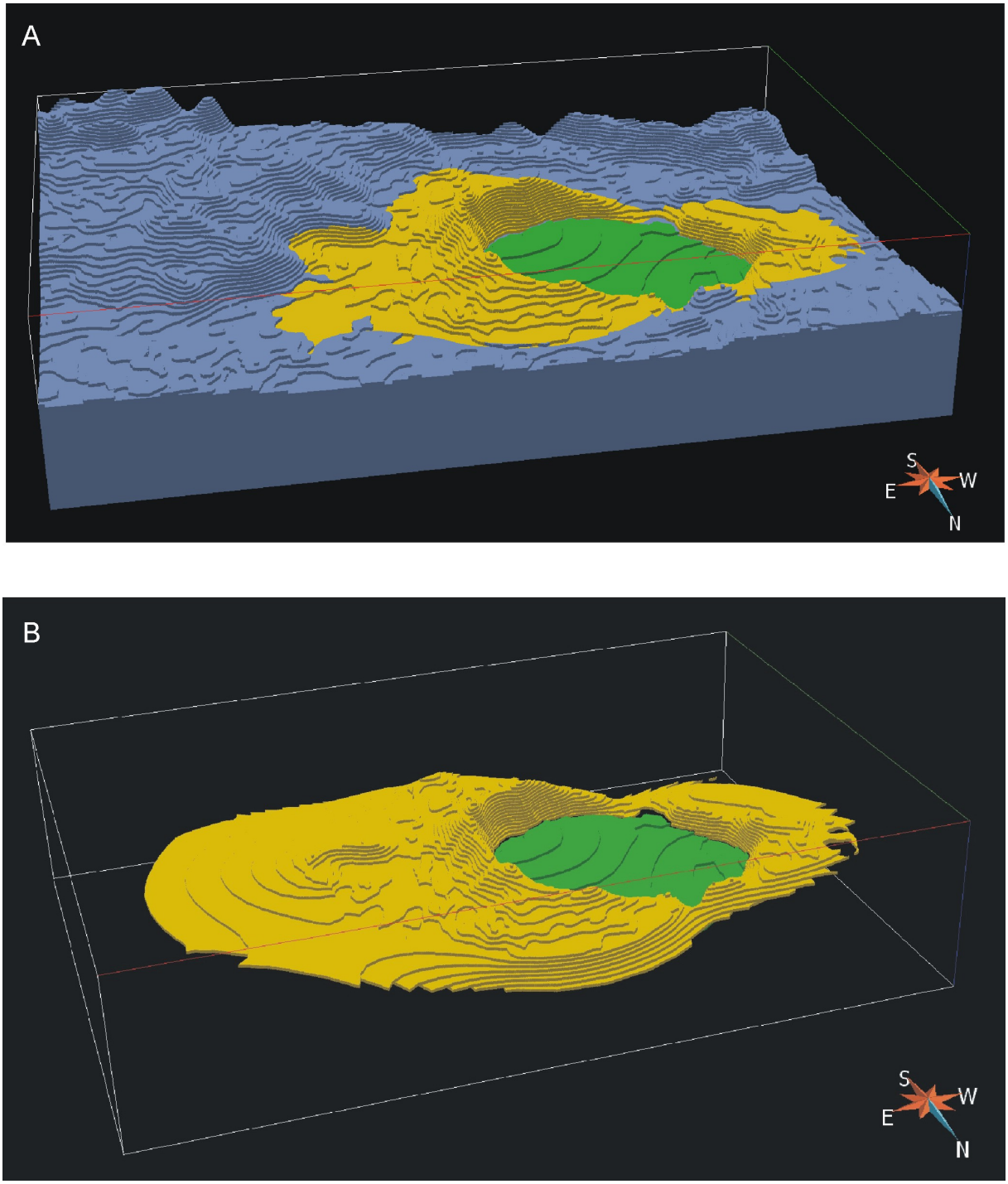

Figure 2.4: 3-D models of the topography and the pyroclastic material around Lake Purrumbete (A) and of the volume of the pyroclastic material (B) (blue: surrounding country rock, yellow: pyroclastic material, green: Lake Purrumbete crater).

2.4 Methods

2.4.1 Field work

Detailed mapping of the pyroclastic maar rim succession and logging of seven important sections were used for lithofacies characterisations and lateral stratigraphic correlations (Appendix 2; images of crater walls). The transport direction of pyroclastic density currents was determined by measuring crossbed orientations (Appendix 3). In addition, impact angle and direction of ballistic ejecta were used together with other properties, including shape, type and size, to reconstruct the trajectories of these ballistics with the computer program Eject version 1.3 by L. G. Mastin (Table 2.1). Structural data was collected such as bedding and orientation of fault planes. Samples of the different lithofacies were collected for laboratory analysis, including grain size, petrography, back-scattered electron (BSE) imaging and geochemistry.

Table 2.1: Primary data including impact angle and direction of ejecta measured at Lake Purrumbete, with distance of the possible vent location calculated using Eject 1.3 by L. G. Mastin.

coordinates	type	size (cm)	impact angle	impact direction	distance (m)
0696343/5760347	basalt	22	34°	N	850
	basalt	16	66°	E	652.5
0696355/5760399	basalt	20	20°	NE	599.9
0696392/5760574	basalt	3	90°	S	0
	basalt	2	55°	S	179.7
	basalt	2	25°	S	196.2
0695864/5759585	basalt	30	60°	S	789
0695721/5759684	basalt	50	40°	E	930
0695657/5759651	basalt	110	40°	SE	858.4
0694732/5759472	basalt	60	50°	SE	943.9
	basalt	20	40°	S	894.9
	basalt	100	30°	S	856.1
0695053/5759394	basalt	25	50°	SE	899.9
0695241/5759421	scoria	5	30°	S	138
	scoria	2	30°	S	72
	scoria	2	20°	S	69.5
0696403/5760604	tuff	10	65°	E	500.8
	basalt	7	95°	E	565.7
	scoria	12	95°	E	457.4
0696407/5760725	basalt	25	30°	NE	553.7
	basalt	25	20°	E	452.4
	basalt	16	35°	E	484.6
0696400/5760759	basalt	35	35°	E	876
0696405/5760861	basalt	50	20°	NE	601.4
	basalt	30	70°	NE	592.9
0696251/5761142	basalt	30	30°	E	588.5

Continued on next page

Table 2.1: Primary data including impact angle and direction of ejecta measured at Lake Purrumbete, with distance of the possible vent location calculated using Eject 1.3 by L. G. Mastin.

coordinates	type	size (cm)	impact angle	impact direction	distance (m)
	basalt	40	40°	E	690.6
	basalt	37	45°	E	933.5
	basalt	17	55°	E	839.1
0696232/5761224	basalt	45	40°	SE	932.3
0696225/5761279	basalt	40	25°	NE	732.5
	basalt	40	35°	NE	673.6
0696155/5761465	basalt	6	30°	E	411.9
	basalt	6.5	55°	NE	371.9
	basalt	13.5	45°	NE	874.7
	basalt	3	45°	NE	261.1
	basalt	22	20°	NE	595.8
	basalt	30	60°	NE	794.4
0695489/5761720	basalt	2.5	35°	N	205
	scoria	1.8	60°	N	28
	basalt	12	72°	N	234.5
	basalt	4.5	50°	N	298.8
0695402/5761727	basalt	25.5	50°	N	577
	basalt	60	40°	N	939.1
	basalt	35	35°	N	880
	basalt	36	50°	N	907.2
0695373/5761748	basalt	21	35°	N	848.2
	basalt	35	35°	N	880
	basalt	25	30°	N	623.9
0695341/5761734	basalt	29	35°	N	871
	basalt	30	40°	N	910.2
	basalt	21	60°	N	783.1
	basalt	56	45°	N	954
0695299/5761736	basalt	32	15°	NW	480.1
	basalt	8.5	30°	NW	846.9
	basalt	12	35°	NW	831.6
0695261/5761740	basalt	60	20°	N	630
	marl	24	20°	NW	601.3
	basalt	18	60°	N	767.8
	marl	13	50°	N	842.6
0695214/5761754	basalt	29	35°	N	872.3
0694137/5760027	basalt	6	35°	W	424.2
0694057/5760069	basalt	18	25°	S	458.9
0694046/5761528	basalt	21	50°	W	890

2.4.2 Grain size analysis

The grain size distribution was determined using two different methods. Coarse grained, unconsolidated samples were dried in an oven at 90 °C and sieved with a mechanical shaker using a stack of sieves with half ϕ-spacings, ranging from -3 to 4 ϕ. Afterwards the grain

size fraction within each sieve was weighed.

The grain size distribution of consolidated fine ash was determined using BSE images of polished thin sections, photographed with the JEOL 840A scanning electron microscope at the Monash Centre for Electron Microscopy. Ten images per sample at varying magnifications were used and the clasts in each image were outlined manually using Gimp2 software. The shape parameters of the clasts were then calculated using ImageJ software. Classification into bin sizes is based on the Minimum Feret Diameter of each clast, which is the shortest distance between two parallel line segments that enclose a 2-dimensional clast outline (Appendix 4).

2.5 Lithofacies

The following description of the different lithofacies types of the Lake Purrumbete Maar rim succession is based on field observations and grain size analyses. The maar rim succession comprises six different ash lithofacies, six lapilli lithofacies, two scoriaceous lapilli lithofacies, two block and bomb lithofacies and an epiclastic, volcanogenic sandy gravel lithofacies.

2.5.1 Ash lithofacies types

Six types of ash lithofacies occur in the field: 1) massive accretionary lapilli rich fine ash (F1), 2) cross laminated fine ash (F2), 3) finely stratified ash (F3), 4) cross laminated lapilli coarse ash (F4), 5) planar laminated coarse ash (F5) and 6) massive, clast rich fine ash (F6). A creamy, yellow colour, high abundance of fine ash and lithification are characteristic for these lithofacies. They are also characterised by a unimodal grain size distribution with a median grain size around 5.5 ϕ for fine ash lithosfacies and around 0 ϕ for coarse ash.

The F1 lithofacies forms up to 70 cm thick, massive, well sorted layers and consists of 85 % fine ash, 10 % blocky, juvenile clasts and 5 % marl lithic clasts. The clast fraction ranges in size from coarse ash to very fine lapilli. The fine ash matrix contains abundant ash aggregates (30 %) (Figure 2.5A), classified as ash pellets after Brown et al. (2010), with a few cored pellets.

Layers of F2 are <1 m thick, moderately sorted and show small scale cross bedding, laminations and dune forms (Figure 2.5B). Eighty percent of the deposit is fine ash, with 20 % blocky, very vesicular juvenile lapilli. Bedding sag structures and centimetre to decimetre size ballistic ejecta are common, with concentrations of ash pellets and cored pellets on the top layer.

The moderately sorted F3 lithofacies is the most common type of fine ash lithofacies. F3 units vary in thickness between 1 and 2 m and are characterised by alternation of centimetre - decimetre thick horizons formed by planar, thinly laminated fine ash and planar or cross bedded, dark grey to black coarse ash. Overall the lithofacies consists of

65 % fine ash, 25 % blocky, moderate vesicular juvenile lapilli, 5 % marl lithic lapilli and occasionally basaltic lithic lapilli (<5 %).

F4 lithofacies units are 40 to 180 cm thick, poorly sorted and matrix supported, with variations in the amount of fine ash matrix (40-70 %) and juvenile lapilli abundance (25-55 %). The content of lithic clasts is relatively low at 5 %.

F5 lithofacies units are 20 to 180 cm thick and predominantly planar laminated, with minor cross laminations. The lithofacies contains 70 % coarse ash matrix, 25 % blocky juvenile lapilli and 5 % marl lithics lapilli.

The F6 lithofacies varies widely in thickness (2-100 cm) (Figure 2.5C), which is caused by pinching and swelling of the deposit. It is generally massive with occasional slump structures and very small ripples. Eighty percent of the material is fine ash matrix and the remaining 20 % consist of coarse ash and fine lapilli juvenile fragments scattered throughout the matrix (Figure 2.5D).

2.5.2 Lapilli lithofacies types

Lapilli lithofacies comprise 1) cross bedded ash lapilli deposits (L1), 2) planar stratified ash lapilli (L2), 3) clast supported, ash poor lapilli deposits (L3), 4) ash poor, hydrothermally altered lapilli deposits (L4), 5) ash rich planar bedded ash lapilli deposit (L5) and 6) chaotic, block-bearing coarse lapilli deposits (L6). The lapilli lithofacies are typically unconsolidated, poorly sorted and unimodal in grain size distribution with a median grain size between 0.5 ϕ and -1.5 ϕ, however some horizons can be semi-consolidated.

L1 deposits are 0.5-2 m thick, with common depositional structures, such as cross bedding, dune forms, undulating layers and climbing dune cross beds (Figure 2.5E). The units vary from light creamy colour, to light and dark grey. The light creamy colour is caused by ash coating of the usually darker lapilli clasts. The material consists of 30-60 % ash, 20-50 % juvenile lapilli , 5-20 % marl and 5 % basaltic lithic lapilli.

L2 units are typically 1-2 m thick, grey in colour, and consist of two domains, planar stratified clast supported lapilli horizons and planar to cross stratified matrix supported coarse ash horizons (Figure 2.5), varying in thickness between 10 and 20 cm. The lapilli layers consist of 60-80 % lapilli and 20-40 % fine ash matrix in contrast to the ash layers, with 80 % fine ash and 20 % lapilli. The lapilli fraction consists predominantly of juvenile clasts with 10 % marl lithic clasts.

L3 lithofacies units range in thickness between 10 cm and 2 m. The typically dark grey

Figure 2.5 *(following page)*: A F1 lithofacies containing abundant millimetre to centimetre sized accretionary lapilli. B Contact between F2 and L2 facies. C Thick F6 lithofacies unit thins out rapidly into D a 2 cm thick horizon consisting predominantly of fine ash with randomly scattered larger black juvenile clasts. E Cross stratification in the L1 facies. F Sharp contact between F3 and S1 lithofacies units. G Large boulders and abundant very coarse clasts in the bottom part of L4 lithofacies. H The clast supported layers of the L4 facies are characterised by thermally altered red and white clasts.

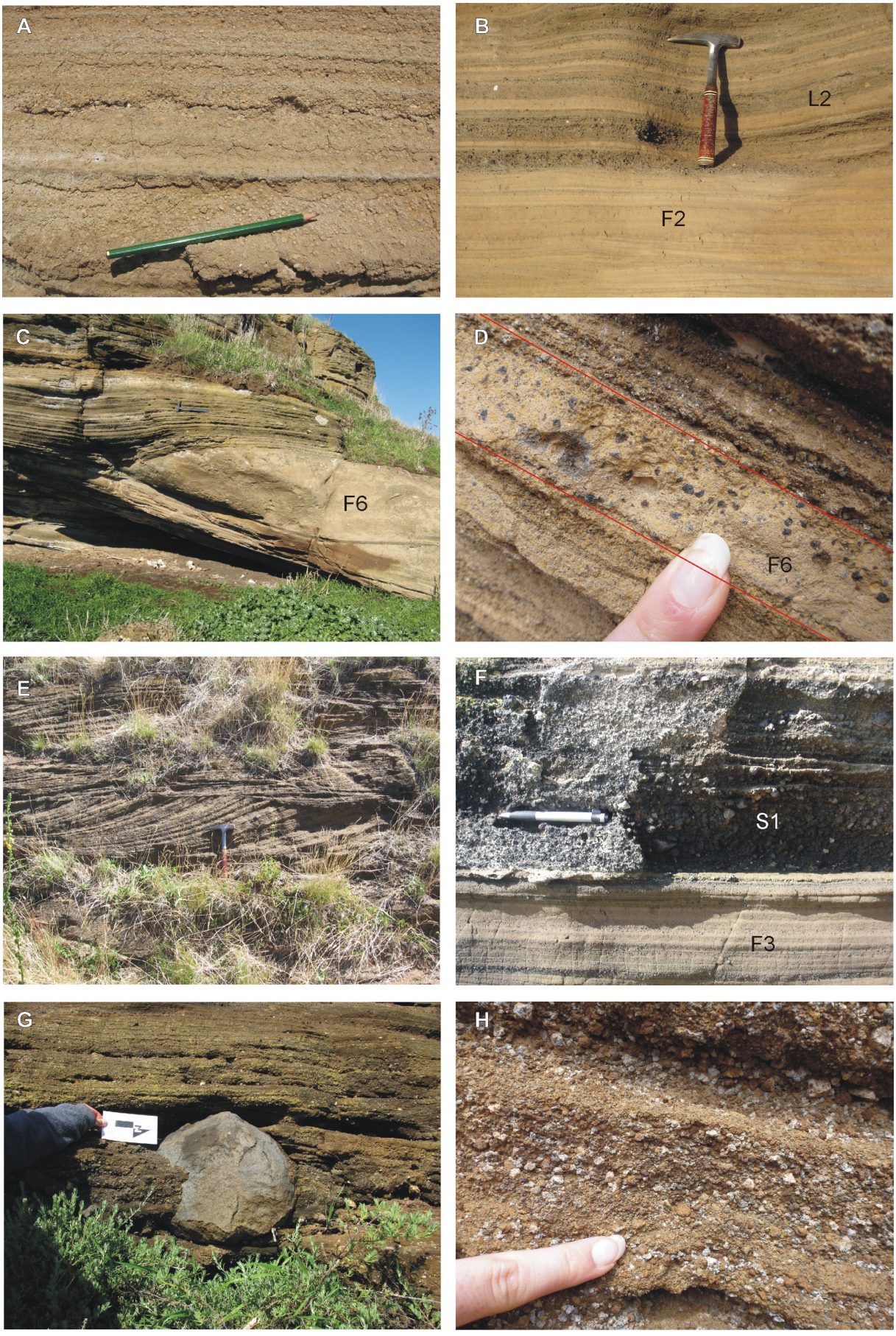
A
B
L2
F2
C
F6
D
F6
E
F
S1
F3
G
H

to black layers show thin planar bedding or small scale cross bedding. Components are 85 % blocky, poorly vesicular juvenile lapilli with 5 % accessory marl lithic lapilli and 10 % coarse ash matrix.

The L4 lithofacies consists of alternating bands of thick massive to planar bedded, moderately to well sorted, coarse lapilli and thinner cross bedded, moderately to well sorted coarse ash. While the contact between lapilli layers and underlying ash layers is sharp, the contact with overlying ash layers is diffuse. Layers are between 50 and 100 cm thick, but wedging on topographical highs is common. Overall the lithofacies thickness is up to 3 m. The lapilli clasts are formed by 20 % marl lithics, 20 % dense basaltic lava flow lithics, and 60 % red, hydrothermaly altered, poorly vesicular basaltic clasts (Figure 2.5H). Ash makes up 10 % of the coarse lapilli layers and <45 % of the coarse ash layers. The ash fraction contains a unique clast type of juvenile cuspate glass shards, which increase in abundance from the bottom (zero) to the top (80 %). Occassionally blocks and boulders occur at the bottom of the unit (Figure 2.5G). Furthermore, a few lapilli sized mantle xenolith fragments were observed.

L5 lithofacies form dark, ash rich, poorly sorted and planar bedded units. The lithofacies consists of ca. 50 % ash matrix, 40 % very vesiculated juvenile clasts and 5 % of each marl and dense basaltic lithics.

L6 lithofacies is ca. 15 cm thick, clast supported and poorly sorted, containing block and lapilli size clasts, while ash is minor (10 %). The clasts consist of 40 % limestone, and 50 % juvenile fragments.

2.5.3 Scoriaceous lapilli lithofacies types

This lithofacies occurs as diffusely bedded scoriaceous lapilli deposits (S1), and massive scoriaceous lapilli deposits (S2). Both lithofacies appear to be moderately to well sorted, whereas results of grain size analysis show poor sorting and a bimodal distribution, which is the effect of the ash content. Especially for the S2 facies type, the ash is likely the result of contamination from the overlying ash facies. The mean grain size is between -0.5 ϕ and -1.5 ϕ.

S1 lithofacies units are typically <50 cm thick, except for one ca. 10 m thick unit in the southern maar sector. S1 shows diffuse planar and cross bedding with very thin ash lenses (Figure 2.5F). This lithofacies is clast supported, poorly sorted and dark grey coloured, containing 40 % scoria clasts, 20 % blocky, poorly vesicular juvenile clasts, 5-15 % marl lithics, 5 % basaltic lithic clasts and 5 % feldspar crystals. Ash contents vary between 15 and 25 %. In the southern thick unit, fragments of Pele's hair were found in the coarse ash fraction.

S2 lithofacies units are only 0.5-30 cm thick and massive. The dark grey colour reflects the high abundance of scoriaceous (70 %) and poorly vesicular juvenile lapilli (10 %). Basaltic and marl lithic lapilli occur only as accessories and the amount of ash is very low (10 %).

2.5.4 Ballistic ejecta

Ballistic ejecta occur in two different lithofacies, either as concentrations of ballistics in block fields (B1) or as single bombs scattered within the fine ash lithofacies (B2). These two lithofacies differ in size, shape and composition.

Most B1 ballistics in the block fields are not in situ, but were eroded out of the crater rims and are preserved at the lake shore. However, blocks found in situ give evidence for the original depositional horizon, together with preserved impact structures (Figure 2.6). The 0.1-1 m large bombs are predominantly spherical in shape and consist mainly of microcrystalline basalt, originating from the underlying NVP lavas. The basaltic bombs show varying degrees of vesicularity, with a majority of bombs being highly or slightly vesicular and a minority of medium vesicular bombs. A few some sedimentary blocks were also observed.

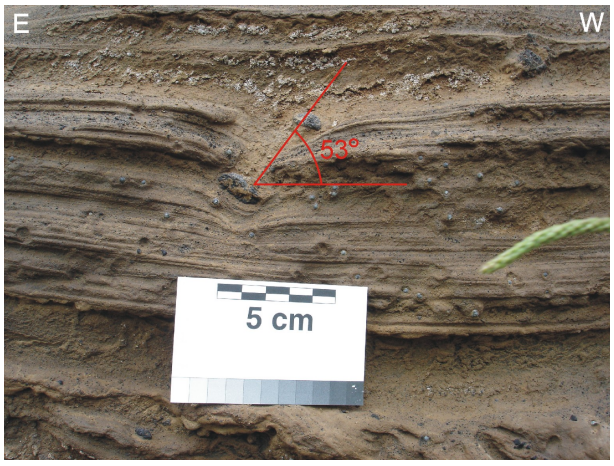

Figure 2.6: Ballistic bomb with impact sag within F2 lithofacies at the bottom of profile A.

Smaller (10 cm) isolated bombs (B2) are scattered over the whole rim succession with a preferential occurrence in the fine ash lithofacies. The majority consist of spindle bombs and rounded basaltic blocks from the underlying NVP lavas. Rounded marl clasts are minor.

2.5.5 Epiclastic, volcanogenic sandy gravel

This lithofacies forms thin, dark, poorly sorted, massive layers, with erosional features at the bottom, including erosional scours with small intraclast blocks from the underlying volcanic layers. Some of these blocks are not fully disconnected from their original layer and can be found in the form of a jigsaw structure. The material consists of 65 % rounded, black volcanic clasts, 5 % exotic clast and 10 % bone material in a fine sand matrix (10 %) (Figure 2.7). The volcanic clasts have a smooth surface and range in grain size from pebbles to sand size. The exotic clasts consist of mantle xenoliths, mudstone, tuff and rounded quartz pebbles. Well preserved bones were identified as a wombat tooth and parts of a kangaroo jaw.

Figure 2.7: Kangaroo jaw with preserved teeth within the epiclastic, volcanogenic sandy gravel deposit. The well rounded shape and smooth surface of the abundant basaltic clasts are characteristic of tractional processes.

2.6 Componentry

Componentry was determined by field observation and manual counting of grains, resulting in two different data sets. The main observed clast types in the field are highly vesicular and poorly vesicular juvenile clasts, dense basaltic lithic clasts from the NVP lava flows, and marl lithic clasts from the Gellibrand Marl.

Detailed componentry analysis by counting manually grains under the binocular microscope was carried out on 29 unconsolidated samples of several lithofacies types, using three different grain size fractions, -1, 1 and 2 ϕ. Five hundred grains of each grain size were identified and classified in six main clast types: clean juvenile clasts; ash coated juvenile clasts; crystals; hydrothermally altered basaltic clasts, sandstone fragments; and accessory lithic clasts including marl fragments, fragments of shells and dense basaltic clasts (Appendix 5). Two uncommon clast types were recorded in two lithofacies; fragments of Pele's hairs in S1 and cuspate glass shards in L4. Analysis of the sandstone fragments in thin section show angular to sub-rounded fine sand sized quartz grains in a mud matrix suggesting origin from the Black Rock Sandstone. Minor amounts of sandstone clasts have a slightly more calcitic matrix with less quartz grains, which may originate from the sand layers of the Gellibrand Marl. The quartz grains in all sandstone fragments are similar to quartz grains observed in thin section of a lateritic sandstone bomb found at Lake Purrumbete. The occurrence of lateritic sandstone is characteristic for the Black Rock Sandstone (Edwards et al., 1996).

Variations within the componentry datasets occur between sequences but not between lithofacies; this applies especially for the microscope data. Figure 2.8 shows the percentage of clast types for each data set and sequence. The field data show that the amount of dense basaltic lithics is relatively low at 5 % and constant in all sequences, except for the bottom part of sequence 5. The amount of marl lithic clasts, however, ranges from 5 % in sequences 2, 4b and the top part of sequence 5, to 15-20 % in sequences 1, 3, 4a

and 5. These variations are not captured in the point counting data of the smaller grain sizes (Figure 2.8), where the abundance of marl and basaltic lithic clasts is so small that they were grouped together as accessory lithic clasts. To test if the similar appearance of both dense basaltic clasts and clean juvenile clasts under the binocular microscope is the reason for the low amount of dense basaltic clast in this data set, we compared the data of random samples to point count data of thin sections. The result shows that the abundance of dense basaltic clasts derived from point counting is within the <5 % abundance derived from field observations. However, it is still very low compared to the abundance of the other clast types. As a result, the componentry data determined using the binocular microscope has errors in the exact percentage of clean juvenile clasts and dense basaltic clasts, but the overall ratio of the distribution of the main clast types is not affected.

The small abundance of marl clasts cannot be the result of identification problems, but may be the result of weathering. The larger marl clasts observed in the field are often very weathered and disaggregate into fine dust when touched. Smaller clasts would weather faster than larger clasts and therefore would be less likely to be preserved. In addition, water percolating through the deposits from the surface, especially in the unconsolidated coarse deposits, is also likely to dissolved any small carbonate clasts. Precipitation horizons of white calcareous material in outcrops are evidence for this process.

The point counting data set shows variations in sandstone fragment abundance between sequences. Sequence 1-4a show relatively high sandstone fragment abundances with the highest amount in sequence 3, whereas sequence 4b-5 have very low contents of sandstone fragments.

2.7 Facies interpretations

2.7.1 Ash lithofacies

The very fine grain size of the F1 and F2 facies is evidence for intense fragmentation typical for phreatomagmatic eruptions. Wohletz (1983) and Kokelaar (1986) suggest that the most intense fragmentation and highly explosive phreatomagmatic eruptions are produced by an optimum magma/water ratio of 0.3. However, White (1996) proposes that this ratio could be smaller if vents are filled with a suspension of loose material and water. The high abundance of accretionary lapilli and the occurrence of soft-sediment deformation structures, such as impact sags of ballistic bombs, are characteristic for wet deposits and can occur in both fall and surge deposits (Dellino et al., 1990, Gençalioğlu-Kuşcu et al., 2007). The well sorted character, the uniform thickness of the units and the extremely high amount of ash pellets and cored pellets indicate deposition of F1 by fall out either from a moisture laden wet eruption cloud or from a co-ignimbrite ash cloud, as described by Brown et al. (2010) for ash pellets and cored ash pellets in ash units at Tenerife. The near vent location of the outcrops makes it impossible to determine if the ash pellets fell

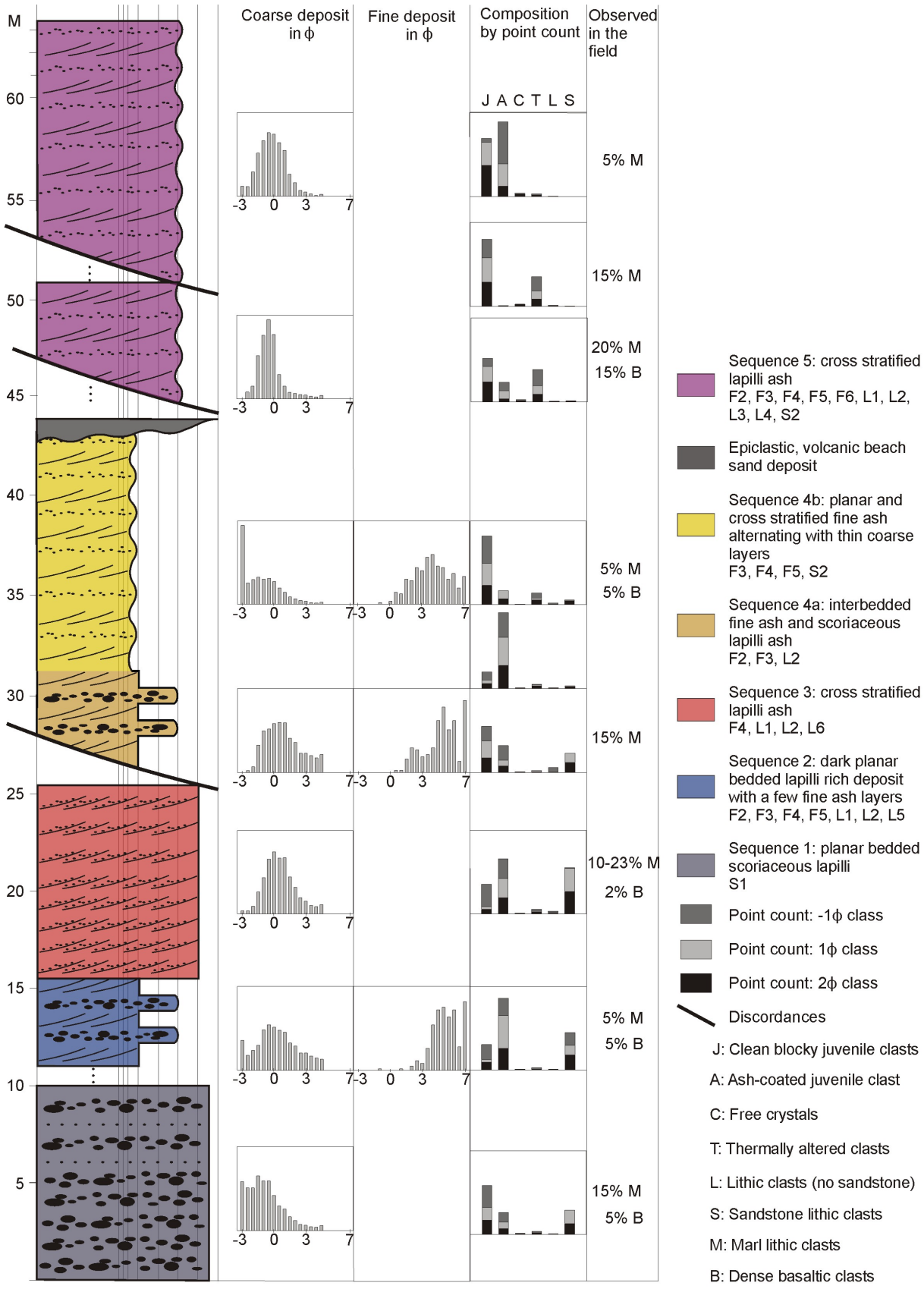

Figure 2.8: Composite stratigraphic column comprising five main pyroclastic sequences, which are cut by three major discordances. Each sequence is characterised by a certain grain size distribution and a unique clast componentry. The abundance of lithic clasts changes throughout the stratigraphy, but the main type of marl clasts occurs in all sequences.

out of an eruption cloud or a co-surge ash cloud.

However, fall out of the ash and cored ash pellets of a co-surge ash cloud is most likely for the F2 facies type, where ash pellets and cored pellets are concentrated at the top of the units and deposition by base surges is indicated by small scale cross stratification.

The fine ash grain size of F3 reflects again the formation of the facies by efficient phreatomagmatic fragmentation. The absence of accretionary lapilli shows that the conditions in the eruption column and/or in the surge were drier than during the formation of F1 and F2. However, the solidified character of the deposit indicates that moisture existed within the deposit. The dominant structure is the alternation of planar stratified fine ash and cross stratified coarse ash. The coarse parts represent the material transported by the main surge whereas the fine ash was deposited from suspension, after the passage of the main surge, from the trailing tail ash cloud (Sohn and Chough, 1989). Therefore each set represents one single surge event (Frazzetta et al., 1989, De Rosa et al., 1992). The contact between individual surge sets is diffuse, indicating continuous pulsatory phreatomagmatic activity rather than separate discrete surge events.

The coarse ash grain size of the F4 ash facies and the abundant juvenile lapilli indicate that the fragmentation was less effective than for F1, F2 and F3. Cross stratification is typical for more dry surge deposits (Dellino et al., 1990) but the poorly sorted character and the relatively high ash content indicate that the depositing surge was relatively wet (Sohn and Chough, 1989).

Occasionally occurring cross beds indicate that the F5 facies type is the product of surges rather than of fall out, while its moderately sorted character suggests that these base surges were relatively dry (Sohn and Chough, 1989).

The F6 facies type is interpreted as the result of a pyroclastic flow event. The massive, structureless character of the deposit, together with the scattered coarser fragments in a very fine matrix is typical of ignimbrite deposits, indicating deposition by a pyroclastic flow. The increased thickness of the deposit in a topographically low area, and the rapid thinning on adjacent, higher palaeotopography creating a veneer type facies (Walker et al., 1981, Pittari et al., 2006), further supports this interpretation.

2.7.2 Lapilli lithofacies

The coarser grain size of the lapilli lithofacies is generally caused by a lower degree of fragmentation, probably due to a less than optimum magma/water mixing ratio.

Ash coating on clasts in the L1 lithofacies indicates deposition by moist surges (Walker, 1984), where varying degrees of ash coating of different depositional units reflect variations in the amount of moisture within different base surges. However, decimetre scale cross beds and dune structures are typical for dry base surges (Walker, 1984, De Rosa et al., 1992).

L2 units were formed by dry surges. The stratification of lapilli and coarse ash layers was caused by the sorting and separation of the material within the surge and then

successive pulses of deposition, each with a varying energy level and clast carrying capacity. The finer fraction was transported in suspension whereas the coarser lapilli fraction was transported by saltation or traction at the bottom of the surge (De Rosa et al., 1992).

The dark colour of the L3 lithofacies reflects clean surfaces of juvenile clasts and low ash contents. The latter indicates, together with planar bedding, deposition by fall out, but small scale cross beds reflect lateral transport by surges. This may be the result of surge modified fall out (Cas and Wright, 1987), which should be common in near vent positions.

The L4 facies occurs only as one unit and is the result of a distinct event. The high amount of blocks and boulders at the bottom of the unit indicates either the opening of a new vent or the reopening of an older vent. The red and white colours of the basaltic clasts are characteristic of hydrothermal alteration and indicate that these clasts are fragments of basaltic material which stayed behind in the conduit after an earlier eruption and was hydrothermally altered. The presence of mantle xenoliths indicate that the magma ascent rate was faster during this eruption event than for earlier eruptions. Cross stratifications and wedging on topographical highs is again evidence for deposition by base surges (Sohn and Chough, 1989). The more distinct contact between ash layers and overlying lapilli layers, together with the cyclicity of the unit, indicates deposition by several distinct base surges, which may be the result of the pulsating character of the eruption. This suggests a phreatomagmatic eruption style, however, the very low ash content of the material, the lack of ash coatings and the occurrence of hydrothermally altered clasts and cuspate glass shards seem to contradict this interpretation. During the eruption the amount of erupted fresh juvenile material increased, documented by the increasing abundance of cuspate glass shards in the coarse ash fraction towards the top of the unit. These fragments also show, that the fresh magma was highly vesiculated with relatively large bubbles and fragmented into fine particles, resulting in a lack of lapilli sized fresh juvenile clasts. This lithofacies appears to represent a transition from relatively dry phreatomagmatic to magmatic explosive activity.

Even though the L5 facies type is planar bedded, the poorly sorted character of the material reflects deposition by base surges. The high vesicularity of the juvenile scoriaceous clasts suggests a largely magmatic driven eruption, consistent with a low country rock lithic content and abundant black juvenile clasts. However, the high ash content also suggests a phreatomagmatic influence. We believe that a combination of both dry phreatomagmatic and explosive magmatic exsolution of volatiles drove this eruption.

The massive structure and the very poorly sorted character of the L6 lithofacies, together with a high content of country rock lithic clasts, is consistent with this lithofacies being formed by a pyroclastic flow. This lithofacies type occurs only once in the maar rim succession and may mark the explosive opening or deepening of a vent, during which an explosive plume became overloaded with solids, collapsed gravitationally, and produced a small volume pyroclastic flow.

2.7.3 Scoriaceous lapilli lithofacies

The S1 lithofacies is interpreted as a surge modified scoriaceous fallout deposit. The predominantly planar bedded structure, and the high abundance of scoria clasts formed manly by fall out, but the thin ash lenses and occasional small scale cross stratification evidence some minor surge activity. The relatively large amount of highly vesicular scoria clasts and the occurrence of ash size Pele's hair shows that the eruption involved a significant magmatic influence. However, laboratory experiments have demonstrated that phreatomagmatic explosions can produce Pele's hair, and that the formation of hair is promoted by the high exit velocity and low viscosity of the melt (Zimanowski et al., 1997b, Büttner et al., 2002) therefore Pele's hair are not unique to magmatic deposits.

The thin S2 facies type was formed by scoria fallout most likely during very short periods of micro-plinian activity (Francis et al., 1990). The well sorted character and the lack of ash are typical for fall out deposits, and the highly vesicular scoria clasts give evidence for magmatic activity.

2.7.4 Ballistic ejecta

The B1 lithofacies contains only lithic blocks, that were formed by fragmentation of the underlying NVP lavas. The rounded shape of these blocks may be the result of vent milling processes inside the conduit, where large blocks remaining in the conduit are rounded by collision with other material and the vent walls. The concentration of these blocks in distinct block fields leads to the interpretation that these blocks were finally ejected either by directed blasts or from different vents during excavation of the crater by phreatomagmatic explosions.

The B2 lithofacies is interpreted as the ballistic fraction of phreatomagmatic eruptions. The accumulation of small bombs in horizons within depositional units indicate that these units were formed by separate surges rather than one single surge (Sohn and Chough, 1989). The predominantly juvenile bombs evidence that fine fragmentation of the magma did not occur in all parts of the conduit and their typically rounded shape indicates plastic deformation of the ejected molten magma clasts during flight. The few lithic blocks also have a rounded shape, produced by vent milling.

Modelling of the possible source vents locations for the ballistic ejecta resulted in 3 different vent locations, which can only be roughly estimated. For accurate calculations, however, the ejection velocity has to be known. Nevertheless, changes in the ejection velocity will only influence the approximate distance between the impact sag and the estimated eruption point, but not the direction. Büttner et al. (2002) observed ejection velocities of over 100 m/s during molten fuel coolant experiments and Zimanowski et al. (1997b) found that Pele's hairs were formed if the ejection velocity is in the range of 75 to 100 m/s. Velocities of ca. 100 m/s were also determined be Self et al. (1980) for the ejection of large blocks at Ukinrek maar. Therefore we use 100 m/s as a general velocity for the calculation of the ejection point.

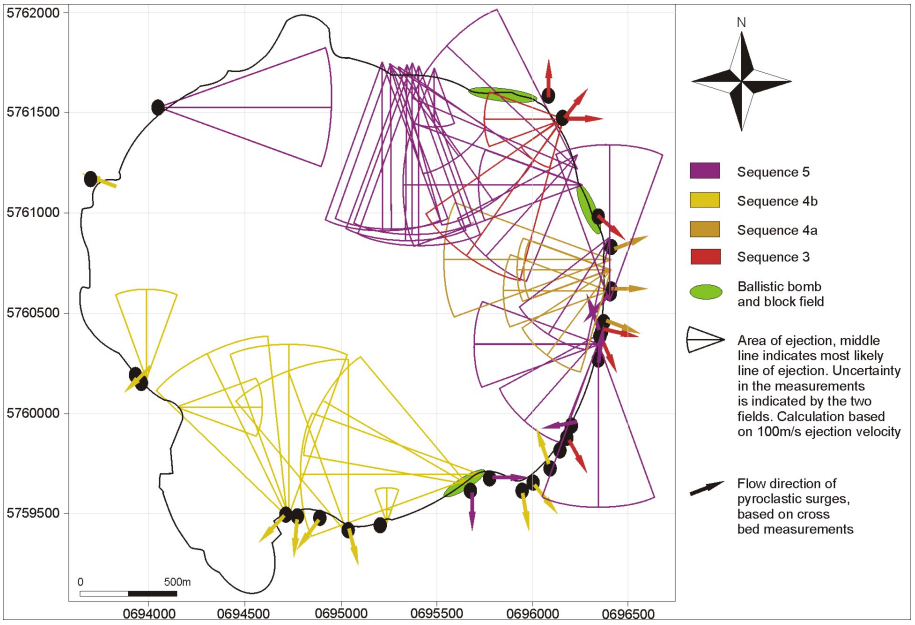

Figure 2.9: Map of the ballistic ejecta distribution and possible source regions. The possible ejection area of each measured ballistic bomb is shown with a sector of a circle, where the middle radius marks the most likely path and the two segments mark the possible error in the measurement of the trajectory direction. The radius is set by the calculated distance using an ejection velocity of 100 m/s.

Figure 2.9 shows a plot of the estimated ejection points with three clusters located, one in the southwest, one in the east and one in the north of the lake. Each cluster is formed by ballistic bombs occurring in the same cluster specific sequence.

2.7.5 Epiclastic, volcanogenic sandy gravel

This lithofacies may have been formed at a lake shore. The dark volcanic clasts of the deposit are reworked juvenile clasts from the maar rim sequence. The smooth surface and the well rounded shape indicate abrasion and rounding by tractional processes caused by waves on the shoreline or by a river. Some of the exotic clasts, such as mudstone fragments and quartz pebbles, indicate some sedimentary input from outside the volcanic system. Small tuff blocks preserved in the moment of breaking of the underlying tuff layers, forming a jigsaw structure, evidence deposition in a relatively calm environment, such as the maar beach shoreline, rather then a river environment. This interpretation is also supported by the large amount of delicate bones.

2.8 Stratigraphic architecture

The maar deposits were divided into five sequences based on the differences in the stratigraphic order of lithofacies, and spatial distribution, and by the occurrence of discordances. Each sequence has a relatively distinctive overall lithofacies character and assemblage that makes them distinguishable in the field (Table 2.2).

Table 2.2: Lithofacies types of each sequence are listed in order of their stratigraphical appearance.

sequences	1	2	3	4a	4b	4c	5
top unit	S1	F4	F4	S2	F3	F2	F4
		F3	L2	L2	F3	F1	L3
		L1	L1	F2	S1	F4	F3
		L2	L1	L2	F3	F1	L1
		L5	L2	F3	S1	F3	F5
		F5	L1	L2	F3		S2
		L5	L1		F4		F2
		F5			F5		L1
		F3					L2
		F5					F4
		F2					F3
							L3
							L4
							F6
							L2
bottom unit							F3

2.8.1 Sequence 1

Sequence 1 occurs only along the southern maar rim below all other sequences, with a single 10 m thick exposure (Figure 2.10). The upper and lower boundaries are not exposed. The sequence consists only of the S1 lithofacies, which generally strikes parallel to the maar rim and dips away from the crater.

2.8.2 Sequence 2

Sequence 2 occurs in the southern maar rim (Figure 2.10), with a minimum observed thickness of 4.5 m in profile A. It contains at least 6 units, varying in lithofacies from fine ash lithofacies to lapilli lithofacies (Table 2.2). The number of units observed in profile A decreases towards profile E and F due to pinching out of single units. The thickness of the remaining units, however, generally increases towards profiles C and E (Figure 2.10). The sequence strikes with a gentle outwards dip along the crater walls and has conformable contacts to the underlying and overlying sequences.

Figure 2.10 *(following page)*: Correlation of the seven stratigraphic logs, showing in detail the Lake Purrumbete pyroclastic succession. The graphic logs are positioned relative to each other on the basis of their stratigraphical position. The correlation of the five sequences throughout the profile is displayed in different colours, whereas the more intense colours indicate the correlation of single units or packages.

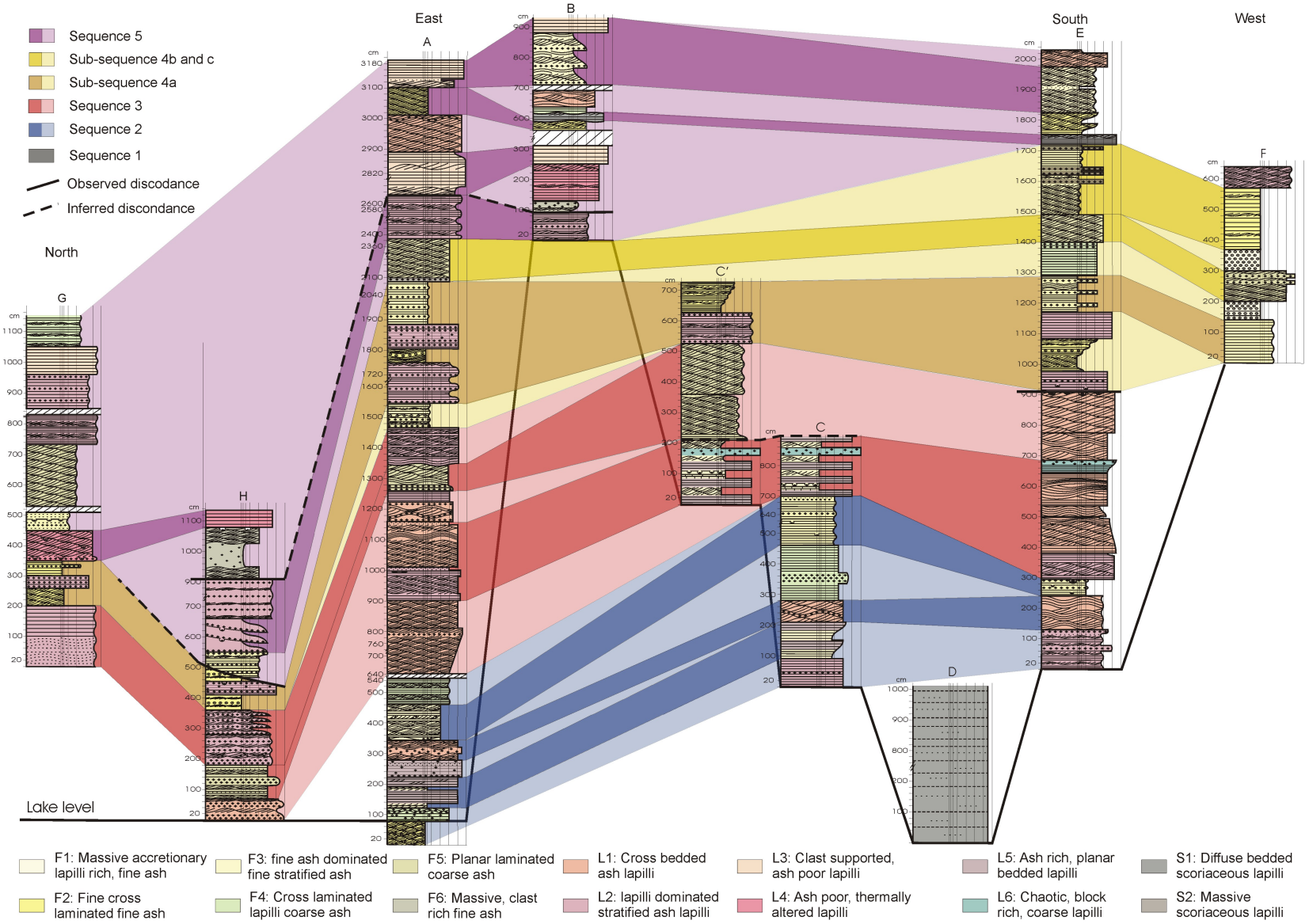
Sequence 5
Sub-sequence 4b and c
Sub-sequence 4a
Sequence 3
Sequence 2
Sequence 1
Observed discodance
Inferred discondance
North
East
South
West
G
H
A
B
C'
C
D
E
F
Lake level
F1: Massive accretionary lapilli rich, fine ash
F2: Fine cross laminated fine ash
F3: fine ash dominated fine stratified ash
F4: Cross laminated lapilli coarse ash
F5: Planar laminated coarse ash
F6: Massive, clast rich fine ash
L1: Cross bedded ash lapilli
L2: lapilli dominated stratified ash lapilli
L3: Clast supported, ash poor lapilli
L4: Ash poor, thermally altered lapilli
L5: Ash rich, planar bedded lapilli
L6: Chaotic, block rich, coarse lapilli
S1: Diffuse bedded scoriaceous lapilli
S2: Massive scoriaceous lapilli

2.8.3 Sequence 3

Sequence 3 occurs in the eastern maar sector, with a maximum thickness of 10 m, exposed in profile A (Figure 2.10). Along the inner crater rim the thickness reaches ca. 5-6 m, but it thins and pinches out towards both the north and south. The sequence is dominated by L1 lithofacies units, interbedded with thin ash horizons, with a unique layer of L6 in the middle of the sequence, which is used as a marker horizon for profile correlations. It also contains ballitstic ejecta of B1, which form one of the block fields in the north, consistent with one of the estimated ejection clusters. Figure 2.10 shows that there are more units in the outer rim profiles A and E, than in the inner rim profile C, where many units are deposited only as thin layers. The general unit thickness in the outer rim ranges from 40 and 200 cm.

The general strike is along the crater rim with an outwards dip, but the sequence is intensely faulted and therefore the orientation can change within micro blocks. Cross bedding measurements at four locations indicate transportation from the north eastern corner of the maar. L2 units in the top part of this sequence are diffuse and planar bedded in the north indicating a more proximal facies type than the cross stratified L2 units further to the south (Sohn and Chough, 1989). The upper contact of the sequence is represented by a discordance, which is only visible at one location in the southern crater rim, while the lower contact is conformable.

2.8.4 Sequence 4

Sequence 4 consists of three subsequences 4a and 4b in the eastern maar sector and subsequence 4c in the western sector. Subsequence 4a at the bottom of the sequence discordantly overlies the older sequences in some parts of the maar rim. It is characterised by interbedding of F3 and L2 lithofacies (Table 2.2) and is <6 m thick (exposed in profile A). In the eastern maar sector sub-sequence 4a is truncated by the discordance to sequence 5 on the inner crater walls, where the maximum exposed thickness is 3 m. To the south, single units pinch out between different profiles (Figure 2.10), whereas to the north, the units change from a more proximal variation of the L2 facies to a more distal variation, indicated by thinning of the deposits and the occurrence of cross stratifications.

The transition to the upper subsequence 4b is gradual. Sub-sequence 4b is characterised by F3 units interbedded with thin scoriaceous S1 and S2 units, forming the vertical walls in the southern maar sector. The maximum thickness of 4.5 m occurs in the south, but it thins to the west and north east and disappears in profile A. The units strike along the crater rim and dip outwards. Displacement of the units along fault lines occurs only in subsequence 4a. However, in the south, a discordance between sequence 4 and the older sequence 3 is exposed. Dip directions measured at this point are to the northwest, indicating deposition on the inner slope of the crater wall. The top of the sequence is truncated by another major discordance to sequence 5.

Subsequence 4c is predominantly formed by fine ash lithofacies, whereby the F1

lithofacies is unique to this sub-sequence (Table 2.2). The sequence is <8 m thick, but pinches and swells. It dips into the ground towards the depressions in the crater walls in the northern and the southern maar sector. This is caused by the lineament cutting through the maar rim parallel to the dip direction.

The majority of the units in subsequence 4a and 4b show cross bed orientations indicating transportation from the eastern maar sector, however, a minority of units in sub-sequence 4b show transportation from the south western corner. B2 ballistic ejecta occur within sub-sequence 4a and their modelled ejection point is located in the east, while the cluster in the west is the modelled ejection point for B2 ballistic ejecta within sub-sequences 4b and c. The block field in the south is formed by B1 ballistics within sub-sequence 4b, which are sourced from the same ejection point as the B2 ballistics.

2.8.5 Sequence 5

Sequence 5 consists predominantly of ash and lapilli lithofacies (Table 2.2). The F6 and L4 lithofacies are unique to sequence 5 and directly overlie the major discordance between sequence 4 and 5 in the south east. In the east they cover a discordance within the bottom part of sequence 5 (Figure 2.10), while the discordance between sequence 4 and 5 is overlain by the basal units of sequence 5. It is characteristic for the thickness of units overlying the discordances to increase on the flat area of the former crater floor, and to thin dramatically on the crater slopes. In the top part of sequence 5 truncated cross beds and small channels indicate erosion by surges. The units in this part are 15-50 cm thick, which is relatively thin compared to units of lower sequences. Cross bedding shows a wide range of flow directions, with some indication for tangential flow along the crater walls.

In the eastern maar sector sequence 5 forms gently inward dipping slopes, overlying discordantly the older sequences and covering most of the pyroclastic succession (Figure 2.11). In both northern and southern maar sectors, sequence 5 lies concordantly on top of sequence 4. But the sequence thins to only 3 m thick in the south, while it is at least 15 m thick in the north.

The base of sequence 5 is formed by the epiclastic, volcanogenic sandy gravel. It is preserved only in a very small area in the east and occurs in two different levels on top of the remnants of the crater walls.

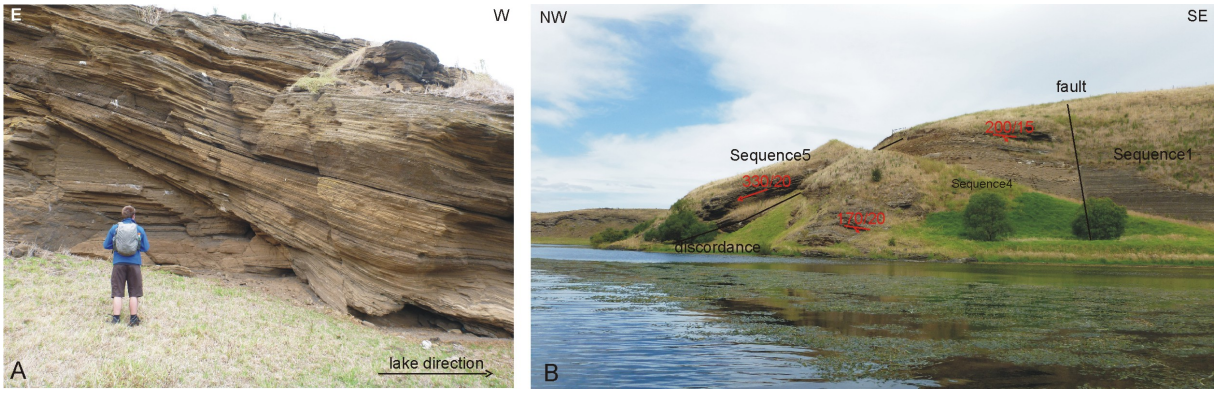

Figure 2.11: A) Discordance between the F6 and L4 units of sequence 5 and the underlying units of sequence 4a. B) View of the discordance between sequence 5 and 4 in the souther maar sector and of the southern part of the ring fault. Units of sequence 5 dip towards the crater (left) while units of the underlying sequences dip steeply away from the crater.

2.9 Interpretation of the volcanology and evolution of the Purrumbete maar, based on the stratigraphic and facies architecture

2.9.1 Sequence 1

Sequence 1 represents the initial vent opening of a transitional magmatic influenced phreatomagmatic eruption. It occurs only in a small area in the south, which may reflect a relatively small eruption and a vent location in the southern maar sector. The thick and uniform S1 lithofacies indicates relatively steady eruption conditions and a phreatomagmatic eruption style with a significant magmatic influence. The predominantly coarse material with a high abundance of relatively highly vesicular clasts shows that fragmentation was less effective than for pure phreatomagmatic eruptions, but ash coated juvenile clasts give evidence for moist conditions in the eruption column (Walker, 1984). The high amount of coarse lapilli sized lithic fragments, both basaltic and marl clasts, is due to explosive excavation of country rock.

2.9.2 Sequence 2

Sequence 2 represents phreatomagmatic eruptions that were controlled by the availability of water and the fracturing of the substrate. The alternation of fine grained lithofacies (F2 and F3) and coarser grained lithofacies (F5 and L5) reflects fluctuations in the effectiveness of the fragmentation, resulting in dry and wet phreatomagmatic eruptions. This sequence only appears in the south eastern maar sector, suggesting that the eruption point was located in close proximity. Because the average grain size is coarser in the east compared with the southern part, the vent was likely closer to the eastern rim than to the southern rim. The very low amount of lapilli sized lithic clasts implies that the eruption took place from the same vent as sequence 1 and the explosion foci did not deepen further.

2.9.3 Sequence 3

Sequence 3 reflects vent migration to the north and dry phreatomagmatic eruptions. Flow directions measured within sequence 3 indicate transportation from the north eastern corner to the south east. Therefore, the thickest part of the deposit is to be expected in the eastern maar sector, which correlates very well with the thickness of sequence 3 observed in profile A (Figure 2.10) and the distribution of the sequence overall (Figure 2.12). The eruption point moved from the south and opened a new vent in the north. This is supported by the large increase of lithic clasts, which again is interpreted as the result of a vent opening event. The high abundance of marl lithic clasts indicates that the explosion level was located within the Gellibrand Marl (Figure 2.8).

The lithofacies and the grain size distribution of sequence 3 reflect predominantly dry phreatomagmatic eruptions and transport of the material by base surges. However, the occurrence of abundant ash coated juvenile clasts indicates the presence of moisture in the eruption column (Walker, 1984). The L6 marker horizon is the deposit of a small pyroclastic flow event, indicating a sudden increase in the volume of ejected material and the eruption intensity. The large amount of marl lithic clasts in this horizon (40 %) is evidence for an increase in the fragmentation of the country rock. This may be the result of magma tapping a water reservoir in the underlying marl, where the sudden availability of a large amount of water caused a sudden increase in the explosive intensity (Aranda-Gomez and Luhr, 1996).

2.9.4 Sequence 4

Sequence 4 represents reactivation of the south vent with phreatomagmatic eruptions that were controlled by the availability of water, and the opening of a new vent to the west with wet phreatomagmatic eruptions. The alternations of wet phreatomagmatic fine ash lithofacies and dry phreatomagmatic lapilli lithofacies may be the result of changes in the availability of water. The fine ash lithofacies reflect most intense magma fragmentation caused by magma/water mixing ratios of 0.3 (Wohletz, 1983, Kokelaar, 1986), whereas the coarse lapilli lithofacies had less water. Based on the measured flow directions, the eruption point was located in the south eastern maar sector. This is supported by the occurrence of a more distal facies to the north and thinning out of units towards the south. It is further supported by the discordance at the bottom of the sequence and the large proportion of lapilli sized marl lithic clasts reflecting excavation of the Gellibrand Marl, consistent with vent migration and deepening of the diatreme.

Sub-sequence 4b differs from sub-sequence 4a in the dominance of F3 lithofacies, indicating changes in the eruption system to a more wet phreatomagmatic, more explosively efficient eruption style. However, intercalated scoriaceous units reflect fluctuations to relatively drier conditions. The change between these two very different lithofacies might be caused by the simultaneous activity of two vents. Evidence for the existence of two vents is given by cross bedding in the south suggesting two different flow directions, one towards the

southeast, and the other to the southwest. This leads to the assumption that a new crater had opened in the western maar sector with predominantly wet phreatomagmatic eruptions. The south crater was active at the same time, and was still alternating between dry and wet eruption styles, although drier conditions prevailed. The general drier conditions of the south vent suggests that this is the source vent of the scoriaceous units. Additionally, the low lithic clast content of the scoriaceous lithofacies is indicative of a more magmatic eruption style.

Although some of the units of sub-sequence 4c do not occur in the southern maar sector, sub-sequence 4c is interpreted as the lee side deposit of sequence 4a and 4b. The majority of pyroclastic flows of subsequence 4b were travelling towards the south east, while in the western maar sector F1 and F2 units were deposited by the same eruption. The few coarser grained units within sub-sequence 4c correlate with units in sub-sequence 4a and b and were formed by surges coming either from the west or the south crater (Figure 2.10). The west crater seems to have been formed on top of the N-S lineament.

2.9.5 Sequence 5

Sequence 5 represents another new eruption phase, after a significant volcanic hiatus, with phreatomagmatic eruptions and vent migration from the south to the north.

The epiclastic, volcanogenic sandy gravel deposit overlying an erosional discordance at the bottom of sequence 5 indicates a volcanic hiatus of unknown duration and the existence of a crater lake. The south crater and probably the north and west crater as well were filled with water. The sandy gravel was deposited at the shoreline of the south crater lake. This deposit occurs at two different levels of the crater walls, which be could either the result of changes in the water level of the lake or subsidence of parts of the crater wall. A volcanic hiatus is further indicated by the hydrothermal alteration of clasts in the L4 lithofacies.

The new phase of activity started out with the reopening and widening of the western part of the south crater and is reflected in the large amount of lapilli sized lithic clasts observed in the field and the large blocks and boulders at the bottom of L4. The occurrence of cuspate glass shards indicate a change to more magmatic eruptions at the end of L4. The deposits discordantly drape the remnants of the earlier parts of the crater wall to the east, indicating that the eruption point was located further to the west. An increase in the eruption intensity is indicated by the ash-rich F6 lithofacies.

Later on, the activity moved again to the north, indicated by the large thickness of ca. 15 m of sequence 5 in the north, compared to the thin deposits preserved in the south and west. The random orientation of the cross bedding in the eastern part may be the result of reflection of the surges off the crater walls.

2.10 Fault lines

Several faults occurred in the eastern crater rim as a result of collapse and crater wall subsidence into the crater. This part of the maar is defined by two fault structures, which are tangential to the crater wall and are interpreted as forming a larger ring fault structure (Figure 2.3). According to Lorenz (1986) and Sohn and Park (2005), ring faults are common in maar volcanoes and are syn-depositional features formed by partial crater wall collapse. The part between these two faults consists of several individual blocks, separated by smaller normal faults. These faults are oriented either parallel or perpendicular to the crater rim. While sequence 1 is cut off by the southern part of the major ring fault, all fault structures occur in sequences 2-4; with some reaching into the lowest units of sequence 5 (Figure 2.12), suggesting that faulting caused by subsidence occurred after the deposition of sequence 4. The extension of some of the faults into the basal units of sequence 5 shows that the movement of the blocks ended during the eruption of this sequence.

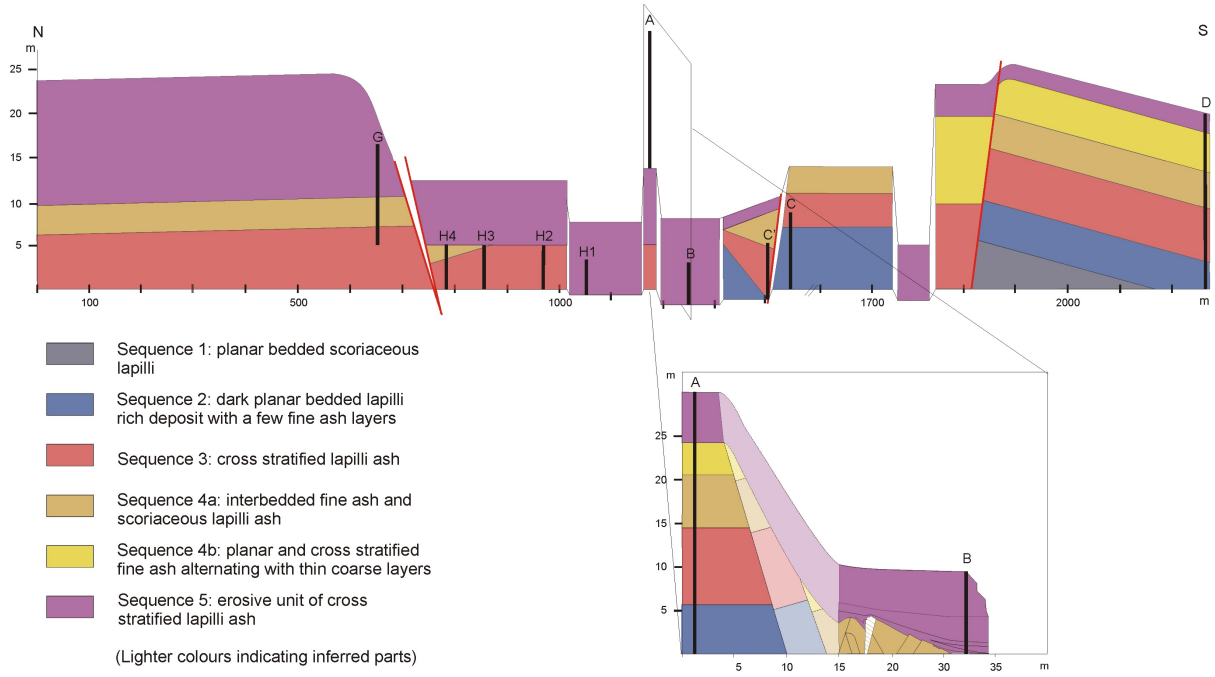

Figure 2.12: Cross section along the eastern crater rim which shows the two major normal faults marked in red. The part in between these two faults is further segmented, but the majority of the faults cannot be displayed in this graphic due to resolution constraints. The large purple blocks between the two faults indicate discordantly inward dipping (towards the reader) units of sequence 5 covering the underlying sequences. Profile A is located in a quarry behind the crest of the rim, indicated by the disappearance of the column, with increased thickness of the sequence near the rim crest. The relationship between profile A and B is shown in the square cross section which is perpendicular to the crater wall. Profile H is a composite profile which is shown by multiple black columns H1-H4. The location of the cross section is marked with a red line in figure 2.3.

The ring fault structure may be the surface expression of the underlying maar diatreme. It forms a half circle, which traces the shape of the estimated south crater, very well.

2.11 Discussion

2.11.1 Dependence of eruption history and aquifer dynamics

Based on the differences in the vent location and the timing of vent migration we divided the eruption of Lake Purrumbete in three main stages: stage 1) start of the eruption in the south crater and vent migration to the north (sequences 1, 2, 3); stage 2) reactivation of the south crater and vent migration to the west (sequence 4); and stage 3) reactivation of the south crater after a significant volcanic hiatus and vent migration to the north (sequence 5).

Eruption stage 1

The first stage started with the opening of the south crater (Figure 2.13A) and very dry phreatomagmatic explosions. The increased amount of marl lithic clasts is evidence that the fragmentation level was within the Gellibrand Marl aquitard. The water for the phreatomagmatic explosions was either provided by interbedded sandy layers in the top part of the Gellibrand Marl (Edwards et al., 1996) or by fractures. The presence of major N-S crustal lineaments indicates that there were at least some fractures in the Gellibrand Marl.

The decrease in the amount of lithic marl clasts in sequence 2 shows that little Gellibrand Marl was further excavated, instead increasing amounts of lithic material from the Black Rock Sandstone, including quartz grains and sandstone fragments, were excavated from the overlying stratigraphy in the south crater (Figure 2.13B). This is a strong indication that the fragmentation level was close to the top of the Gellibrand Marl and not deeper. Excavation of the overlying stratigraphy was caused by widening of the crater due to wall rock collapse, which is a common process in maars, tuff rings and tuff cones (Lorenz, 1986, Houghton and Nairn, 1991, White and McClintock, 2001, Sohn and Park, 2005, Auer et al., 2007). Arcuate faults and sets of normal faults in the maar rim are evidence for this process (Sohn and Park, 2005) and can be observed in the south crater walls. The overlying Black Rock Sandstone is considered one of the major aquifers in the area (Tweed et al., 2009), and was presumably water saturated. In the study of other maars, Houghton and Nairn (1991) and Sohn and Park (2005) proposed that the sudden infill of the crater with water saturated sediment can cause a change to more intense phreatomagmatic eruptions. This could be a reason for the wet phreatomagmatic units in sequence 2. Aranda-Gomez and Luhr (1996) suggested that fracturing of the country rock caused by shock waves of the explosions opens pathways for the groundwater, resulting in increased availability of water, and may cause a change to wet phreatomagmatic eruptions. However, these pathways may become damaged by successive explosions, which again might lead to a drying out of the system. A combination of these two processes may have caused the alternations from dry to wet phreatomagmatic eruptions.

Deposition of sequence 2 ended with a shift of the activity to the north along the N-S

trending fault line (Figure 2.13C). Sohn and Park (2005) described vent migration as the result of clogging of the original vent due to crater wall collapse, which is a plausible explanation for abandonment of the south vent. The occurrence of the B1 lithofacies and increased amounts of marl lithic clast within sequence 3 are evidence again for vent opening and migration (Figure 2.13D). The marl lithic clasts also indicate that the fragmentation level was located within the Gellibrand Marl. However, as mentioned previously, the Gellibrand Marl is an aquitard and only small amounts of water would be available along fractures, causing very dry, magmatic influenced, scoriaceous deposits. Alternations between wet and dry phreatomagmatic explosions may occur if the permeability is enhanced during the eruption. Sequence 3, however, is characterised by sustained dry phreatomagmatic eruptions. White (1996) suggested that sustained phreatomagmatic eruptions result from mixing of magma with sediment laden water, due to the enhanced efficiency of mixing caused by the higher density of the sediment-water mixture. In the case of the north crater, any water was likely mixed with sediment derived from Black Rock Sandstone, as supported by the large amount of ash size sandstone fragments in the deposits (Figure 2.8). The supply of the water saturated sediment must have been larger or more constant than during the eruption of sequence 2, to create sustained phreatomagmatic eruptions. White (1996) and Auer et al. (2007) suggested that water saturated sediment can be liquified by shock waves, causing it to flow into the crater. The result of this process would be lateral widening of the crater. Mixing of material of the Black Rock Sandstone with the magma is reflected by the occurrence of aggregates of quartz grains and single quartz grains inside juvenile clasts observed in thin sections. Recycling of water and pyroclastic material could be another factor causing the sustained eruptions during sequence 3. Volcanic debris and water may stay inside the crater if the explosion is not sufficiently violent to eject material over the crater rim or due to collapse of the eruption column, whereby some volcanic debris and water fall back into the crater, supplying the system with water saturated debris for long lasting phreatomagmatic eruptions (White and McClintock, 2001).

Eruption stage 2

This stage started with the reactivation of the south crater, as indicated by sub-sequence 4a (Figure 2.13D). It is not clear from the depositional record what caused this change. Features, indicating a major hiatus, such as paleosoil horizons or fluvial erosion surfaces are absent. Sub-sequence 4a shows the typical alternating character of the south crater, nevertheless, the interbedded fine ash units are thicker than in sequence 2, indicating that more water was available for a longer period of time. The ring fault and normal faults in the eastern crater wall are evidence for wall rock collapse due to phreatomagmatic explosions, and are characteristic of hard-substrate maars (Lorenz, 1986, Auer et al., 2007). The fragmentation level is therefore inferred to be deeper in the Gellibrand Marl, with alternations of the eruption style being influenced by the opening and closing of water pathways, rather than by short lived crater wall collapse events and incorporation of sediment from the Black Rock Sandstone, as suggested for stage 1. This is supported

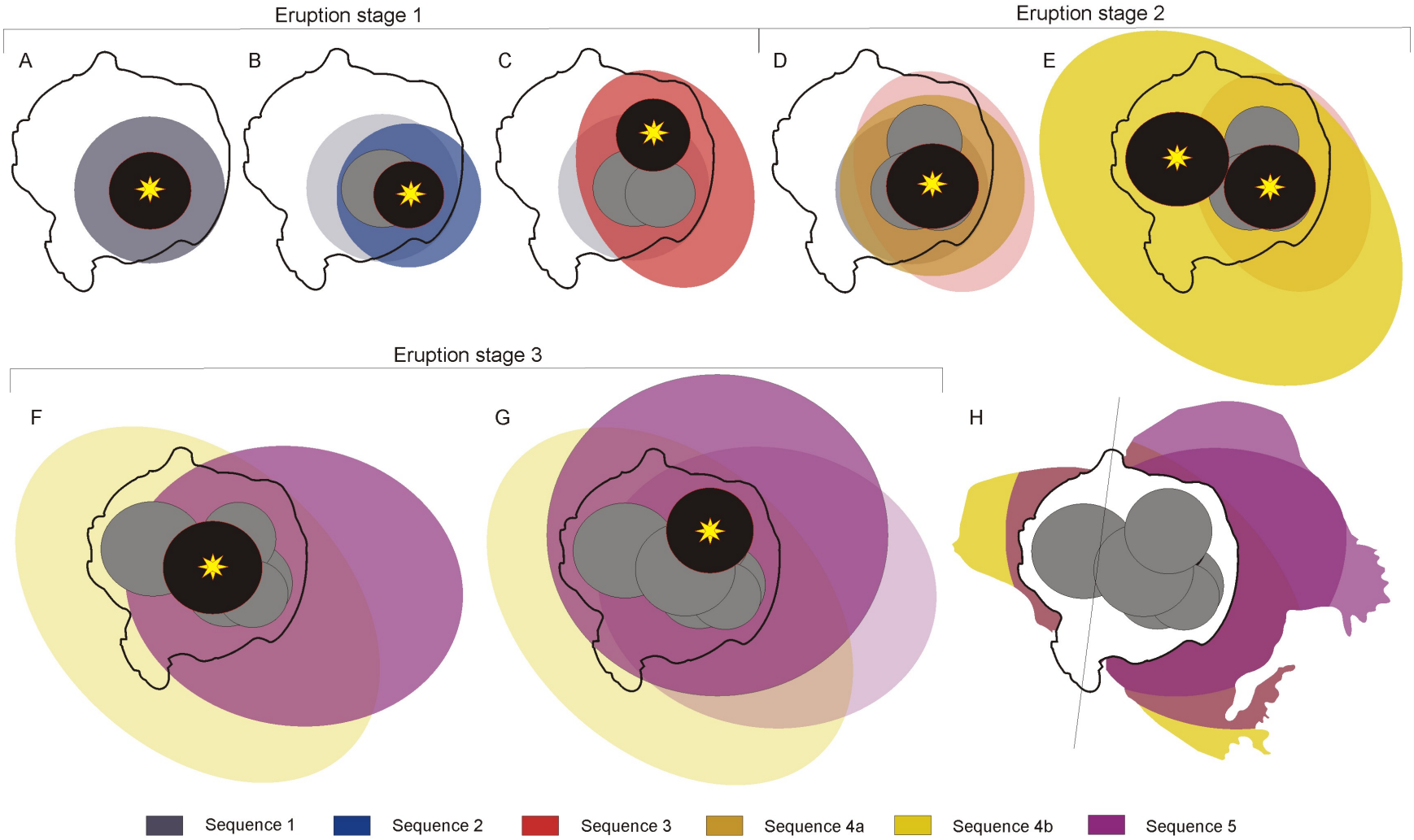

Figure 2.13: The evolution of the Lake Purrumbete Maar: The first stage of the eruption is shown in figures A-C, with the deposition of sequences 1-3. Figures D and E show the second eruption stage with the deposition of sub-sequence 4a (D) and 4b and 4c (E). Eruption stage 3 is shown in figure F and G, with the early phase in the south (F) and later vent migration to the north (G). Figure H shows the current deposit distribution, to the SE it is covered by younger lava flows, while it was eroded away in the N and SW.

by the smaller sandstone fragment abundance in sub-sequence 4a compared to the larger abundance in sequence 2 (Figure 2.8).

The different measured transport directions of base surges in sub-sequence 4b indicate the simultaneous activity of two vents, including the south crater and a newly opened west crater (Figure 2.13E). Opening of a new vent is supported by the B1 lithofacies within sub-sequence 4b and the block and bomb field in the south. While the eruptions of the south crater are characterised by alternating wet and dry phreatomagmatic explosions, activity in the west crater seems to have been predominantly wet phreatomagmatic. This is supported by the very fine grain size of the deposits and the high abundance of accretionary lapilli (Gençalioğlu-Kuşcu et al., 2007). The quite large thickness of the deposits indicate that water was constantly available in large quantities. This is very different to the activity of the north and south crater, where water supply was restricted. The west crater is located on the N-S trending fault line, a topographical lower area, located within the groundwater table, which is reflected by swampy areas to the north and south of the lake. The formation of the epiclastic, volcanogenic sandy pebble deposit in the eastern maar sector and its stratigraphic position 2 m above the recent water table shows that the groundwater table was higher in the Pleistocene. As a result, it is likely that the low area above the N-S fault line was covered with surface water at the time of the eruption of the west crater, also causing wet phreatomagmatic eruptions.

The formation of the epiclastic, volcanogenic deposit in the east also marks the end of the second stage of the eruption and a period of volcanic quiescence. The shape of the pebbles suggests that the length of the volcanic hiatus was sufficiently long to produce well rounded clasts, but too short for the development of any palaeosoil horizons. Using the highest borehole yield of 7.2 l/sec in the Black Rock Sandstone (ANRA, 2002), and the highest amount of rainfall per year (400 mm/year) over the last 120 years (Tweed et al., 2009), it would take 18 years to fill Lake Purrumbete up to its present water level. However, the exact crater size at the end of the second eruption stage is unknown, but it was certainly smaller than the present day crater, therefore the time must have been shorter.

Eruption stage 3

The third eruption stage began again in the south crater but further to the west, as indicated by the inwards dipping units of sequence 5 at the eastern crater rim (Figure 2.13F). As we described before, the occurrence of the L4 lithofacies near the bottom of sequence 5 shows that magma from the earlier stages remained in parts of the conduit, which may have clogged partly the conduit. The faster ascent rate of the magma, indicated by the preserved mantle xenoliths, together with a partly clogged conduit, may explain the presence of F6 lithofacies, where the small volume pyroclastic flow may be the result of a discrete vent clearing vulcanian eruption (Carey and Bursik, 2000).

Afterwards, the vent migrated again further to the north, reflected by the larger thickness of the upper part of sequence 5 in the north (Figure 2.13G). This part of the

sequence is very similar to sequence 3 which was also formed by the activity of the north crater, therefore, the same processes are inferred for this part of the eruption as for sequence 3.

Evolution after the eruption ended

The maar filled up with water after the end of the eruption and a small portion of the deposits were incorporated into the swamps to the south and north of the lake. The crater rim underwent only minor erosion, reflected in the still vertical crater walls, the preserved fault structures and mantling surge deposits. Aggradation due to sediment input was minimal, due to limited water inflow from the surrounding area. The maar deposits were covered to the southeast by lavas from Mt Porndon.

2.11.2 Maar size and subsurface structure

Lake Purrumbete Maar shows features of both maars and tuff rings. Ring faults, such as the ring fault around the south crater, and the occurrence of inward dipping beds, are typical for tuff rings (Aranda-Gomez and Luhr, 1996, Sohn and Park, 2005). The absence of country rock exposure in the crater walls and the shallow present day lake floor at a depth of 45 m are also characteristic for tuff rings (Lorenz, 1986). The shallow depth of the crater is reflected in the relatively low amount of excavated lithic clasts (5 and 20 %), which can be up to 80 % (Lorenz, 1986) in other maar volcanoes. However, the low bedding angles of the pyroclastic deposits and the mainly dry phreatomagmatic character are evidence that Lake Purrumbete is a maar volcano.

Lorenz (1986) suggested in some of his figures that the ratio between crater diameter and diatreme depth is 1:1 in maars. If this is the case, than the diatreme underneath Lake Purrumbete should be 3000 m deep. Assuming that Lake Purrumbete represents a single maar with a 3000 m diameter, half of the diatreme would reach into the Palaeozoic basement, which should occur at 1030 m beneath Purrumbete (Edwards et al., 1996). The absence of any lithic clasts deeper than the Gellibrand Marl support the interpretation of a shallow diatreme structure. Valentine (2012), however, argued that lithic clast from deep stratigraphic levels are not necessarily ejected during the eruption. Phreatomagmatic explosions can occur in different parts of the diatreme, whereas the debris jets of deep explosions transport the material higher into the diatreme infill while the actual eruption column and pyroclastic density currents are generated by shallow phreatomagmatic explosions. Valentine (2012), however, found at least very small amounts of lithic clasts from deep stratigraphic levels at Dry Lake Maar, USA, in contrast to Lake Purrumbete, where no deep lithic clasts were observed. It seems unlikely that during multiple eruption events all deep lithic clasts would stay within the diatreme infill, while only shallow lithic clasts were ejected. The interpretation of the origin of Lake Purrumbete by coalescence of multiple shallow craters, rather than deep excavation of a single large diatreme, presented here based on geological constraints, is consistent with the emerging results of a geophysical

research project on the maar, which also indicates multiple, coalesced, sub-surface craters (J. van den Hove, pers. comm.).

Other authors (Carn, 2000, Cas and Wright, 1987, Gençalioğlu-Kuşcu et al., 2007) suggested that a higher ratio between diameter and depth of a maar volcano is the result of widening of the crater by erosion of the crater walls and therefore reflects the age of the maar. This was observed by Gençalioğlu-Kuşcu et al. (2007) at the Cora maar in Central Anatolia where the crater diameter is 1200 m, twice the size of the sub-surface crater at 615 m. Ukinrek maar in Alaska also demonstrates the rapidity of erosion after 30 years (Pirrung et al., 2008). However, the crater walls at Lake Purrumbete do not show any sign of intensive posteruptive erosion. Instead the preservation of features including blocks half subsided into the crater during the eruption and vertical crater walls, shows that the crater walls are more or less in their original form. Atexcac crater in Mexico also has a large diameter (1150 m) compared to a relatively shallow floor (100 m), but extensive erosion of the crater walls is not reported (Carrasco-Núñez et al., 2007). However, multiple vent migration events were determined by Carrasco-Núñez et al. (2007). This similarity to Lake Purrumbete shows that the shallow depth may be the result of multiple vent migrations, which may not allow the formation of a deep diatreme due to the short time of activity at each location, and the shallow depth of source aquifers.

It would be expected that these multiple vents would cause a multi-lobate shape of the lake, which is in contrast to the circular shape of Lake Purrumbete. However, a slightly lobate shape is observed in the bathymetry data together with a shallower area to the west (Figure 2.3). The circular shape may be the result of the interplay of the active N-S trending fault line and enlargement of the craters by mass flow of water saturated soft sediment into the crater as described by many authors (White and McClintock, 2001, Sohn and Park, 2005, Auer et al., 2007). The lower part of sequence 5 also shows that activity in the single crater was not fixed to the same point, but moved to different areas within the crater, which would cause further enlargement. The cirular shape of the maar is therefore interpreted to be the result of multiple vent locations, multiple events of vent migration and reopening of former vents and enlargement of the crater due to both liquefaction of the soft substrate of the Black Rock Sandstone and wall rock collapse of the hard substrate of the Gellibrand Marl. Furthermore, any lobate structure to the west might have been destroyed by erosion along the N-S trending lineament due to post volcanism activity of the fault line.

2.11.3 Tectonic influence on the magmatic system

The Lake Purrumbete Maar eruption was strongly influenced by the tectonic setting. Magma emplacement occurred in the NVP predominantly along NW-SE Mesozoic-Cenozoic structures (Lesti et al., 2008), therefore it is most likely that the NW-SE fault line at Lake Purrumbete was also the main magma propagation line. The intersection of the Mesozoic fault with the N-S striking Palaeozoic fault structure marked a weakness in

the area which was used by the magma to reach the surface and erupt during the first stage. The opening of the north crater occurred parallel to the N-S Palaeozoic fault line in contrast to the opening of the west crater which was controlled by further propagation of the magma along the NW-SE Mesozoic fault. Son et al. (2012) found that diatreme deepening and vent migration at the Yangpori diatreme were controlled by movement along a fault line. Tectonic activity along either of the two fault lines cannot be ruled out for Lake Purrumbete and may have played a role during vent migration, given that the NVP volcanism occurred while the crust of SE Australia was in compression (Hare and Cas, 2005) and the Otway Basin experienced basin inversion.

The Mesozoic fault line is the predominant subsurface structure in the area. Other volcanic centres, such as Lake Gnotuk, Mount Leura and Mount Sugarloaf to the north-west, and Mount Porndon to the south-east, are located on the same NW-SE structural trend. However, the Wiridgil Hills volcanic centre to the north of Lake Purrumbete is aligned on the N-S Palaeozoic structure, indicating that both trends strongly influenced the location of the volcanic centres. This is in agreement with the general alignment of eruption points along NW-SE Mesozoic-Cenozoic, N-S Paleozoic and E-W Cretaceous structures within the NVP (Lesti et al., 2008).

2.12 Conclusions

- Lake Purrumbete Maar volcano is characterised by a typical maar rim sequence consisting predominantly of dry and wet phreatomagmatic deposits sourced from low density currents and minor interbedded magmatic influenced dry phreatomagmatic scoriaceous deposits.

- The maar crater has a shallow bowl shaped subsurface structure. The large diameter to depth ratio is caused by shallow aquifers and multiple vent migration events.

- Vent migration was mainly caused by clogging of the original vent by wall rock collapse and crater infill, but processes including tectonic activity along the basement structures and a new magma influx may have further influenced vent migration.

- The evidence for at least one volcanic hiatus and reactivation of the system afterwards raises the question if maar volcanoes are strictly monogenetic.

- We showed that each vent has a unique eruption pattern corresponding to characteristic deposits. The eruptions were strongly influenced by the underlying aquifers of the fractured Gellibrand Marl and the porous Black Rock Sandstone.

3

Partial melting and channelised melt transport in the mantle underneath the Newer Volcanics Province, southeastern Australia: Geochemical evidence from the Lake Purrumbete Maar

S.C. Jordan, S.M. Jowitt and R.A.F. Cas

Abstract

The Pleistocene Lake Purrumbete Maar eruption sequence in southeastern Australia records stratigraphic, temporal and geochemical variations that cannot be explained by crustal processes, such as crystal fractionation and crustal contamination. The geochemistry of samples from the Lake Purrumbete Maar have distinct trace element trends that correlate with stratigraphic height, indicating that the most evolved melts were ejected during the earliest eruption stages, with the most primitive melts erupted in the final stages. Variations in La/Sm ratios and Sm concentrations suggest that these melts were formed by partial melting of the mantle, consistent with other volcanic centres within the basaltic cones subprovince of the Newer Volcanics Province. However, the small temporal and volumetric scale of the eruption suggests that partial melting alone is probably not responsible for the changes in the trace element geochemistry observed within the eruption sequence, changes that also cannot be explained by crystal fractionation or crustal contamination. Instead, the data presented here are best explained by a model where melt differentiation occurred during the flow of partial melts through highly porous channels within the mantle, with decreasing incompatible element concentrations from the centre of the channel towards the margins. This suggests that the geochemical variations at Lake Purrumbete and within the

basaltic cones subprovince of the Newer Volcanics Province are the result of channelized melt transport in the mantle, and tapping of different parts of these melt channels by volcano-related conduit systems, with the most evolved melt originating from the interior parts of these channels, and less evolved melts originating from the margins.

3.1 Introduction

Monogenetic volcanoes are generally considered to be formed by small, single, short-lived eruptions (Walker, 1993), with geochemical variations that occur over entire monogenetic volcanic fields, rather than in individual volcanoes. However, recent research on single monogenetic volcanoes has indicated that these variations can also occur within eruption sequences of single monogenetic volcanoes (e.g. Strong and Wolff (2003), Németh et al. (2003), Blondes et al. (2008), Smith et al. (2008), Needham et al. (2011)). Various processes have been used to explain these geochemical variations, with Blondes et al. (2008) explaining continuous geochemical variations for single basaltic eruptions in the Big Pine Volcanic Field, California, using a model involving mixing of magmas derived from different sources. Different mantle sources were also suggested by Strong and Wolff (2003) for the magmas which erupted in the volcanic fields of the southern Cascades, whereas Németh et al. (2003) suggested that geochemical variations observed in the Waipiata volcanic field, New Zealand, were related to the mixing of a basanitic magma with a melt that evolved to tephritic composition in a magma chamber. In addition, geochemical trends observed at monogenetic volcanoes in the Auckland volcanic field, New Zealand, are ascribed by Smith et al. (2008) and Needham et al. (2011) to crystal fractionation during magma ascent.

However, basaltic magmas in intraplate monogenetic volcanic fields are thought to rapidly rise through the crust and are therefore unlikely to be modified by within-crust differentiation processes (Reiners, 2002, Smith et al., 2008). This suggests that the geochemical variations observed in these fields reflect differentiation processes in the mantle rather than crustal processes. Reiners (2002) found that many basaltic systems have similar temporal-compositional trends, that are associated with mantle processes. In addition, Spiegelman and Kelemen (2003) showed that these geochemical variations may be the result of magma transport through highly porous channels in the mantle, and are caused by differences in flow patterns and melting processes, which lead to elevated concentrations of incompatible trace elements in melts transported through the channel centre. Here we present data from the Lake Purrumbete Maar, part of the Newer Volcanics Province (NVP) of southeastern Australia, where geochemical variations suggest that magmas erupted in the study area were formed during the transport of melt through high porosity channels in the mantle.

These interpretations are based on stratigraphic changes in major and trace element concentrations in the pyroclastic Lake Purrumbete Maar sequence. Lake Purrumbete is an ideal field area for geochemical investigations on a maar volcano, with continuous outcrop

and good preservation of the entire pyroclastic sequence, as previously described in detail by Jordan et al. (2013a, chapter 2).

3.2 Geological setting

Lake Purrumbete is located in the basaltic, intraplate NVP, in southeastern Australia (Figure 3.1B), a volcanic province that has been active since the early Pliocene (Price et al., 1997). The youngest eruptions in the NVP occurred arround 5 ka at Mt. Gambier, with recent activity of the NVP evidenced by natural hot springs and mantle derived CO_2 in the region (Lesti et al., 2008). The basaltic products of the NVP cover an area of ca. 25000 km^2, which were erupted from over 440 eruption points (Joyce, 1975). The source for the volcanism in the NVP is still controversial. Early workers suggested that volcanism in the eastern part of Australia was mantle plume-related (Wellman and McDougall, 1974); however, the NVP volcanic centres do not have the systematic temporal and spatial relationships that are indicative of mantle-plume associated magmatism. More recent work suggests that NVP volcanism is related to the break up of Gondwana and rifting between Australia and Antarctica, although volcanism occurred in the NVP ca. 60 Ma after rifting had stopped at the end of the Cretaceous and after a change in the tectonic regime from extension to compression (Hill et al., 1995, Perincek and Cockshell, 1995, Price et al., 1997, Miller et al., 2002). An alternative hypothesis for generation of the NVP is provided by Price et al. (1997), who suggest that asthenospheric mantle diapirs formed during rifting continued to interact with shallow mantle material and are responsible for the NVP volcanism. In addition, Lesti et al. 2008 suggest that NVP volcanism is related to trans-tensional decompression of the lithosphere in locations where the regional southeast-northwest orientated compressional stress field interacts with existing major crustal structures.

Vogel and Keays (1997) divided the NVP basalts into three compositional groups according to geochemistry: the alkaline cones, transitional plains and tholeiitic plains basalts. The most fractionated rocks occur in the tholeiitic plains basalts, with SiO_2 concentrations above 50 wt%. The transitional plains basalts are less fractionated than the tholeiitic plains basalts, and have SiO_2 concentrations less than 50 wt%, with the highly geochemically variable alkaline cones basalts being SiO_2 undersaturated (Vogel and Keays, 1997).

Lake Purrumbete itself is a very large (3 km diameter) maar volcano (Figure 3.1A), that is characterised by multiple vent migration events. The pyroclastic maar sequence consists of lapilli and ash facies and was divided by Jordan et al. (2013a, chapter 2) into six sequences using facies patterns and distributions. These sequences were formed during three main eruption stages, which were determined on the basis of vent location and migration events. The first eruption stage started in the southern part of the maar, with dry magmatic-influenced phreatomagmatic eruptions, as evidenced by scoriaceous lapilli deposits, and with later alternating dry and wet phreatomagmatic eruptions, that formed

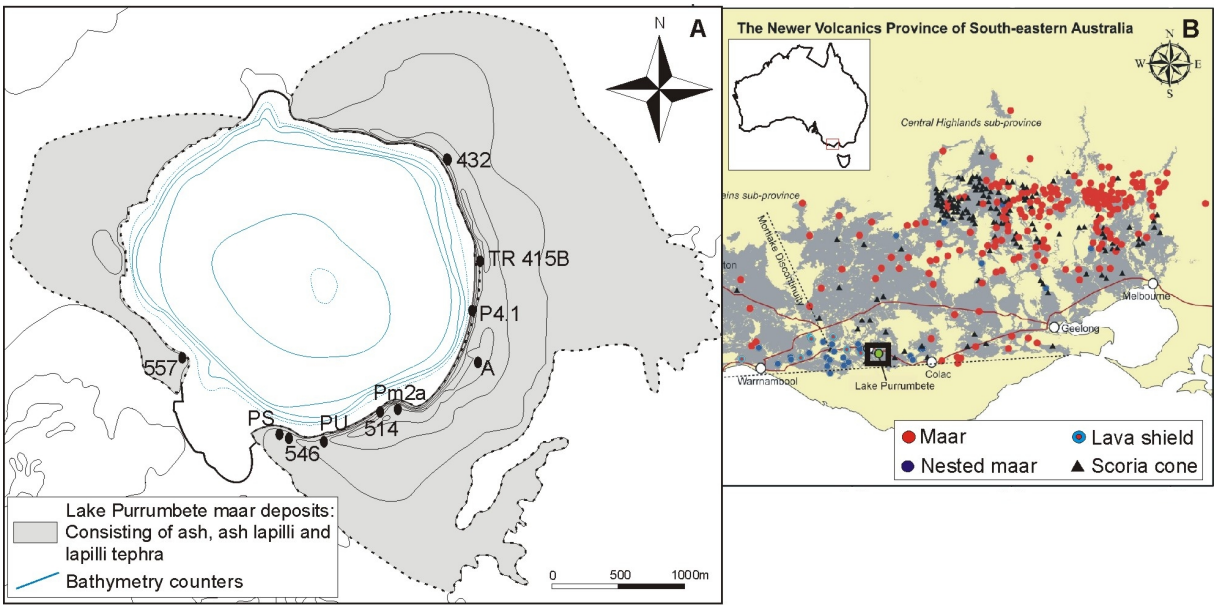

Figure 3.1: A) Lake Purrumbete map with sample locations. B) map of the NVP with the location of Lake Purrumbete Maar.

intercalated lapilli-ash and fine ash units (Jordan et al., 2013a, chapter 2). The first eruption stage ended after vent migration and the opening of a new crater to the north, with sustained dry phreatomagmatic eruptions. The second eruption stage started again in the southern part of the maar with alternating dry and wet phreatomagmatic eruptions, but with a new vent opening to the west and producing consistently wet phreatomagmatic eruptions. The simultaneous activity of both vents is evidenced by the interbedded deposits that were produced by both vents. After the second eruption stage ended the study area underwent a significant volcanic hiatus, indicated by the formation of a crater lake. The last eruption stage began in the southern part of the maar, with relatively violent eruptions shifting over time to the north where it produced dry phreatomagmatic deposits (Jordan et al., 2013a, chapter 2).

3.3 Sampling and analytical techniques

Representative samples were taken from well defined units of the 5 different sequences of the Lake Purrumbete Maar succession. Petrographical studies were conducted on thin sections of juvenile clasts from the samples, with back-scattered electron (BSE) imaging of clasts undertaken to identify chemical zoning within phenocrysts. BSE images were acquired using a JEOL 800 scanning electron microscope at the Monash Centre for Electron Microscopy, using an 8 mm working distance and a 15 kV accelerating voltage.

Prior to whole-rock geochemical analysis, samples were sieved and lapilli sized fresh juvenile clasts separated. Any adhering ash was carefully removed from these clasts by hand using a plastic brush, before further cleaning in an ultrasonic bath. After 1 min in the ultrasonic bath the distilled water was changed and cleaning recommenced until the water surrounding the clasts remained clean, with the wet clasts dried in an oven at 90 °C before

pulverisation in a tungsten carbide mill. Major element concentrations were determined using an aliquot of powder and a Bruker-AXS S4 Pioneer X-ray Fluorescence (XRF) Spectrometer at the Advanced Analytical Centre, James Cook University. Analytical precision and accuracy were assessed using basalt standards. Trace element concentrations were determined using inductively coupled plasma-mass spectrometry (ICP-MS) and a Thermo Finnigan X series II quadrupole instrument at the School of Geosciences, Monash University. Prior to analysis, samples were digested using a low pressure 3-acid digestion method, with initial HF and HNO_3 digestion followed by a later HCL digestion stage. External standardisation of ICP-MS count rates was undertaken using calibration curves based on an in-house basalt standard, with In and Bi used as internal standards, and repeated analysis of dummy standards throughout the analytical session used to correct instrument drift. The precision and accuracy of analysis undertaken during this study is around 5 % for all elements. Loss of ignition (L.O.I.) was determined by ignition prior to XRF analysis with all samples recalculated to anhydrous compositions before interpretation. The original XRF and ICP-MS data are given in Table 3.1.

3.4 Results

3.4.1 Petrography

Juvenile clasts of the Lake Purrumbete samples are dominated by olivine and clinopyroxene with minor K-feldspar in fresh glassy matrices. All crystals are free of zoning or resorption in both transmitted light and BSE images. The crystal content of the juvenile clasts is constant over the entire maar sequence, but the abundance of free feldspar and minor olivine in the pyroclastic material increases in the top part of the maar sequence. Microlites in juvenile clasts consist of plagioclase and minor clinopyroxene, and vary in abundance between single clasts within the same sample.

Juvenile clasts can contain country rock xenoliths, which show only minor resorption. These xenoliths are sandstone fragments comprising angular quartz grains in a carbonaceous clay matrix, are similar to country rock xenoliths within the volcanic deposits and have been interpreted by Jordan et al. (2013a, chapter 2) to originate from the underlying Black Rock Sandstone and sandy layers of the Gellibrand Marl. These xenoliths are also thought to have been included in the magma during mixing and recycling in the maar diatreme. Juvenile clasts containing these country-rock xenoliths also contain other evidence of recycling in the maar diatreme, such as ash coating and alteration of glass matrices. It should be noted that only fresh and clean juvenile clasts were used during geochemical analysis, thereby avoiding contamination of the geochemical data by these recycling processes. Country rock xenoliths from deeper crustal sections are absent in the Lake Purrumbete deposits.

Table 3.1: Geochemistry of samples analysed during this study; samples are in stratigraphical order and are divided into sequences according to the descriptions of Jordan et al. (2013a, chapter 2). Major element concentrations were determined using XRF, whereas trace element concentrations were determined by solution ICP-MS.

Sequence	1	2	2	2	3	3	3	3	3
Sample no.	514	A3	A5	A17	532	432	A6	P4.1	PU
wt%									
SiO_2	46.5	35.15	45.3	46.1	46.6	45.6	45.6	44.4	41.9
TiO_2	2.74	2.13	2.65	2.67	2.74	2.63	2.69	2.73	2.62
Al_2O_3	14	10.9	14.1	14.1	13.9	14.0	13.7	13.4	12.5
Fe_2O_3	12.3	9.59	12.2	12.4	12.3	12.5	12.3	12.3	11.5
MnO	0.16	0.14	0.18	0.17	0.16	0.18	0.16	0.16	0.14
MgO	5.68	4.53	5.4	5.9	5.24	5.67	6.45	6.74	5.9
CaO	7.95	17.77	8.56	7.96	7.69	8.44	8.71	9.04	12.0
Na_2O	4.26	4.2	5.56	4.83	3.46	5.08	4.52	3.81	3.22
K_2O	2.72	2.11	2.91	2.77	2.57	2.75	2.57	2.3	2.25
P_2O_5	1.14	1.32	1.21	1.16	1.12	1.12	1.17	1.16	1.08
SO_3	0.08	0.12	0.09	0.08	0.08	0.07	0.08	0.07	0.09
L.O.I.	2.3	11.12	1.69	1.27	4.08	1.84	1.52	3.81	6.79
Total	99.8	99.07	99.8	99.4	100.0	99.8	99.6	99.9	99.9
ppm									
V	128.33	96.63	120.95	127.35	120.36	126.26	142.70	137.68	125.77
Cr	97.1	63.84	105.31	114.53	80.69	108.62	142.00	136.56	92.11
Co	39.88	30.33	38.3	40.21	38.31	38.91	43.01	42.95	38.72
Ni	92.66	65.58	83.81	102.69	83.7	102.44	118.41	121.42	100.78
Cu	130.6	24.5	31.98	32.1	137.75	30.18	74.37	32.96	104.08
Zn	217.14	135.65	170.81	167.45	222.36	165.46	186.58	148.82	188.45
Ga	26.01	21.36	27.0	26.31	26.11	26.19	25.65	24.06	22.77
Rb	65.59	55.14	69.85	66.93	60.2	66.01	62.9	56.16	54.95
Sr	1375.94	1618.0	1640.59	1515.8	1260.83	1475.99	1411.44	1318.93	1366.26
Y	33.8	28.87	36.99	35.97	32.0	35.37	33.88	30.65	29.66
Zr	508.48	436.32	542.97	516.79	515.36	516.79	463.93	429.75	452.34
Nb	114.09	99.43	106.76	119.74	122.25	118.49	107.18	107.29	102.39
Mo	6.9	7.47	9.22	8.74	5.65	8.78	7.2	5.65	5.3
Sn	3.58	2.87	3.16	3.6	3.57	3.6	3.71	3.23	3.15
Cs	1.11	0.94	1.19	1.15	1.09	1.19	1.27	1.08	0.95
Ba	711.75	617.55	774.81	759.94	740.62	743.12	711.43	655.75	666.17
La	84.93	81.75	103.13	98.75	79.75	96.44	84.42	74.29	73.59
Ce	174.28	155.18	210.13	207.76	152.93	182.44	161.4	143.16	142.41
Pr	18.07	16.8	21.13	20.32	17.18	19.96	17.91	16.11	15.97
Nd	68.37	62.26	78.73	75.82	64.93	74.44	67.77	61.57	60.63
Sm	12.88	11.5	14.55	14.05	12.35	13.81	12.87	11.71	11.59
Eu	3.96	3.53	4.43	4.32	3.8	4.21	3.93	3.6	3.55
Gd	11.1	9.87	12.4	12.07	10.62	11.89	11.07	10.21	10.02
Tb	1.46	1.28	1.62	1.58	1.4	1.55	1.46	1.35	1.31
Dy	7.12	6.21	7.87	7.69	6.83	7.57	7.15	6.56	6.38
Ho	1.17	1.01	1.29	1.26	1.12	1.24	1.18	1.08	1.05
Er	2.69	2.3	2.93	2.89	2.55	2.84	2.71	2.47	2.39
Tm	0.32	0.27	0.34	0.34	0.3	0.33	0.32	0.29	0.28
Yb	1.75	1.5	1.89	1.88	1.68	1.85	1.78	1.65	1.59
Lu	0.23	0.19	0.24	0.24	0.22	0.24	0.23	0.21	0.21
Hf	9.86	8.3	10.36	9.97	9.89	9.92	9.03	8.47	8.33
Ta	6.52	3.91	3.3	6.78	5.1	6.72	6.1	5.03	5.31
Pb	7.05	6.15	7.58	7.41	6.95	7.38	8.65	6.01	6.28
Th	11.33	9.9	12.56	12.09	11.14	12.12	10.69	9.81	9.57
U	2.82	3.42	3.33	3.12	2.6	3.07	2.74	2.4	2.43

Continued on next page

Table 3.1: Geochemistry of samples analysed during this study; samples are in stratigraphical order and are divided into sequences according to the descriptions of Jordan et al. (2013a, chapter 2). Major element concentrations were determined using XRF, whereas trace element concentrations were determined by solution ICP-MS.

Sequence	4	4	4	4	5	5	5	5	5
Sample no.	A13.5a	557	546	PS1	WQ5a	An22	An28	Pm2a	TR415B
wt%									
SiO_2	44.3	46.2	44.3	43.8	46.1	45.2	46.3	45.4	40.6
TiO_2	2.71	2.76	2.76	2.81	2.89	2.84	3.0	2.95	2.53
Al_2O_3	13.3	13.8	13.3	13.3	13.8	13.5	13.9	13.8	12.3
Fe_2O_3	12.1	12.7	12.3	12.4	13.0	12.7	13.2	13.0	11.1
MnO	0.15	0.16	0.17	0.17	0.16	0.16	0.17	0.16	0.14
MgO	6.01	6.69	6.59	7.27	6.99	7.06	6.91	6.96	5.67
CaO	9.17	7.93	9.5	9.76	6.71	8.79	7.46	7.9	13.4
Na_2O	3.51	4.16	3.83	3.86	3.08	3.1	4.26	4.05	3.67
K_2O	2.48	2.34	2.32	2.27	2.4	2.23	2.43	2.51	2.24
P_2O_5	1.18	1.05	1.18	1.29	1.04	1.09	1.15	1.12	1.14
SO_3	0.08	0.07	0.1	0.08	0.07	0.07	0.09	0.09	0.12
L.O.I.	4.72	2.14	3.35	2.79	3.52	2.36	1.07	2.02	6.71
Total	99.7	100.0	99.7	99.8	99.8	99.1	99.9	99.9	99.7
ppm									
V	133.94	148.01	140.83	146.44	148.8	148.9	151.26	146.54	123.11
Cr	106.5	127.9	116.55	151.04	141.64	155.1	140.53	133.24	99.59
Co	40.42	43.64	43.67	45.17	46.74	46.56	47.01	45.71	38.48
Ni	105.23	125.42	122.98	133.68	141.94	135.94	132.43	125.55	99.86
Cu	32.22	33.77	72.39	82.27	37.85	37.99	36.9	37.49	139.32
Zn	149.81	151.8	172.3	178.01	152.55	151.8	158.14	156.64	201.36
Ga	24.22	24.67	24.16	23.9	24.3	24.67	25.52	25.29	22.58
Rb	59.84	55.82	56.47	53.27	59.21	55.29	57.46	58.74	54.4
Sr	1358.73	1267.29	1276.97	1267.29	1321.08	1252.23	1270.52	1355.5	1244.7
Y	30.75	33.33	31.72	32.59	33.54	32.01	33.7	32.2	29.75
Zr	452.03	431.09	431.29	416.82	422.06	409.84	426.88	431.29	410.15
Nb	106.45	95.34	104.01	96.61	98.89	101.84	106.03	97.66	83.36
Mo	5.7	5.89	6.22	5.57	4.83	5.87	6.34	6.32	5.8
Sn	3.3	2.96	3.15	3.06	3.15	3.14	3.11	3.25	2.87
Cs	1.06	1.07	1.02	0.91	0.98	0.91	0.98	1.02	1.03
Ba	686.25	673.98	636.11	688.42	705.24	639.9	741.16	683.21	610.17
La	76.75	81.18	78.49	77.06	81.82	76.67	81.5	79.38	73.18
Ce	150.78	150.35	150.46	145.63	152.82	148.31	157.65	155.82	138.76
Pr	16.64	17.23	16.95	16.63	17.75	16.73	17.7	17.36	15.76
Nd	63.29	65.47	64.37	63.77	67.84	63.84	67.86	66.33	59.91
Sm	12.05	12.5	12.26	12.22	13.01	12.21	13.02	12.62	11.42
Eu	3.69	3.83	3.75	3.77	3.98	3.76	3.98	3.89	3.49
Gd	10.4	10.87	10.6	10.69	11.25	10.58	11.21	10.92	9.87
Tb	1.37	1.43	1.39	1.41	1.47	1.39	1.47	1.43	1.29
Dy	6.63	7.01	6.78	6.87	7.16	6.82	7.16	6.93	6.31
Ho	1.09	1.16	1.12	1.14	1.18	1.12	1.18	1.13	1.03
Er	2.5	2.66	2.55	2.62	2.7	2.56	2.69	2.59	2.37
Tm	0.29	0.32	0.3	0.31	0.32	0.3	0.32	0.3	0.28
Yb	1.64	1.78	1.7	1.72	1.75	1.7	1.77	1.68	1.56
Lu	0.21	0.23	0.22	0.22	0.22	0.22	0.23	0.22	0.2
Hf	8.82	8.5	8.46	8.25	8.36	8.22	8.51	8.55	7.94
Ta	4.02	4.14	4.9	5.5	4.84	3.81	3.71	4.91	2.91
Pb	23.52	6.34	6.13	12.07	6.03	5.87	6.14	5.97	5.91
Th	10.14	10.19	9.87	9.51	9.66	9.37	9.68	9.6	9.32
U	2.49	2.4	2.41	2.35	2.02	2.32	2.37	2.33	2.49

3.4.2 Rock classification

The majority of the samples are classified on a Na_2O+K_2O vs SiO_2 total alkalis versus silica (TAS) diagram (Figure 3.2) as alkaline basanites, with a few samples classified as trachy-basalts. The distribution of these samples is random and there is no compositional relationship between this major element-based classification and the stratigraphic position of the samples.

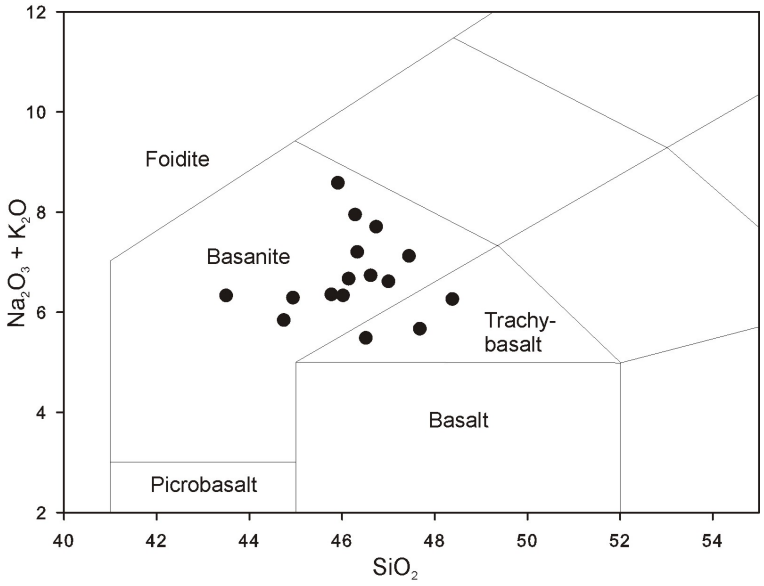

Figure 3.2: Classification of the Lake Purrumbete samples in a TAS diagram (Le Bas et al., 1986).

3.4.3 Major and trace element variations

Highly incompatible elements, such as K_2O and Zr, significantly decrease with increasing stratigraphic height and define distinct geochemical trends within individual eruption stages (Figure 3.3), whereas MgO concentrations increase during the first two eruption stages, but then slightly decrease during the last eruption stage. In comparison, SiO_2 concentrations are relatively constant over the entire sequence, but can be split into three distinct negatively correlating trends with stratigraphic height within single eruption stages. Figure 3.3 also indicates that the most evolved magma was erupted first, with more primitive magmas erupted later in the eruption sequence.

The relatively constant SiO_2 concentrations throughout the stratigraphic sequence mean that the highly incompatible element Zr was used as a monitor of igneous evolution and as a comparator for other major and trace elements. Differentiation trends are evident in a number of trace elements (Figure 3.4), with incompatible elements, including Rb, Sr, Y, Ba, La and Ce, positively correlating with Zr concentrations, whereas compatible elements, such as Ni and Cr, negatively correlate.

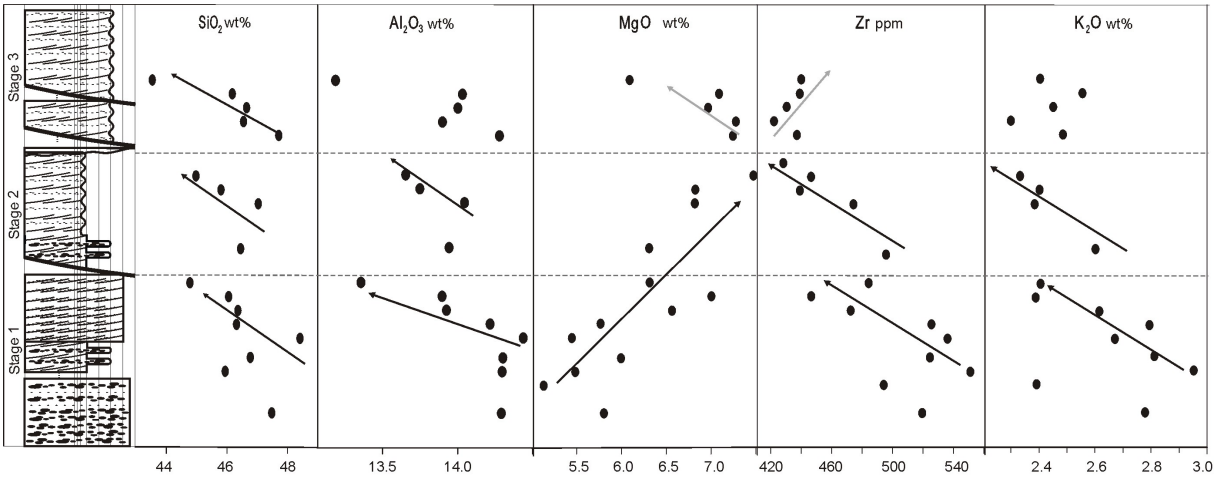

Figure 3.3: Geochemical variations within the stratigraphic sequence. Significant trends are shown by MgO, Zr and K_2O, while the concentration of SiO_2 and Al_2O_3 is relatively constant (stratigraphical column modified after Jordan et al. (2013a, chapter 2)).

3.4.4 Trace element systematics

All samples have near-identical trends in a chondrite-normalised rare earth element (REE) diagram (Figure 3.5; normalised to chondrite values of McDonough and Sun (1995)). All samples are light rare earth element (LREE) enriched with no significant anomalies, although the degree of LREE enrichment varies slightly and correlates with the stratigraphic order of the samples, with samples containing the lowest LREE concentrations being from the bottom part of the pyroclastic succession, and samples from the top of the succession have the highest LREE concentrations. A primitive mantle-normalised trace element spidergram (Figure 3.5) indicates that the Lake Purrumbete samples have uniform trace element distributions and are generally potassium depleted, with these melts having trace element characteristics similar to, but slightly more enriched than, typical ocean island basalts (OIB; Sun and McDonough (1989)) (Figure 3.5).

3.5 Discussion

Different processes, including crustal assimilation, crystal fractionation and partial melting, can control the geochemistry of a batch of magma, such as those observed in the Lake Purrumbete stratigraphic succession. Here, we discuss the influence of each process on the magma and explain why the processes involved in the transportation of partial melts in the mantle are the most likely reason for the observed trends.

3.5.1 Crustal assimilation

One possibility that might explain the geochemical variations at Lake Purrumbete is crustal contamination and the assimilation of crustal material by the magmas during or prior to eruption. All of the Lake Purrumbete samples are slightly SiO_2 undersaturated, with no distinct trend of increasing SiO_2 with evolving melt composition. Assimilation of crustal

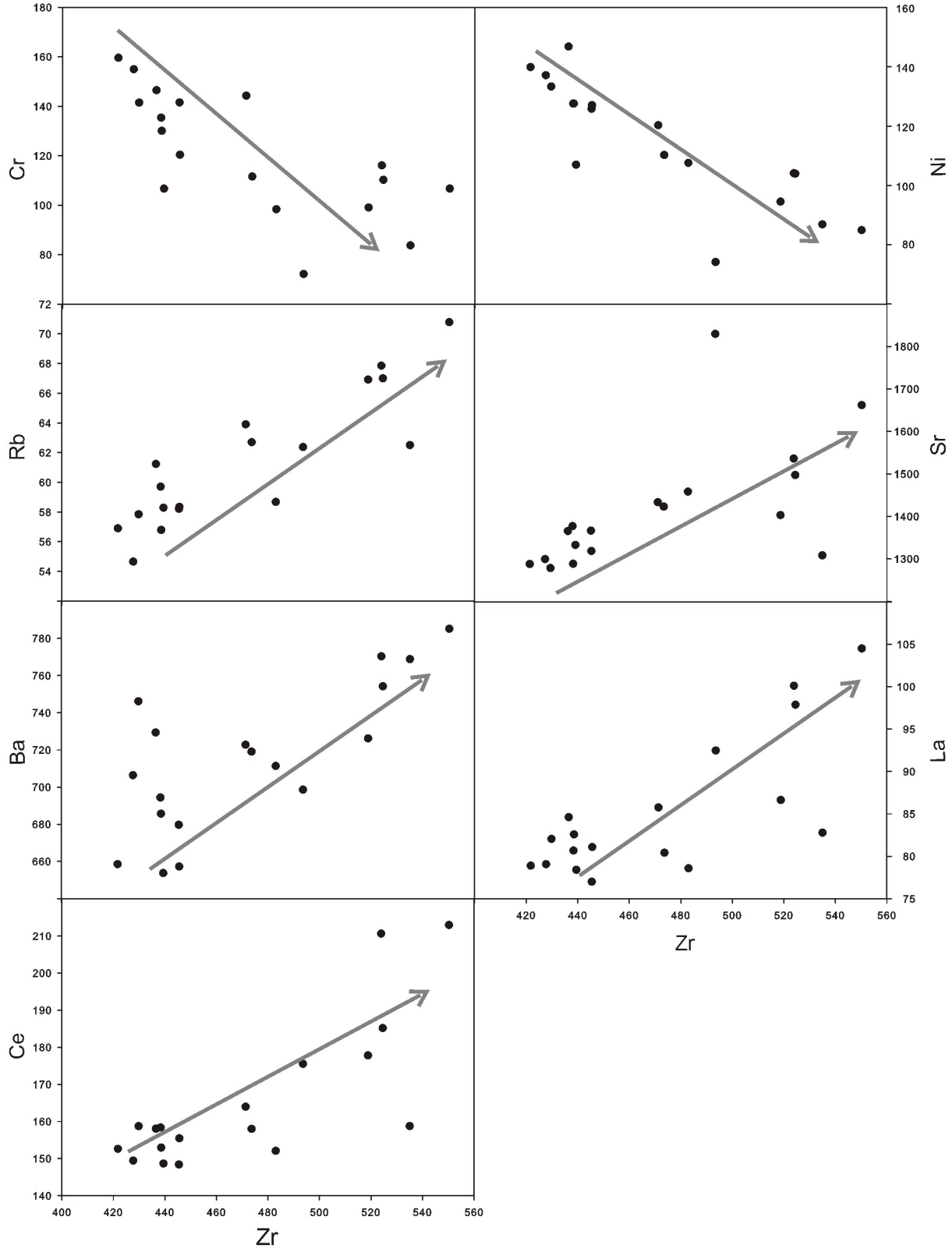

Figure 3.4: Diagram showing geochemical variations of the trace elements compared to the highly incompatible element Zr (values in ppm).

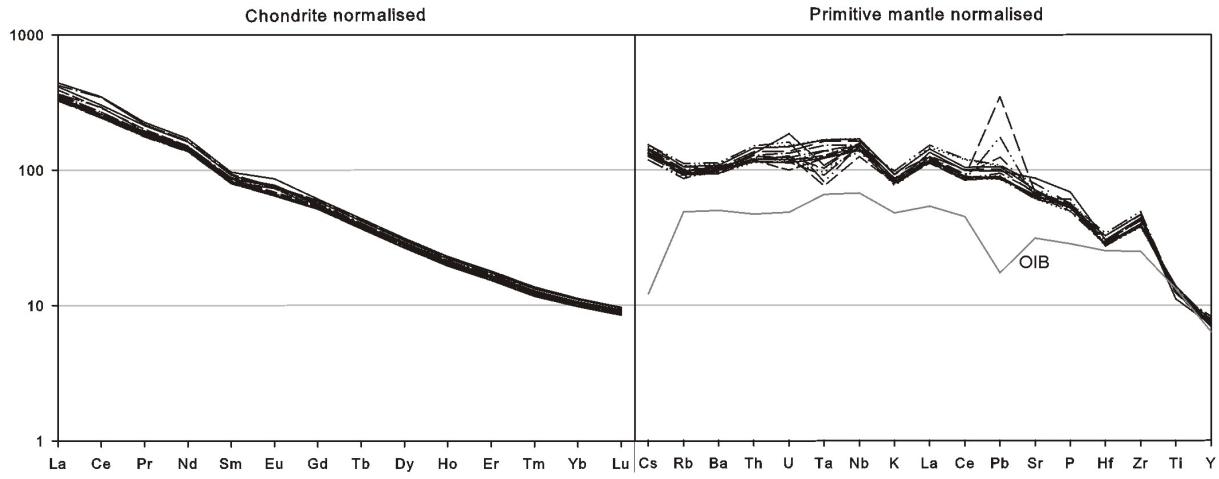

Figure 3.5: Chondrite normalized diagram of the REE indicates all samples were formed by melts of the same source. Mantle normalized diagram of the trace elements shows an OIB signature (OIB values are from Sun and McDonough (1989)). Primitive mantle and chondrite values for normalising of the samples were used from Sun and McDonough (1989) for primitive mantle and McDonough and Sun (1995) for chondrite.

material, however, would mean these primitive magmas would have assimilated more SiO_2-rich material and therefore should have caused an increase in the SiO_2 concentration of these samples. In addition, crustal contamination can be excluded using a Zr/Y vs Nb/Y diagram, with the Lake Purrumbete data plot in the field defined by OIBs associated with recycled components, including EM1, EM2 and HIMU compositions (Condie, 2005), without any evidence of crustal contamination (Figure 3.6). Magmas associated with monogenetic volcanism are thought to ascend quickly from the mantle to the surface, as evidenced by the presence of mantle xenoliths (Reiners, 2002). This means that the potential time for assimilation of crustal material is extremely short, and contamination of the ascending magma is unlikely. However, the presence of country rock xenoliths may indicate crustal contamination, but the country rock xenoliths in juvenile clasts of the Lake Purrumbete samples originate from shallow subsurface rocks and indicate mixing between fragmented country rock and magmas within the maar diatreme (White, 1996, Jordan et al., 2013a, chapter 2), rather than any systematic crustal contamination. This is supported by the only minor amount of resorption textures, reflecting incorporation of the country rock xenoliths into the magma shortly before fragmentation, with little time for the mixture to equilibrate. The absence of any deeper country rock xenoliths indicate that interaction of the melt with surrounding crustal material did not occur prior to eruption.

3.5.2 Crystal fractionation

Crystal fractionation is another process that may have generated the geochemical variations evident in the Lake Purrumbete Maar. Crystal fractionation can occur during the storage of magma in a chamber, but is relatively uncommon in monogenetic volcanism, that involves fast magma ascent directly from the source (Reiners, 2002). However, the existence of a magma chamber has been reported for the Lachersee maar and two other maar volcanoes

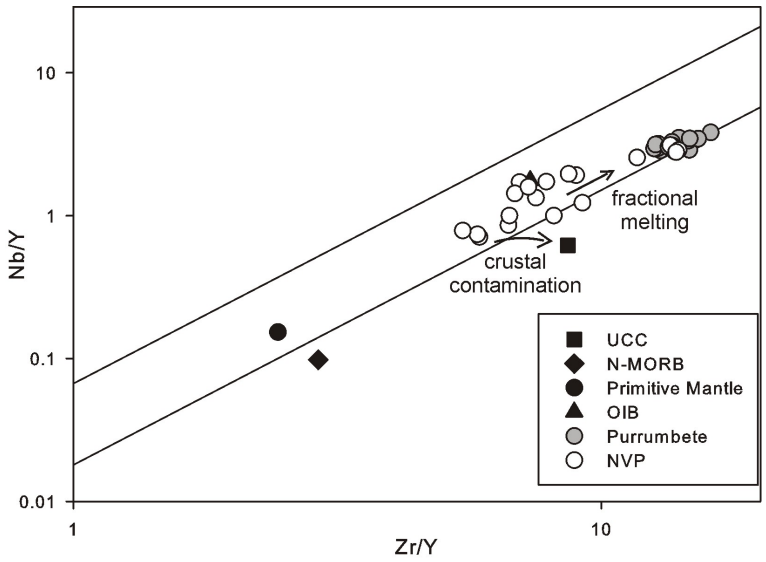

Figure 3.6: Diagram showing partial melting trends and source relationship with OIB of the Purrumbete and NVP samples. The linear trends clearly indicates that crustal contamination of the melts can be excluded as a differentiation process (modified after Fitton et al. (1997), Condie (2005)).

in Germany (Wörner and Schmincke, 1984, Harms et al., 2004). During emptying of a zoned magma chamber, the more evolved material is generally ejected at the beginning of the eruption, consistent with the presence of the most evolved basaltic material at the bottom of the Lake Purrumbete pyroclastic sequence. In addition, the negative correlation of Cr and Ni with Zr may indicate olivine and orthopyroxene fractionation (Ginibre et al., 2004), as further supported by the negative correlation of MgO and Zr.

Crystal growth in a magma chamber typically results in zoned crystals or exsolution features and crystal intergrowths (Ginibre et al., 2004, Ban et al., 2008). However, none of these features were observed in the samples of Lake Purrumbete, indicating that the olivine phenocrysts were in equilibrium with the melt.

Samples of the youngest sequence that contain mantle xenoliths suggest that these melts ascended quickly, as a quick ascent is needed to preserve these mantle xenoliths, indicating that the Lake Purrumbete magmatism did not involve storage in a magma chamber. Needham et al. (2011) suggested that olivine fractionation can occur in the ascending magma column, a process associated with the gravitational sinking of crystals through the magma column, leading to an increase in the number of crystals with depth. As a result, samples with the most primitive melt compositions should contain more crystals than samples with a more evolved melt compositions. In addition, these crystals should show evidence for changes of the melt composition such as zoning or reaction rims, that form as these crystals sink through a melt column with different geochemical composition. However, none of these indicators are present in the Lake Purrumbete pyroclastic sequence, although the youngest sequence contains slightly more crystals than the rest of the pyroclastic sequences. Smith et al. (2008) described a different process of crystal fractionation for the monogenetic Crater Hill volcano, New Zealand, where crystals grew onto dyke walls during magma ascent, removing them from the melt. Crystal

fractionation, however, would produce more distinct major element trends, that were, for example, observed by Smith et al. (2008) in samples from Crater Hill volcano; however, this is clearly not the case for the Lake Purrumbete samples. Furthermore, the majority of samples analysed in this study define a steep trend in a La/Sm vs Sm diagram (Figure 3.7A), a trend that is opposite to the gentler trend that would be produced by crystal fractionation (Pearce et al., 1995). The geochemical variations shown in the Zr/Y vs Nb/Y diagram (Figure 3.6) also cannot be explained by crystal fractionation, given that this diagram is insensitive to low-pressure fractional crystallization (Fitton et al., 1997).

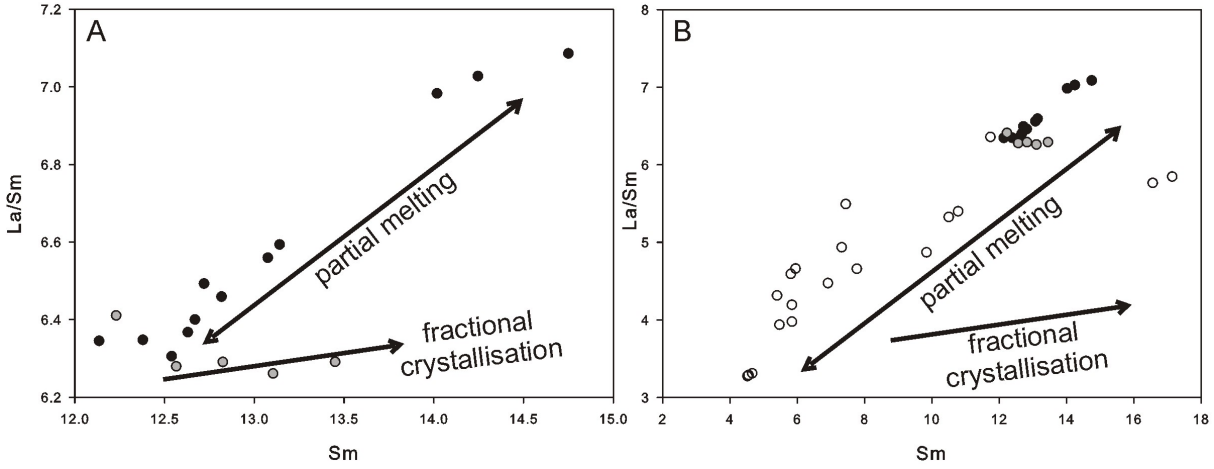

Figure 3.7: La/Sm versus Sm diagrams for the Lake Purrumbete samples (A) and for the rest of the Newer Volcanics Province (B). A) The majority of the Lake Purrumbete samples (black dots) follow a partial melting trend, with only the samples from the youngest sequence (grey dots) preserving evidence of crystal fractionation. B) Lake Purrumbete samples (black and grey dots) plot on the same trend as the NVP cones basalt samples (white dots), indicating a regional partial melting control on magma composition (data from Vogel and Keays (1997), and plots modified after Pearce et al. (1995)).

However, an increase in free crystals is recorded in sequence 5. The majority of the material in sequence 5 is formed from magma that remained in the conduit system after the earlier eruption (Jordan et al., 2013a, chapter 2) and therefore could have been affected by crystal fractionation. This is supported by the fact that these samples plot along a trend suggestive of crystal fractionation in a La/Sm vs Sm diagram (Pearce et al. (1995); Figure 3.7A). The presence of unresorbed mantle xenolith fragments in the same sequence is in contrast with the longer residence times of the magma in the conduit suggested by this crystal fractionation trend. However, this can be explained by transportation of mantle xenoliths in a fresh magma pulse that erupted together with the more crystallised magma, forming the deposits of sequence 5.

3.5.3 Partial melting

Partial melting of a mantle source can also explain the major and trace element variations seen in the Lake Purrumbete samples. The samples define a steep trend a La/Sm vs Sm plot (Figure 3.7), indicative of variations in degree of partial melting (Pearce et al., 1995).

The samples with the highest (La/Sm)/Sm ratios were generated by magmas formed by some of the lowest degrees of partial melting recorded in the NVP and are located at the bottom of the stratigraphic sequence, whereas samples with the lowest (La/Sm)/Sm ratios, indicative of higher degrees of partial melting, are found at the top of the stratigraphic sequence. This is supported by variations in incompatible elements, with low degree partial melts at the bottom of the sequence having higher concentrations of incompatible elements, such as Zr (Figure 3.4) than the higher degree partial melts at the top of the sequence. Comparison of the Lake Purrumbete samples with (La/Sm)/Sm ratios of other NVP cones basalts (Vogel and Keays, 1997) also highlights a regional partial melting trend, with the Lake Purrumbete samples formed from magmas derived from lower degree partial melting than any of the NVP samples that were analysed by Vogel and Keays (1997). This relationship is also evident in Figure 3.7B, where Lake Purrumbete samples plot on the same trend lines as alkaline cones basalt samples. These trends were interpreted by Vogel and Keays (1997) to be the result of partial melting of an enriched mantle source, with crystal fractionation control being ruled out by the existence of mantle xenoliths within many volcanic deposits. Frey et al. (1978), Zou and Zindler (1996), Vogel and Keays (1997) all showed that the alkali cones basalts were derived from 3-10 % partial melting of fertile peridotite mantle material, with Frey et al. (1978) calculating that the magmas at Mt Leura and Mt Porndon, volcanic edifices in the vicinity of Lake Purrumbete that lie on the same structural trend, were formed by between 6 and 6.5 % partial melting of the mantle. The samples of these two volcanoes again plot on the same partial melting trend as the Lake Purrumbete samples (Figure 3.7B). This evidence of a partial melting of a region of enriched OIB-type mantle is also supported by the Zr/Y vs Nb/Y diagram (Condie, 2005, Fitton, 2007), where the Lake Purrumbete samples plot along the same trend as other samples of the NVP and within an OIB and enriched OIB field. This indicates either melting of an enriched region within the mantle (Fitton, 2007) or partial melting of a extremely small volume of mantle material (Fitton et al., 1997). The trend of the NVP samples within the Zr/Y vs Nb/Y diagram is similar to trends of samples associated with rifting of the North Sea and other continental rift systems (Fitton, 2007), in agreement with the tectonic history of the Otway Basin. The NVP and Lake Prurrumbete samples, as well as samples of other rift systems, plot within the mantle plume field defined by the two straight lines on a Zr/Y vs Nb/Y diagram (Fitton et al., 1997, Fitton, 2007) suggesting that NVP magmatism did involve some mantle plume influence.

3.5.4 Differentiation by channelised mantle flow

Channelised flow of melt through the mantle can create geochemical variations similar to partial melting and may be an answer to the question of how partial melting trends can occur in a volcanic sequence produced in a very short time frame.

Monogenetic volcanoes are formed by small and relatively short lived eruptions (Walker, 1993). Three eruption phases are recorded for Lake Purrumbete, but only one significant

time break was observed between the second and third eruption phase (Jordan et al., 2013a, chapter 2). In each eruption sequence, melt compositions change from most evolved at the beginning to the least evolved at the end of the sequence, changes that cannot be explained by crystal fractionation. The magma supply was constant at least during the first two eruption phases and over a relatively short time scale. As discussed above, the geochemical variations in samples from Lake Purrumbete are indicative of variable degrees of partial melting, strongly suggesting that these melts had to be undergoing constant extraction and removal from a region of mantle melting to preserve these variations formed in the mantle Strong and Wolff (2003). The geochemistry of these samples also suggests that these extracted melts ascended quickly and directly to the surface without mixing with each other or undergoing significant differentiation by assimilation of crustal material or crystal fractionation. Extraction of the melt can occur along channels in the mantle, where channelised flow along porous melt channels can cause extreme chemical variations in small areas (Spiegelman and Kelemen, 2003, Blondes et al., 2008). These chemical variations are recorded in trace element compositions, predominantly in the incompatible elements, whereas major element concentrations are generally unaffected by this process (Spiegelman and Kelemen, 2003). This can effectively explain why the majority of the major element concentrations of the Purrumbete samples are invariant, although the distinct SiO_2 and Al_2O_3 trends can be explained by this model. Spiegelman and Kelemen (2003) suggested that melts react with mantle peridotites, dissolving pyroxenes and precipitating small amounts of olivine. This process may be responsible for the distinct trends of increasing SiO_2 and Al_2O_3 concentrations within single eruption stages, while MgO concentrations change only slightly and more constant over the whole eruption sequence.

Melt transport along high porosity channels in the mantle can also explain geochemical variations in the NVP cones basalts. In a region of mantle with multiple high porosity channels, similar geochemical variations would form in each individual channel, forming an overall trend similar to that expected for melting of mantle material at differing degrees of partial melting (Spiegelman and Kelemen, 2003). Each volcano may have tapped different channels, or sections of individual channels, resulting in significantly different chemical compositions. The fast ascent of these magmas through the crust, typical for monogentic volcanism, may be one reason whereby these geochemical variations that originally formed in the mantle are preserved within the NVP.

3.5.5 Model of magma generation for Lake Purrumbete

The Lake Purrumbete magma was produced by partial melting of the mantle, with melts extracted from the source via high porosity channels. In these channels, the melting of pyroxenes and the precipitation of a very small amount of olivine caused changes in the geochemistry of the melt, predominantly by concentrating incompatible trace elements (Spiegelman and Kelemen, 2003). After the melt left the mantle, ascent through the crust was fast, with the magma unable to assimilate significant amounts of crustal material

or undergo extensive crystal fractionation. Each sequence started with the ejection of the most evolved magma, and a progressive change towards more primitive compositions, indicating that this volcanic conduit system most likely tapped the interior section of a high porosity melt channel during the first part of each eruption stage (Spiegelman and Kelemen, 2003). Jordan et al. (2013a, chapter 2) suggest that a pause in eruption between sequence 4 and 5 led to melt ponding somewhere in the conduit system. This is evidenced by the weak crystal fractionation trend the samples from the bottom part of sequence 5 define in a (La/Sm)/Sm diagram. These trends may be caused by crystal fractionation of the melt within the conduit system, also reflected by the increasing trend of Zr in the upper-most samples (Figure 3.3). Reinitiation of the eruption was caused by the arrival of fresh melt that transported mantle xenoliths (Jordan et al., 2013a, chapter 2).

3.6 Conclusions

- The geochemistry of samples from the Lake Purrumbete Maar indicate that the maar formed in an eruption sequence where most evolved melt was erupted first and the most primitive melt was ejected last.
- The observed trace element variations cannot be explained by assimilation of crustal material, primarily as all samples from Lake Purrumbete have relative constant SiO_2 concentrations. In addition, observed trends in (La/Sm)/Sm ratios cannot be generated by crystal fractionation. It is likely that partial melting of a fertile mantle generated the magmas that formed the Lake Purrumbete Maar, although it should be noted that partial melting is a long process compared to the very short-lived eruption of this single monogenetic volcano.
- Melt extraction via high porosity channels in the mantle (Spiegelman and Kelemen, 2003) can explain the distinctive geochemical variations evident at Lake Purrumbete.
- These variations were preserved by fast ascent of the magma through the crust, reducing the time for further differentiation by assimilation of crustal material and/or crystal fractionation.
- The magma remaining in the conduit system was modified by crystal fractionation during quiescence, with subsequent ejection together with fresh melt from the mantle, as indicated by the presence of mantle xenolith fragments.

4

Multi-stage vesicle nucleation in the conduit system of a large maar volcano, Lake Purrumbete Maar, southeastern Australia

S.C. Jordan, P.C. Hayman and R.A.F. Cas

Abstract

The Pleistocene Lake Purrumbete Maar, southeastern Australia, at 3 km diameter, is one of the largest maar volcanoes on Earth. The pyroclastic sequence records multiple changes in the eruption style from wet phreatomagmatic, to dry phreatomagmatic and magmatic influenced dry phreatomagmatic. We used analysis of Bubble number densities and Bubble size distributions to investigate processes in the conduit which were driving the eruption of this large maar volcano. The new data presented in this paper indicates changes in the magma ascent rate prior to fragmentation and two distinct nucleation events, which is supported by vesicle textures observed using transmitted light and back-scattered secondary electron images. The first nucleation event is characterised by nucleation of a small number of vesicles deep in the conduit and low magma ascent rates. The high bubble number densities between $1.79\text{x}10^{7}$ mm−3 and $9.04\text{x}10^{9}$ mm−3 are formed by small vesicles nucleated in the second event near the fragmentation level. These values are in the range of bubble number densities observed in basaltic Plinian eruptions, indicating fast magma ascent in the shallow conduit. Changes of the bubble number densities throughout the sequence further indicate increase of the primary magma ascent rate during the eruption, which is supported by the occurrence of mantle xenolith fragments in the youngest deposits, and their rarity in the oldest deposits. The analysis, presented here, show that magma ascent was influenced by multiple processes in different levels of the conduit and that vesiculation was arrested by phreatomagmatic magma/water interaction. The results highlight the complexity within the plumbing system of maar volcanoes.

4.1 Introduction

Conduit processes can be investigated using vesicles preserved in pyroclasts (Toramaru, 2006, Polacci et al., 2009). Bubble number densities (BND) and bubble size distributions (BSD) have been determined in many studies for basaltic eruptions to investigate fragmentation processes and magma ascent dynamics (Mangan and Cashman, 1996, Shimano and Nakada, 2006, Polacci et al., 2009). Further investigations on BND and the shape of the BSD curve have been undertaken using experimental and numerical methods (Toramaru, 1991, Blower et al., 2002, Toramaru et al., 2008), while nucleation and growth rate of vesicles have been calculated from BNDs by Mangan and Cashman (1996). However, only little work on vesicle textures in phreatomagmatic pyroclasts has been done so far (Tsukui and Suzuki, 1995, Mattsson, 2010, Murtagh et al., 2011) and studies of vesicle characteristics of phreatomagmatic deposits of maar volcanoes have been published to our knowledge only one by Ross and White (2012).

Phreatomagmatic deposits are typically described as poorly vesicular, which is considered to be the result of fragmentation by magma/water interaction prior to optimum magma vesiculation is being achieved (White and Ross (2011), Ross and White (2012) and references therein). However, Jordan et al. (2013a, chapter 2) showed that the fragmentation level of phreatomagmatic eruptions at Lake Purrumbete Maar, southeastern Australia was very shallow, near the surface. It can be assumed that melt vesiculation was already well advanced at this level within the conduit and vesicle textures are preserved in the pyroclasts. Furthermore, variations in the eruption style from wet phreatomagmatic, to dry phreatomagmatic and magmatic influenced dry phreatomagmatic, are recorded in the pyroclastic sequence of the maar, which give a great opportunity to investigate vesicle textures, BND values and BSD's for different eruption styles formed by the same plumbing system.

4.2 Geological setting and deposit characteristics

Lake Purrumbete Maar is part of the intraplate basaltic Newer Volcanics Province (NVP) in southeastern Australia (Figure 4.1). The NVP overlies the Palaeozoic basement of the Lachlan and Delamerian fold belts in the north and the sedimentary succession of the Cainocoic Otway Basin in the south, formed during the break up of Australia and Antarctica in the Cretaceous (Hare and Cas, 2005). An area of over 25000 km^2 is covered by the volcanic products of over 400 eruption points (Joyce, 1975, Vogel and Keays, 1997, Hare and Cas, 2005). Volcanism began in the NVP in the early Pliocene in a predominantly intracontinental setting that was subject to a regional compressional tectonic stress field (Perincek and Cockshell, 1995, Hare and Cas, 2005).

Many of the volcanoes in the NVP show multiple alternations in the eruption style, from magmatic to wet phreatomagmatic. The ca. 50 ka years old Lake Purrumbete Maar has a diameter of 3 km and is one of the largest maars in the province. The stratigraphy

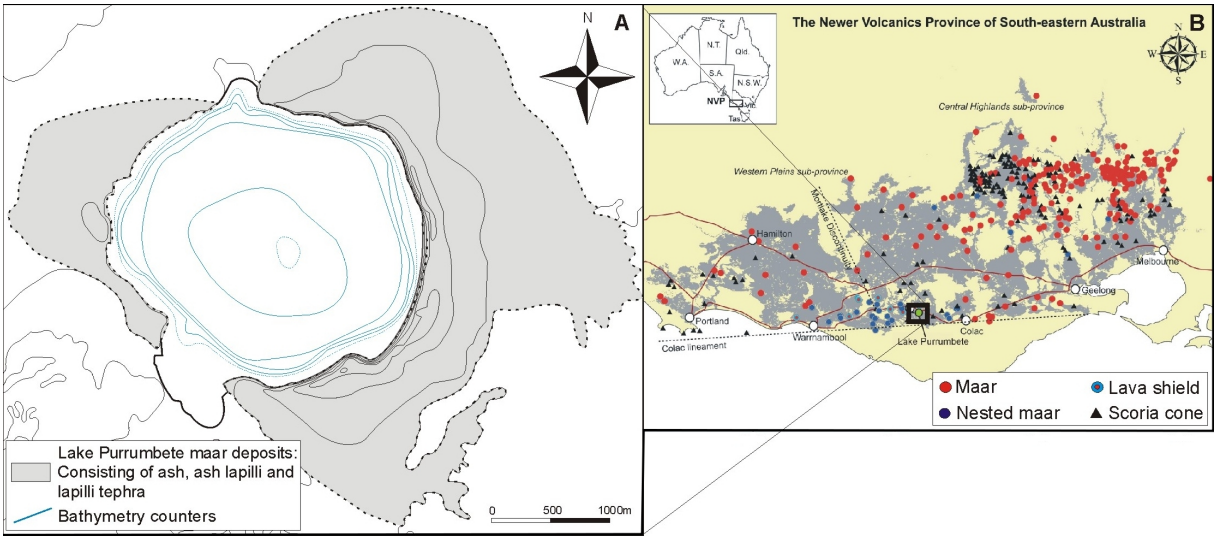

Figure 4.1: A)Topography of the Lake Purrumbete Maar volcano and the distribution of the pyroclastic maar deposits. B) Overview map of the NVP, showing the location of Purrumbete maar (modified after Cas and van Otterloo (2011)).

of the pyroclastic maar rim succession, described by Jordan et al. (2013a, chapter 2), is divided into five litho-stratigraphic sequences, interpreted as partly erupted from three different vent locations (Figure 4.2). The sequences consists of different facies types ranging from magmatic influenced scoriaceous lapilli deposits over dry phreatomagmatic ash lapilli and coarse ash deposits to wet phreatomagmatic fine ash deposits (Figure 4.3). The order of the different facies types appears to be random with no obvious trend of drying out or becoming more wet.

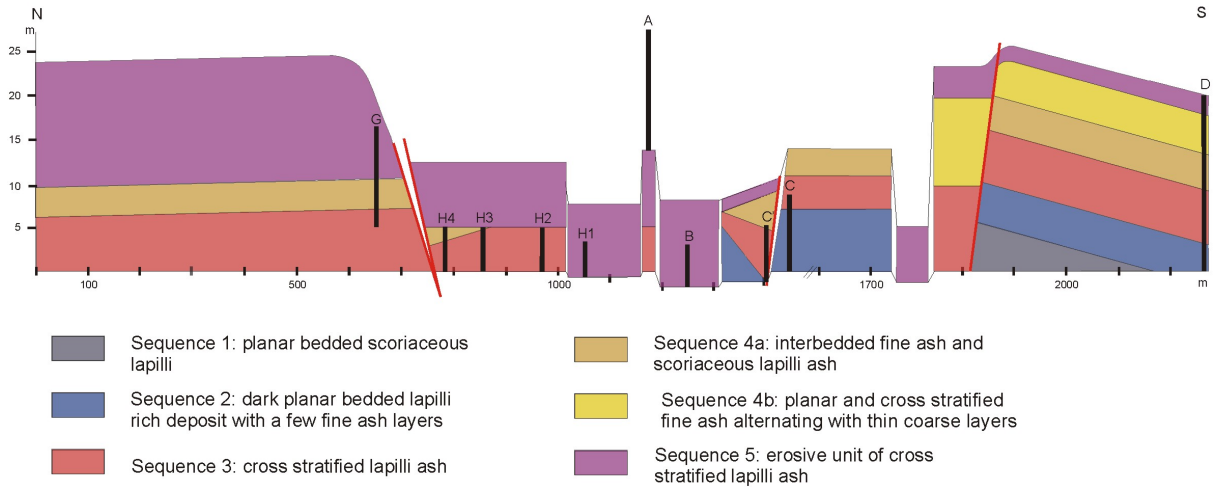

Figure 4.2: Cross section of the Lake Purrumbete pyroclastic sequence along the eastern crater rim (modified after Jordan et al. (2013a, chapter 2)).

The eruption started out in the southeastern corner of Lake Purrumbete with magmatic influenced dry phreatomagmatic eruptions forming scoriaceous lapilli deposits (Figure 4.4). The eruption changed later to alternating dry and wet phreatomagmatic eruptions forming interbedded lapilli-ash and fine ash deposits. Afterwards activity migrated to the north forming a thick sequence of dry phreatomagmatic lapilli deposits. A new

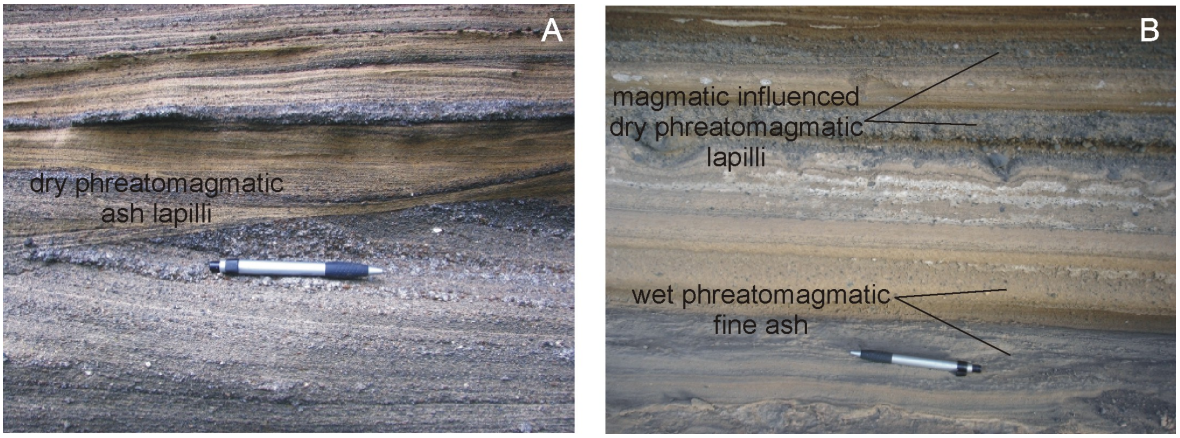

Figure 4.3: Outcrop characteristics of the three main facies types at Lake Purrumbete. A) Cross bedding in dry phreatomagmatic ash lapilli. B) Wet phreatomagmatic fine ash with intercalated layers of magmatic influenced dry phreatomagmatic lapilli.

migration to the southern vent produced another sequence of interbedded fine ash with both magmatic influenced scoriaceous lapilli and dry phreatomagmatic lapilli-ash deposits which is intersected to the south west with a thick deposit of fine ash produced simultaneously at a third vent in the west. After the eruption of the west crater, the volcanic activity underwent a significant hiatus, before the youngest eruptive phase started out again at the southern vent with the formation of very dry phreatomagmatic deposits and some pyroclastic flow events. Activity, however, shifted to the northern vent shortly after the eruption started, producing a thick deposit of dry phreatomagmatic lapilli deposits in the north (Jordan et al., 2013a, chapter 2).

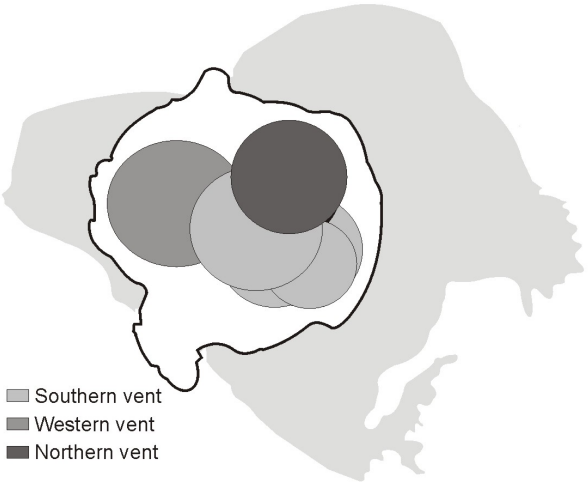

Figure 4.4: Vent locations during the eruption of Lake Purrumbete described by Jordan et al. (2013a, chapter 2).

4.3 Methods

To evaluate vesicle characteristics in the major lithofacies, vesicle sizes and abundances were determined for pyroclasts of different sizes and fifteen samples.

The grain size of the pyroclastic deposits at Lake Purrumbete varies between fine ash and coarse lapilli. Clasts in the lapilli size range are typical for the magmatic influenced scoriaceous lapilli deposits and the dry phreatomagmatic lapilli-ash deposits, with particles smaller than <125 μm being characteristic for wet phreatomagmatic fine ash deposits (Zimanowski et al., 1997b, Büttner et al., 2002). Larger juvenile clasts are very rare in these fine ash deposits and may be cognate, rather then autochthonous juvenile clasts, and are thus not suitable for analysis. Due to the small size of the fine ash particles, vesicles in the erupting magma that were larger than the clast itself will be lost from the record and will be missed in the analysis of vesicle characteristics. To be able to compare these fine clasts with the larger clasts of the coarse deposits we chose two different size classes (-1.5 ϕ>clast>-1 ϕ and 0.5 ϕ>clast>1 ϕ) for the analysis of the coarse samples.

Vesicles in larger clasts may be the result of on-going post-fragmentation vesiculation in the interior of the pyroclast, while the clast is still hot. The distribution of these vesicles within the clasts should be uneven due to no post-fragmentation vesiculation within the chilled margins of the clasts. To avoid the analysis of these vesicles only clasts were used which have an even vesicle distribution from the margin towards the middle and cuspate margins, indicating that bubbles existed prior to fragmentation. The relatively small grain size of the lapilli was also chosen to avoid the effects of post-fragmentation vesiculation because small clasts are chilled at the time of phreatomagmatic magma/water interaction.

Recycling of ejected material, falling back into the crater, is common in maar volcanoes (White, 1996) and is indicate by different degrees of ash coating of the clasts (Houghton and Smith, 1993). It should be noted that only fresh, not altered and not ash-coated juvenile clasts were used for the vesicle analysis (Appendix 6).

Ten clasts per size class and sample were analysed, using transmitted light images for the -1 ϕ size class and Backscattered Electron Microscope (BSE) images for the 1 ϕ size class. BSE images were conducted at the Monash University Centre for Electron Microscopy using a JEOL 800 scanning electron microscope with, 8 mm working distance, 15 kV acceleration voltage and a probe current of 1x10^{-9} A. Images were converted into binary black and white images using the computer program Gimp2. Due to a lack of contrast in the grey scale images, vesicles had to be outlined and filled manually using the software Gimp2. Afterwards size and shape parameters were calculated by using the computer program ImageJ 11. Using transmitted light microscopy, vesicles smaller than the diameter of the thin section will be projected to the surface. Analysing these vesicles will result in a too large number per area of small vesicles. The lower limit for the vesicle analysis of thin sections was therefore set to 700 μm^2, equivalent to a vesicle diameter of 30 μm, to secure analysis of vesicles larger then the diameter of the thin section. The smallest vesicles analysed with BSE methods are 0.3 μm in diameter. For

each run ImageJ produces an image of the outlines of all analysed objects, that was used for comparison with the original image to detect and correct errors in the analysis. In addition, analytical precision and accuracy were determined by assessing the size of seven vesicles of different size classes 10 times. The standard deviation determined in this test is 1-4 %, with a higher standard deviation of 9 % for the smallest vesicle class. Using the computer program CSDCorrections 1.39 by Higgins (2000) the 2D data set was converted into a 3 dimensional size distribution and corrected of the cut-section effect on the basis of the volume calculations described in detail by Higgins (2002, 2006). Binning of the data was done according to Higgins (2000) using logarithmic size bins and 5 bins per logarithmic decade. Bubble number densities (BND) were also calculated by CSDCorrections, representing the number of vesicles (N) per melt area (A_n) in a clast, divided by the mean diameter of the vesicles (D)(Equation 4.1).

$$BND = \frac{(N/A_n)}{D} \tag{4.1}$$

It should be noted that the very small size of the juvenile clasts and their tendency to float in water prevent makes using conventional density measurement techniques impossible. This in turn makes determination of vesicularity using immersion density methods difficult.

4.4 Results

The results for BND and BSD are similar for the three main lithofacies at Lake Purrumbete and are presented in Table 4.1 and graphically shown in Figure 4.7. The vesicularities of the different analysed samples differ a lot between single clasts of the same sample, ranging from 2 to 70 %. The highest values are shown by scoriaceous lapilli and clast supported lapilli ash deposits, with a maximum vesicularity of 40 % in clasts of fine ash deposits (Table 4.1). Based on the vesicularity of the clasts, different clast types were identified: highly vesicular (>50 %), moderately vesicular (50-25 %), slightly vesicular (<25 %) and glass shards (0 %).

Highly vesicular clasts occur as both ash particles and lapilli clasts and are typically angular to subrounded. The highly vesicular clasts have ragged margins and polylobate vesicles indicating bubble coalescence (Figure 4.5 and 4.6). Very small round vesicles occur in the spaces between the larger bubbles.

Both ash and lapilli size fraction contain moderately and slightly vesicular clasts with only a few imprints of burst bubbles on the margins. Some clasts show an uneven distribution of vesicles, but systematic variations, such as decreasing vesicle abundances towards clast rims, were not observed. Large vesicles can be connected and can have polylobate shapes, both of which are signs of bubble coalescence. Smaller vesicles, however, are isolated and typically round in shape. Elongation of vesicles is also a common feature and can affect the whole vesicle population of a single clast or only parts of it.

Glass shards occur typically only in the ash fraction and are the remains of the melt

Table 4.1: BND values and vesicularities listed for the different clast sizes and samples. Samples are listed in stratigraphical order.

BSE image derived				
Sample	eruption style	size range	BND	vesicularity
An28	dry phreatomagmatic	1 ϕ	1.14x10^8	2-43 %
BA	dry phreatomagmatic	1 ϕ	5.03x10^7	4-50 %
BA	dry phreatomagmatic	-1 ϕ	6.61x10^7	3-36 %
WQ5a	dry phreatomagmatic	-1 ϕ	3.32x10^7	10-37 %
PS1	magmatic influenced	1 ϕ	1.55x10^8	4-30 %
PS1	magmatic influenced	-1 ϕ	1.02x10^8	11-47 %
F2.1	wet phreatomagmatic	<3 ϕ	1.79x10^7	4-40 %
A20	wet phreatomagmatic	<3 ϕ	1.96x10^8	1-40 %
A6	dry phreatomagmatic	1 ϕ	2.48x10^8	4-67 %
532	magmatic influenced	1 ϕ	1.64x10^8	15-70 %
A2	dry phreatomagmatic	1 ϕ	1.07x10^8	4-33 %
A1	wet phreatomagmatic	<3 ϕ	5.56x10^9	6-40 %
514	magmatic influenced	1 ϕ	4.59x10^9	9-50 %
514	magmatic influenced	-1 ϕ	9.04x10^9	6-51 %
Micrograph derived				
An28	dry phreatomagmatic	-1 ϕ	9.64x10^2	8-46 %
An22	dry phreatomagmatic	-1 ϕ	7.06x10^2	12-28 %
F1.2	magmatic influenced	-1 ϕ	8.73x10^2	5-42 %
A6	dry phreatomagmatic	-1 ϕ	4.9x10^2	6-32 %
An15	dry phreatomagmatic	-1 ϕ	4.84x10^2	6-20 %
A14	dry phreatomagmatic	-1 ϕ	6.88x10^2	4-50 %
A2	dry phreatomagmatic	-1 ϕ	6.47x10^2	5-40 %

between larger vesicles. The imprints of these bubbles are still visible in the shape of the clasts, indicating that the magma has been vesiculated prior to fragmentation. Due to their very small size and thickness, no vesicles are enclosed within the clast margins and therefore these clasts are not suitable for vesicle analysis.

The BNDs of coarse samples analysed in micrographs are in the range of 4.84x10^2 mm^{-3} to 9.64x10^2 mm^{-3}, while the BNDs of samples analysed in BSE images range between 1.8x10^7 mm^{-3} to 5.6x10^9 mm^{-3} that is, 4 to 7 orders of magnitude higher (Table 4.1). The BND values are similar for the three deposit types of wet phreatomagmatic, dry phreatomagmatic and magmatic influenced dry phreatomagmatic. But a decreasing trend occurs in the BND values from 4.6-5.6x10^9 mm^{-3} to 3-6.6x10^7 mm^{-3} with increasing stratigraphic height, which does not correspond with a distinct transition in the lithofacies types. Samples with the lowest BND number, except of sample F2.1, contain pieces of mantle xenoliths.

The plot of the whole data set in a BSD diagram shows that the two data sets derived from both BSE and trasmitted light images fit very well together forming a curved BSD curve. The very steep part of the curve on the very small vesicle size end of the curve is formed by the BSE data set, while the very gentle slope towards the larger vesicle sizes is

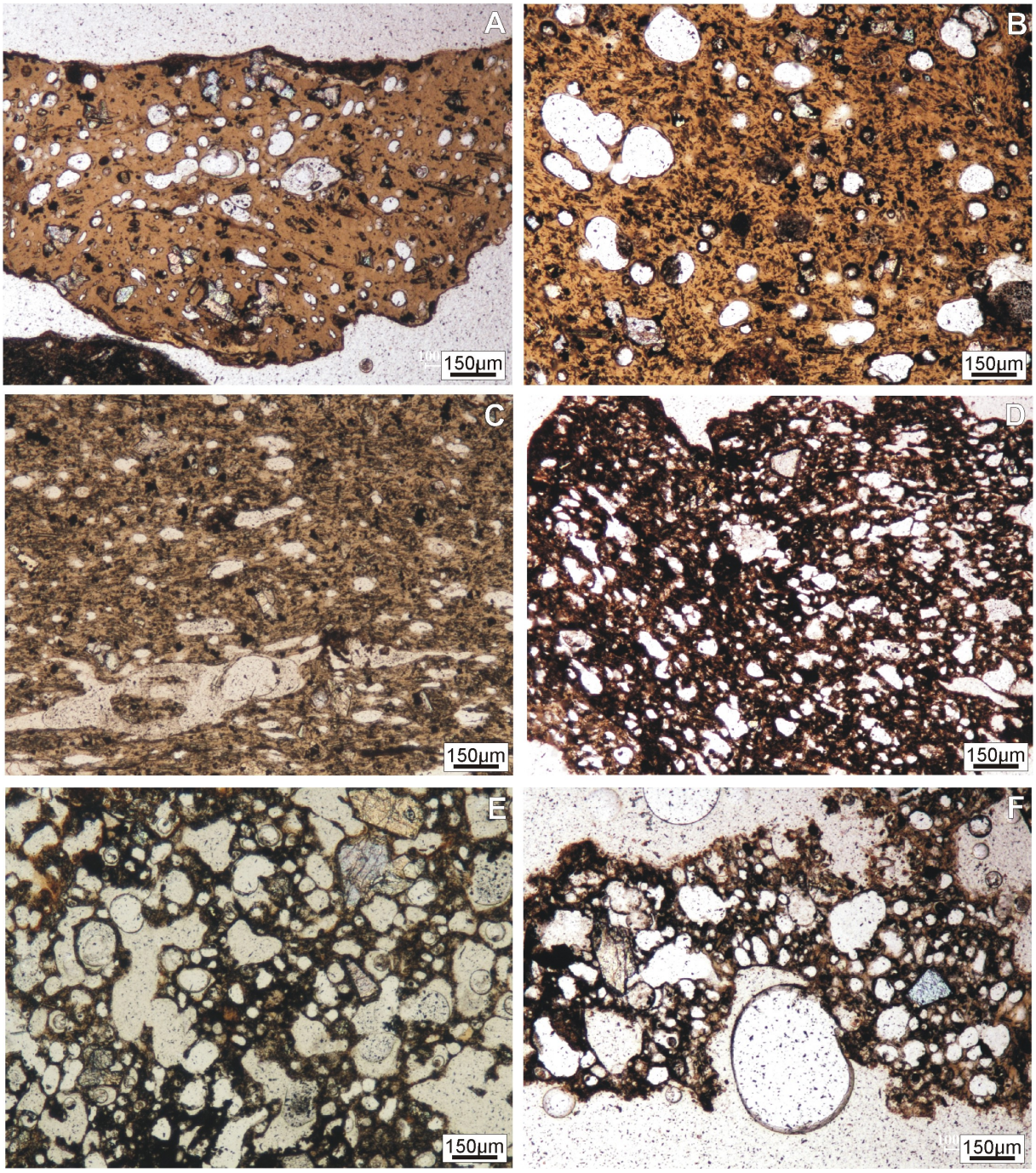

Figure 4.5: A)-F) micrographs of juvenile clasts from lapilli ash and scoriaceous lapilli deposits in the size range of 1 ϕ. A)-C) show slightly vesicular clasts with different textures such as round and lobate vesicles in A) and B) and stretched vesicles in C). Image D) shows a moderately vesicular clast, while highly vesicular clasts are depicted in image E)-F). Bubbles with irregular shape and connected bubbles indicating bubble coalescence occur in all images.

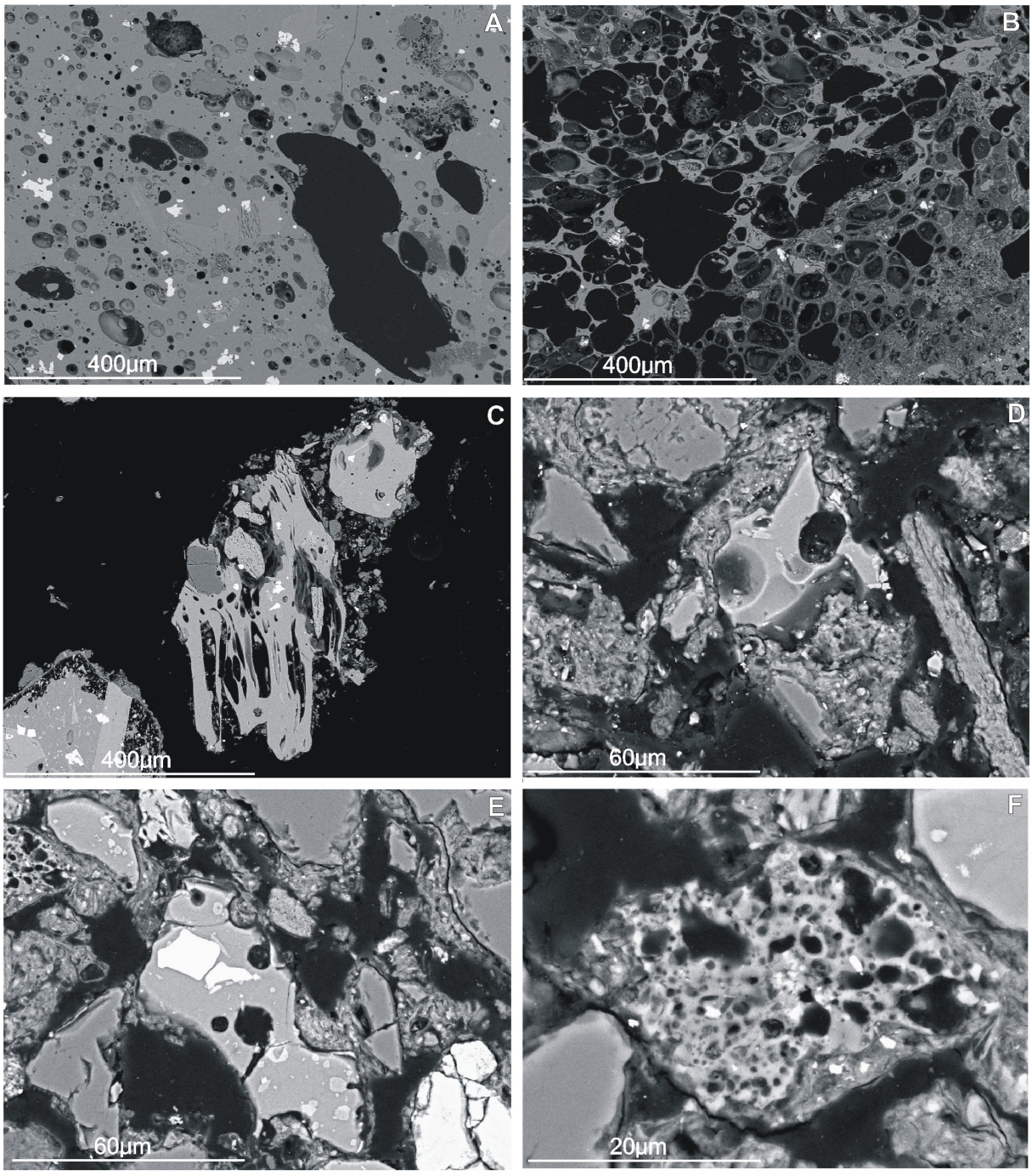

Figure 4.6: A)-C) BSE images of juvenile ash particles of lapilli-ash and scoriaceous lapilli deposits, with A) representing slightly vesicular clasts and B) representing highly vesicular clasts. D)-F) BSE images of fine ash particles indicating highly vesicular melts.

formed by the data set derived from transmitted light microscopy (Figure 4.7).

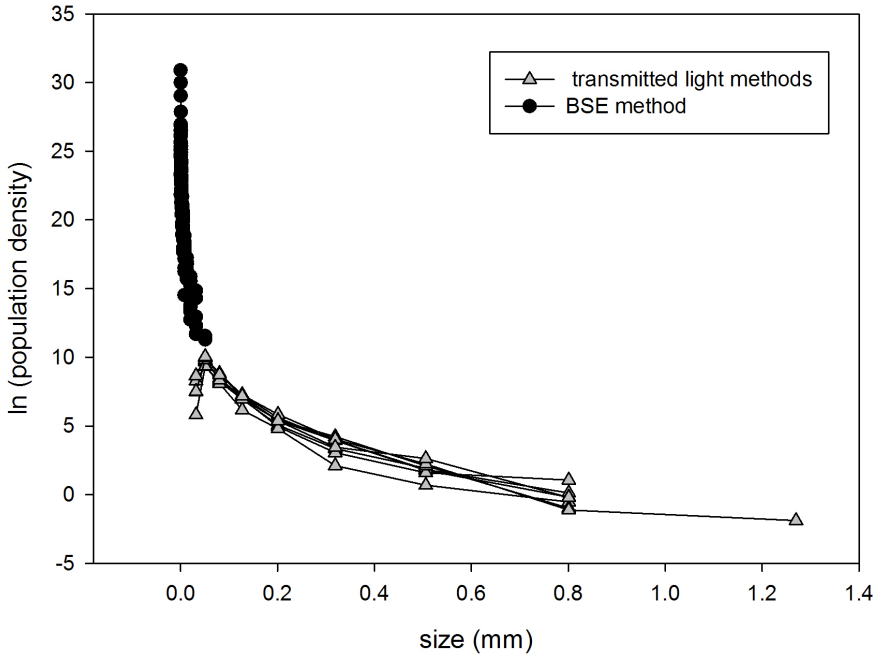

Figure 4.7: BSD of the Lake Purrumbete magma. The steep part of the BSD is formed by very small vesicles observed by BSE imaging while the part with a gentle slope is formed by larger vesicles observed with transmitted light microscopy in lapilli clast.

4.5 Discussion

4.5.1 BND variations between clast sizes

The results of the BND calculations show that there are large variations between the BND values derived by the two different methods. BND values of $4.84\text{x}10^2\,\text{mm}^{-3}$ to $9.64\text{x}10^2\,\text{mm}^{-3}$ (see Table 4.1) calculated from thin section analysis are in the range of BND values found in other studies of phreatomagmatic deposits (Murtagh et al., 2011, Ross and White, 2012). Those previous studies, however, neglect very small vesicle sizes. The BSD diagrams of the Lake Purrumbete samples show that a vast majority of the vesicles are in the very small size range of $<10\,\mu$m. Ross and White (2012) suggest that high BND values are formed by large numbers of small vesicles. As a result of neglecting the very small bubble range, the BND values of these previous studies are too small. In addition, the lower limit set for the analysis of the Lake Purrumbete thin sections, also leads to too small BND values derived by transmitted light methods. The strong dependence of the BND values on the magnification has been also observed by Shea et al. (2010).

BND values derived from the analysis of BSE images are very high ranging between $1.79\text{x}10^7\,\text{mm}^{-3}$ and $9.04\text{x}10^9\,\text{mm}^{-3}$. Similarly high BND values have been found in pumice clasts of the Vesuvius 79 AD eruption (Shea et al., 2010). As a consequence of the high

magnification of BSE images large vesicles, filling out the whole field of view, will be missed, resulting in a bias towards artificially high numbers of small bubbles, as a whole (Gaonac'h et al., 2005).

By comparing the BSD's of different size classes of the same sample, it can be evaluated if the BND calculated for the ash particles is correct. The data set fits very well together in one BSD curve (Figure 4.7) indicating that the two different data sets derived by different methods and clast sizes, describe different size ranges of the same BSD. The BND calculated for ash particles is therefore correct and represents the abundance of very small vesicles in the melt. As shown by the BSD the largest number of vesicles is in the smallest vesicle size range and therefore the BND derived from the small clast size may be closer to the original BND of the magma, than the BND of the larger clasts.

4.5.2 Multiple bubble nucleation events

The curved shape of the BSD may be the result of bubble coalescence and Oswald ripening (Mangan and Cashman, 1996, Higgins, 2006). While Oswald ripening would decrease the amount of very small bubbles, bubble coalescence lowers the amount of the medium sized vesicles and increases the number of large vesicles. The typical shape of a BSD modified by bubble coalescence is kinked (Mangan and Cashman, 1996). Coalesced vesicles are common in the larger clasts of the Lake Purrumbete samples, but rare in the small size class. However, this could be due to coalesced bubbles being larger than the fine ash particles. The curved shape of the BSD of the Lake Purrumbete BSD, however, is difficult to explain only with bubble coalescence.

Curved BSDs were also observed by Higgins (2006), Shimano and Nakada (2006), Polacci et al. (2009), Tsukui and Suzuki (1995) and are explained as the result of different nucleation events. Tsukui and Suzuki (1995) interpreted the curved BSD found in phreatomagmatic deposits of the 1983 Miyakejima eruption as formed by a second nucleation event, which was caused by sudden cooling of the magma by water contact. This process can be excluded for the Lake Purrumbete samples, having curved BSD's in all three different deposit types, including scoriaceous magmatic influenced deposits. This is further supported by the elongation of small vesicles reflecting plastic deformation of the bubbles due to stress in melt prior to fragmentation, and indicating vesicle nucleation prior to magma water interaction. Shimano and Nakada (2006) and Polacci et al. (2009) assumed that the first nucleation event is caused by degassing in the magma chamber and/or the deep part of the conduit, with degassing of the magma being controlled afterwards by bubble growth rather then nucleation of new vesicles. This vesicle population forms the large vesicle class observed in the Lake Purrumbete pyroclasts. The number of these vesicles decreases during ascent due to bubble coalescence and loss of vesicles, which may ascend faster than the magma. The second nucleation event occurs near the fragmentation level by degassing of a very small amount of H_2O due to sudden decompression of the melt, triggered by acceleration of the melt near the fragmentation level (Massol and Koyaguchi,

2005, Shimano and Nakada, 2006, Polacci et al., 2009). Massol and Koyaguchi (2005) suggest that a very low magma flux will cause the melt to become highly supersaturated in volatiles at the time of the second nucleation event, resulting in a large amount of secondary nucleating vesicles. The very small size of these vesicles in the Lake Purrumbete samples indicates vesicle nucleation occurred shortly before fragmentation (Sable et al., 2006) where vesicle growth is slowed by fast ascent rates due to acceleration of the melt (Massol and Koyaguchi, 2005). Shea et al. (2010) explained curved BSD with continuous acceleration of vesicle nucleation and growth, which cannot be completely ruled out for the Lake Purrumbete magmatic system, but vesicle textures and the depletion in medium sized vesicles show that vesicle nucleation either stopped or was very limited until acceleration of the melt close to the fragmentation level.

4.5.3 Variations in the vesicularity

From a textural point of view, the vesicularity of the clasts is a function of the number of vesicles in the clast and the size of the vesicles. While the Lake Purrumbete samples show large variations in the clast vesicularity in each sample, the BND of the clasts is similar within the same sample. The vesicularity is therefore dependent on the size rather then the number of vesicles. Highly vesicular clasts have the same size and amount of large vesicles of the first vesicle population as slightly vesicular clasts. The second vesicle population in the highly vesicular clasts, however, is missing vesicles of the very small size range, which occur in slightly vesicular clasts, indicating that small vesicles had time to grow. This means that the vesicularity of the clasts is dependent on the time interval between nucleation and fragmentation, which should be the same for clasts of the same eruption event. In maar diatremes, however, magma can rise into different levels of the diatreme before coming in contact with water (Valentine, 2012). Magma fragmented deeper in the diatreme and therefore earlier will contain only very small vesicles of the second population and will thus have only low vesicularities while magma which is rising higher into the diatreme will have higher vesicularities due to longer growth time of the vesicles.

Recycling of juvenile material, due to fall back of ejected material into the crater, is also a common process in maar volcanoes (White, 1996). Additionally, material fragmented in a deeper explosion may not be ejected at all, and remain within the confines of the diatreme (Valentine, 2012). Both processes may contribute to the formation of deposits consisting of a mixture of juvenile clasts originating from different explosion events. By choosing fresh, ash free clasts we tried to avoid analysing clasts from earlier explosive events.

4.5.4 Magma ascent rates

Excluding vesicles $<10\,\mu$m, the Lake Purrumbete BND values are in the range of BND values of pyroclasts from Etna's 122 BC Plinian eruption, indicating fast magma ascent rates (Sable et al., 2006). These high BND values, however, are formed by the large

amount of vesicles in the size range of 10 μm<vesicles<20 μm, which can be considered as formed by the second nucleation event close to the fragmentation surface. After the first nucleation event the magma was ascending slowly which is reflected by the polylobate shape of the large vesicle population indicating bubble coalescences. The large amount of the second small vesicle population shows that the melt was highly supersaturated which may be the result of very low magma fluxes, due to low ascent rates (Massol and Koyaguchi, 2005). During and after the second nucleation event the magma ascended rapidly which is reflected in the high BND values.

Magma ascent rates are typically considered to be relatively fast and direct from the mantle for small monogenetic volcanoes, which is supported by the occurrence of mantle xenoliths in deposits of many monogenetic volcanoes (Reiners, 2002). In the Lake Purrumbete Maar deposits fragments of mantle xenoliths are rare and only occur in the youngest sequence (Jordan et al., 2013a, chapter 2), suggesting that magma ascent rates were general too slow to preserve mantle xenoliths, but increased during the youngest eruptive phase. An increase in the primary magma ascent rate would lead to an increase in the magma flux and in the number of vesicles of the first population, as they have less time to coalesce (Figure 4.8), together with decreasing degrees of supersaturation of the magma. Smaller degrees of supersaturation, however, will cause a smaller amount of vesicles to nucleate in the second nucleation event. This may be reflected in a general decreasing trend of the BND values from the bottom to the top of the Lake Purrumbete Maar sequence (Figure 4.8). Progressively deepening of the fragmentation surface due to downwards growth of the maar diatreme, will result also in a decrease of the BND values due to progressively earlier fragmentation. Lake Purrumbete, however, has a very shallow bowl shaped diatreme structure, where downwards growth has not been significant (Jordan et al., 2013a, chapter 2) and therefore is unlikely to be the reason for changes in BND values. In addition, downwards growth of the maar diatreme cannot explain the opposite trend of increasing BND for larger vesicles and decreasing trend for smaller vesicles observed in the Lake Purrumbete samples. Increasing magma ascent rate should cause the first generation bubbles to be smaller because there is less time for them to grow, and fewer and smaller second generation bubbles, again because there is less time.

4.6 Conclusion

- The comparison of BND values and BSD of fine ash deposits with coarser deposits is possible if different size classes of pyroclasts are analysed and compared carefully for all samples.

- Similar BND values and BSD shapes of all Lake Purrumbete deposit types indicate that the eruption style has not been influenced by the vesicularity of the melt.

- BND values and BSD shapes indicate that bubble nucleation occurred in two steps. The first bubble population formed deep in the conduit/ or magma chamber while

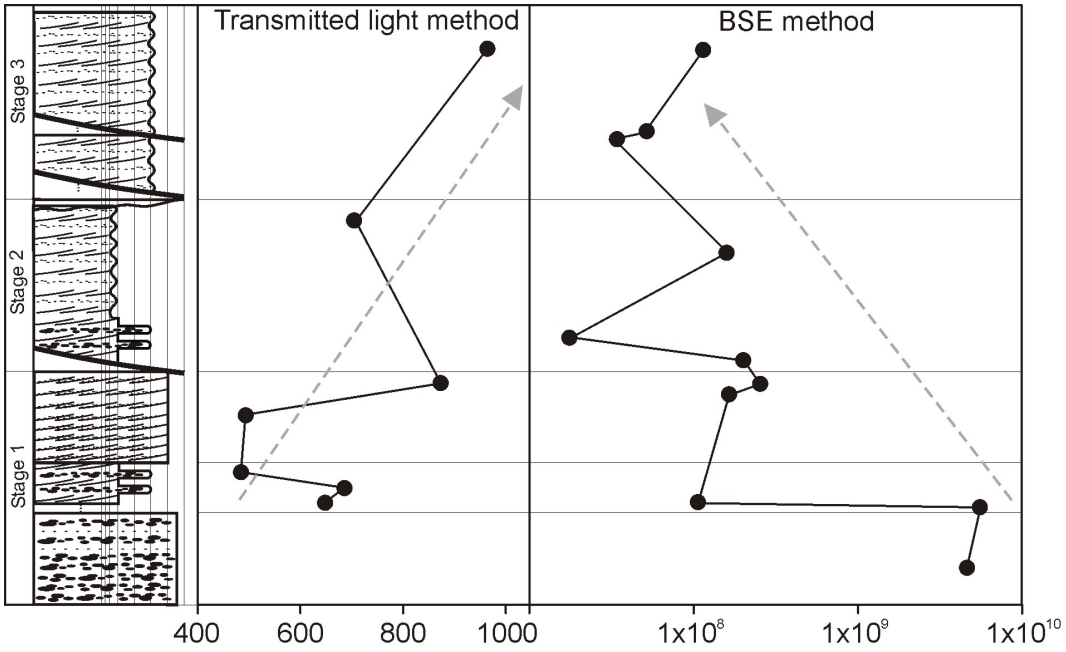

Figure 4.8: Changing BND values within the stratigraphic sequence. Grey arrows indicate general trends with increasing BND values of larger vesicles observed by using transmitted light and decreasing BND values of smaller vesicles determined in BSE images (stratigraphical column modified after Jordan et al. (2013a, chapter 2)).

the second population nucleated in the shallow conduit near the fragmentation level due to supersaturation and acceleration of the melt (Massol and Koyaguchi, 2005, Shimano and Nakada, 2006).

- The initial ascent rate of the magma is changing over the time of the eruption. It is slower at the beginning causing a higher degree of supersaturation of the magma and larger BND values of the second vesicle population. With increasing ascent rate of the magma the degree of supersaturation decreases resulting in smaller BND values due to smaller amounts vesicles of the second vesicle population.

- The large amount of vesicles of the second vesicle population is caused by acceleration of the melt near the fragmentation level and rapid decompression. The high BND values are similar to those observed in pyroclasts of the Etna 122 BC eruption, indicating fast magma ascent rates prior to fragmentation.

5

New perspective of microlite formation

S.C. Jordan and R.A.F. Cas

Abstract

Basaltic juvenile pyroclasts, formed during phreatomagmatic eruptions of the Pleistocene Lake Purrumbete Maar, southeastern Australia, strongly differ in microlite abundances and textures, indicating that microlite formation was heterogeneous throughout the magma that was erupting during the same eruptive event. These heterogeneities cannot be explained by decompression or cooling induced microlite formation, as these processes would affect the whole magma body. The microlites must have formed independently in different parts of the magma, which most likely happened during fragmentation or afterwards. To evaluate the possibility of microlite formation during magma fragmentation, a new type of experiment was performed in which basaltic melt was fragmented under conditions simulating magmatic and phreatomagmatic conditions. The results show that microlites can form in extremely short time scales during the fragmentation process. The relationship between microlite occurrence and clasts forming by brittle fragmentation, strongly suggests that the process of microlite formation is caused by the same internal stress causing the magma to fragment in a brittle way. Stress induced microlite formation may occur during fragmentation processes but also in the conduit itself if the magma is strained during ascent, this will make it difficult to use microlite populations as a proxy for cooling or decompression rates as currently have been used.

5.1 Introduction

In recent research microlite number densities and textures have become an important tool to determine magma ascent rates and conduit processes (Couch et al., 2003, Toramaru et al., 2008, Cichy et al., 2011). Many numerical and experimental studies have been conducted on both cooling (Berkebile and Dowty, 1982) and decompression (Hammer and

Rutherford, 2002, Couch et al., 2003, Cichy et al., 2011) induced microlite nucleation to understand the processes governing microlite formation. Decompression of the magma during ascent results in degassing and undercooling of the magma, and it is widely accepted that this leads to crystal nucleation and growth (Hammer and Rutherford, 2002, Couch et al., 2003, Suzuki and Fujii, 2010). Changes in microlite abundances within eruption sequences have been used to determine changes in magma ascent rates (Suzuki and Fujii, 2010). Other authors explained differences in microlite abundances within clasts of the same eruption event by mixing of different magma batches (Stovall et al., 2012). The study presented here, of microlite abundances and textures in juvenile pyroclasts from the Lake Purrumbete Maar in the Newer Volcanics Province, southeastern Australia, shows that clasts, which formed during the same eruption event, vary widely in the microlite abundance. These variations are difficult to explain with the formation of microlites due to decompression or slow cooling of the magma in the conduit. To investigate the possibility of a different mechanism of microlite formation, fragmentation experiments were used to evaluate the influence of the fragmentation process on microlite formation.

The current models of microlite nucleation are based on experimental work, using decompression experiments. In these experiments volcanic material is typically molten inside a capsule at a certain temperature and pressure. The pressure is than changed and the system is given time to adjust to the new pressure. Afterwards the whole capsule is cooled rapidly below the glass transition temperature, and the glassy material is analysed (Hammer and Rutherford, 2002, Couch et al., 2003). The time period for the melt to adjust to the new pressure is in the range of 1 hr to weeks and the processes within the capsule cannot be observed during this time. Therefore, the moment of microlite formation cannot be observed. The experimental work conducted in this current study, uses dry and wet blow-out experiments described by Büttner et al. (2006) and Austin-Erickson et al. (2008) to determine the factors that influence microlite formation during magma fragmentation. The results of these experiments show that microlites are constrained to particles formed by brittle fragmentation and therefore may be formed by the same processes causing brittle behaviour of the melt, such as strain and rapid deformation.

The natural samples used in this study are from the pyroclastic sequence of the Lake Purrumbete Maar. This Pleistocene maar volcano is located in the basaltic intraplate Newer Volcanics Province (NVP), southeastern Australia (Figure 5.1), which consists of over 400 small eruption points (Joyce, 1975). Activity of the volcanic field started in the early Pliocene (Price et al., 1997) with recent activity of the NVP indicated by natural hot springs and mantle derived CO_2 (Lesti et al., 2008). Volcanism in the NVP is suggested to be the result of the break up of Gondwana and rifting between Australia and Antarctica (Price et al., 1997).

Lake Purrumbete was formed by three eruption phases and multiple vent migration events, resulting in a very large (3 km diameter) maar (Jordan et al., 2013a, chapter 2). The magma feeding the Lake Purrumbete volcanic system ascended directly from the mantle without storing in a magma chamber, whereby magma ascent accelerated near the

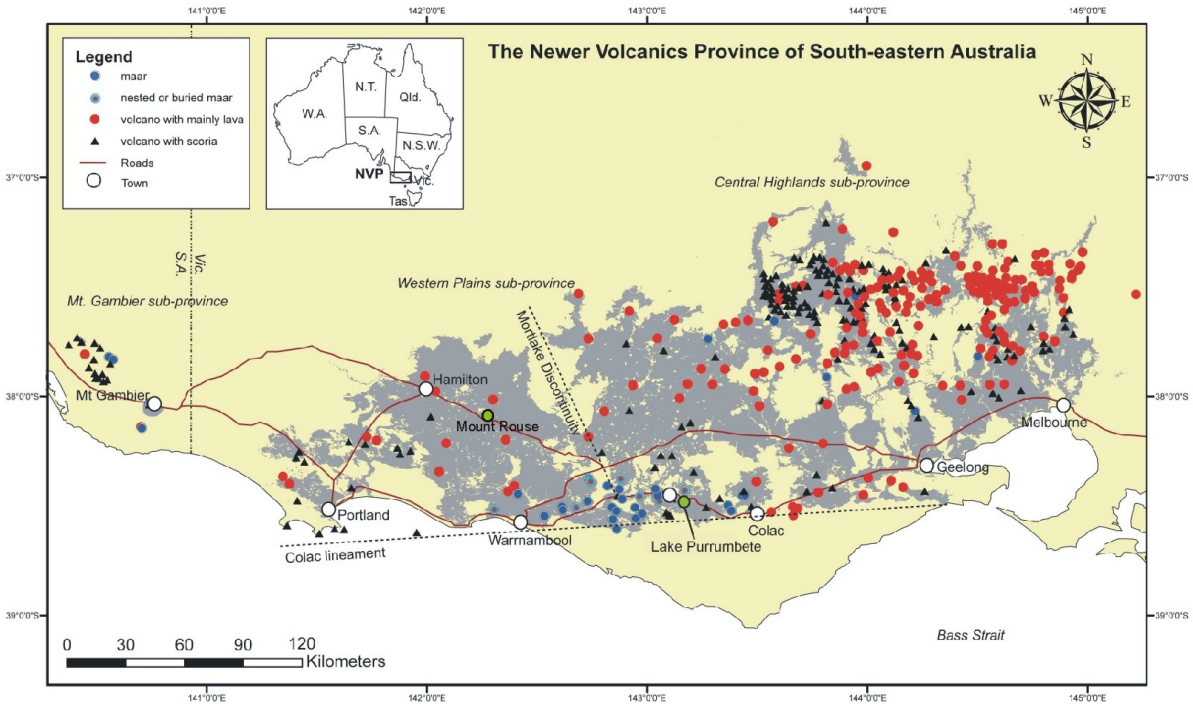

Figure 5.1: Map of the Newer Volcanics Province in southeastern Australia. The location of Lake Purrumbete and Mount Rouse are marked in green (modified after Cas and van Otterloo (2011)).

fragmentation level (Jordan et al., 2013c,b, chapter 2 and 3). The pyroclastic sequence of Lake Purrumbete (Figure 5.2) consists of dry and wet phreatomagmatic deposits with intercalated magmatic-influenced dry phreatomagmatic layers and has been described in detail by Jordan et al. (2013a, chapter 2). The wet phreatomagmatic layers are the product of most intense phreatomagmatic eruptions that generated predominantly fine ash, while dry phreatomagmatic layers consist of ash lapilli deposits which were formed during less efficient phreatomagmatic eruptions. The magmatic-influenced dry phreatomagmatic layers were formed by inefficient phreatomagmatic activity, with parts of the magma being fragmented in a magmatic way, as indicated by the occurrence of abundant scoria clasts within the ash lapilli deposits. The main factor controlling these different eruption styles was the availability of water at the time of the eruption (Jordan et al., 2013a, chapter 2).

5.2 Experimental material

The material of the Lake Purrumbete Maar sequence is not suitable for the conducted experiments due to the relatively fine grain size and the high ash content. In addition, ash coating of the juvenile lapilli clasts is common in the Lake Purrumbete material (Jordan et al., 2013a, chapter 2) and makes it impossible to separate pure juvenile material in large quantities from the deposits, as ash coated juvenile clast would need manual cleaning with a brush. Therefore clean and fresh scoria originating from Mount Rouse, a different volcanic centre of the NVP (Figure 5.1), but with a similar geochemical composition as the deposits of Lake Purrumbete (Table 5.1), was used for the experiments. Mount Rouse is a

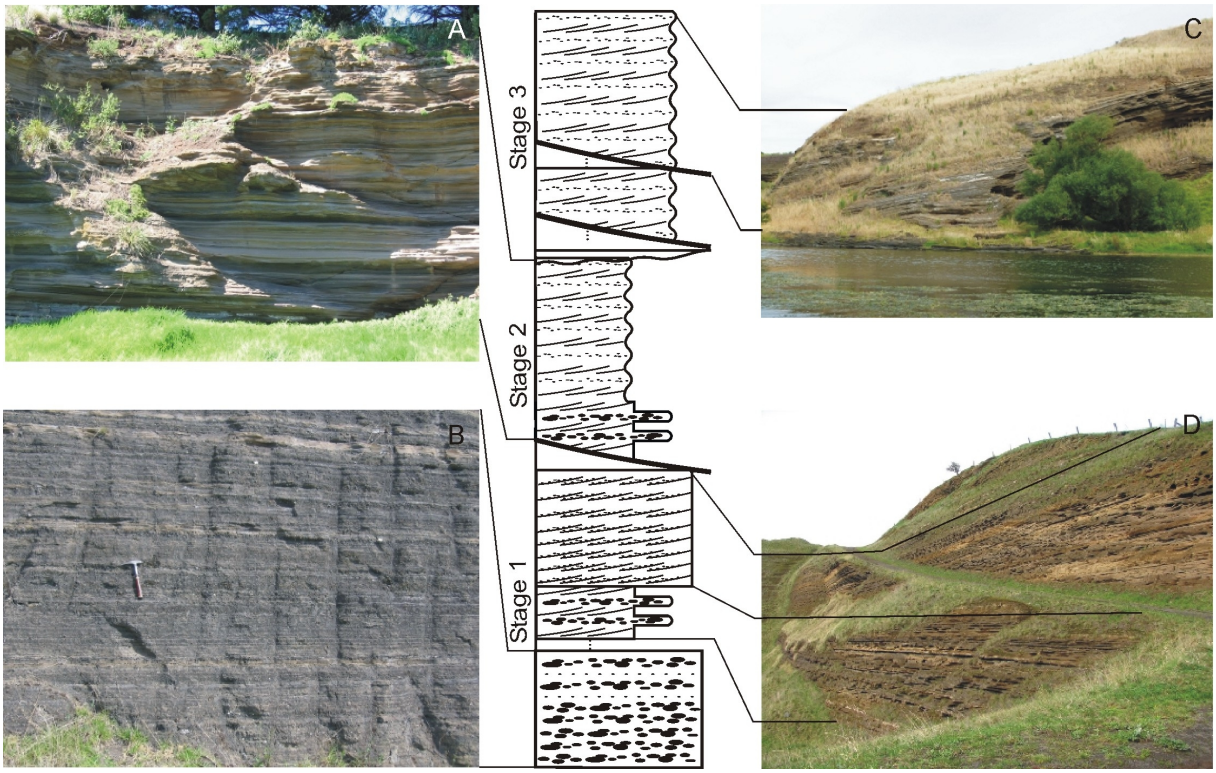

Figure 5.2: Composite stratigraphical log of the Lake Purrumbete pyroclastic sequence, indicating the three stages of the eruption. Field pictures show the out crop characteristics of A) wet phreatomagmatic deposits, B)+D) dry phreatomagmatic deposits and C) magmatic influenced dry phreatomagmatic deposits.

Table 5.1: General geochemistry of Lake Purrumbete and the Mount Rouse material.

	SiO_2	TiO_2	Al_2O_3	Fe_2O_3	MnO	MgO	CaO	Na_2O	K_2O	P_2O_5	LOI
Mt Rouse											
2208-590	47.62	2.4	13.99	12.2	0.16	8.68	8.19	3.59	1.65	0.66	0.4
Lake Purrumbete											
514	46.5	2.74	14	12.3	0.16	5.68	7.95	4.26	2.72	1.14	2.3
WQ5a	46.1	2.89	13.8	13	0.16	6.99	6.71	3.08	2.4	1.04	3.52

volcanic complex including several eruption points (Boyce, 2011) with changing eruption styles from effusive to explosive. The sample material originates from a scoria fall deposit formed during a scoria cone building eruption phase.

The fresh scoria clasts have a light yellow-brown glass groundmass, with a crystal content of 5-10 % and 50 % vesicles. The crystal fraction consists of olivine, clino- and ortho-pyroxene and K-feldspar, whereby olivine and clinopyroxene are dominant. The glass groundmass also contains plagioclas microlites in various amounts.

5.3 Methods

To investigate the formation of micro-textures within juvenile clasts a series of fragmentation experiments were conducted. Three different types of experiments were conducted at the Physikalisch, Vulkanologisches Labor Würzburg, Germany, to investigate pyroclasts

formed by different eruption styles. Dry blow-out experiments, described in detail by Büttner et al. (2006), were used as an analogy for fragmentation during magmatic explosive eruptions, while wet blow-out experiments, described in detail by Austin-Erickson et al. (2008), were used as an analogy for phreatomagmatic fragmentation. Thermal granulation experiments were conducted as a comparative test to investigate the state of the melt prior to fragmentation.

Figure 5.3 shows the experimental setup that was used for dry and wet blow-out experiments. The material is heated in a steel crucible by induction heating using an induction coil around the crucible. The bottom of the crucible has a hole, which is closed by a ceramic lid. This hole is used for the injection of the driving gas via a tube, which is controlled by a valve. The pressure of the gas is measured by a pressure transducer, while the force transducer records the repulsive force of the system. The coolant coil in the lower part of the set-up is used for cooling this part, as both force and pressure transducers are heat sensitive. The lower part is insulated from the crucible by the ceramic breaker plate.

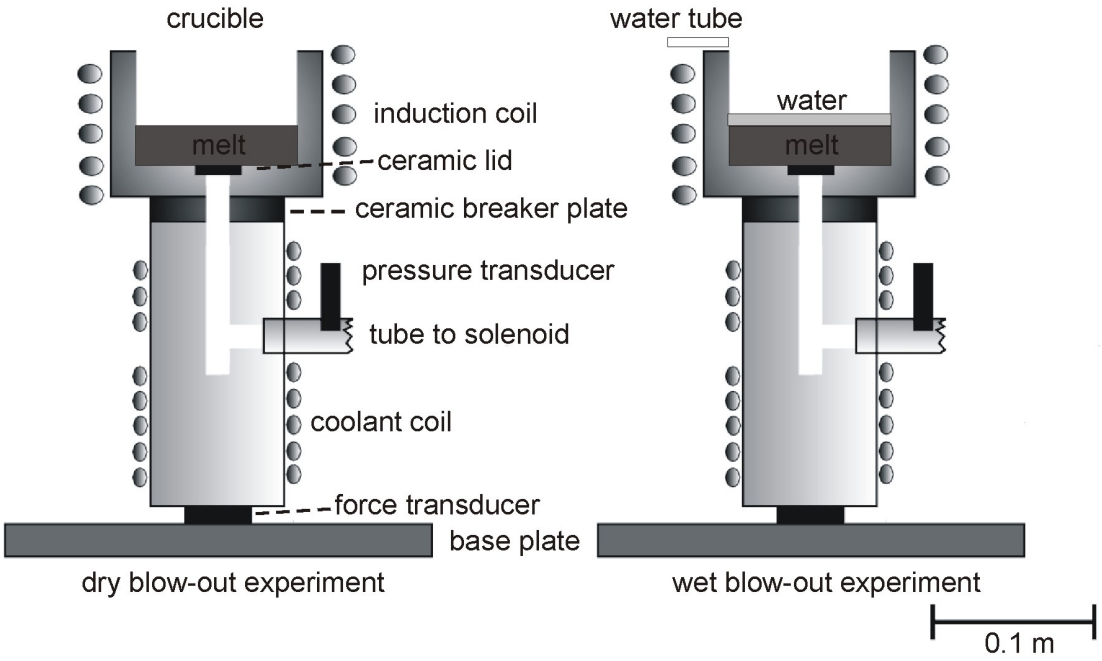

Figure 5.3: Experimental setup of dry and wet blow-out experiments (modified after Büttner et al. (2006) and Austin-Erickson et al. (2008)).

Fresh scoria clasts from Mount Rouse were crushed and sieved to extract material in the grain size range of 0.5-4 mm, which is best for homogeneous melting. For each experimental run 300 g of the material was melted in a crucible using induction heating. Voids included in the scoria and filled with air, will be preserved within the melt if the time the material exists in a liquid state is kept short enough. The time used in the experiments for melting was in the range of 3-4 hr, whereby in each run the time was set longer to allow more and more vesicles to escape from the melt. The temperature was adjusted to 1283-1293 K. By heating the melt over the desired temperature and cooling over a short period of time of exactly seven minutes, the thermal gradient within the melt plug between the margin and the inside was removed.

The experiment of dry blow-out runs is triggered by opening of the valve at the gas tube. Due to the pressure in the tube, the gas is forced into the crucible through the tube at the bottom of the crucible, lifting the ceramic lid and pushing against the melt plug, causing the melt plug to bulge and the formation of microcracks in the melt plug. The high strain rate caused by the deformation of the magma will result in brittle fragmentation of the melt within the crucible, which is similar to the process of magmatic fragmentation in nature (Büttner et al., 2006). Further fragmentation is caused in a ductile way by acceleration of the melt due to expansion of the material at the moment the melt leaves the crucible (Büttner et al., 2002).

The experiment of wet blow-out runs is again triggered by the opening of the valve and the gas forced into the crucible, causing the melt plug to deform. But in wet blow-out experiments water is poured on top of the melt plug via the water tube (Figure 5.3) shortly before the onset of brittle fragmentation of the melt. In the moment of deformation of the melt and the formation of micro cracks, the water will flow inside these cracks of the melt plug (Figure 5.4). This increases the contact area of the melt and the water, resulting in explosive magma/water interaction, known as molten fuel coolant interaction (MFCI) (Austin-Erickson et al., 2008, Büttner and Zimanowski, 1998, Büttner et al., 2002). During MFCI the fragmentation of the melt is caused by simultaneous steam expansion and contraction of the melt due to rapid cooling. The explosivity of this process is controlled by the size of the magma/water interface, where explosions are only caused if the interface is large enough (Büttner and Zimanowski, 1998, Austin-Erickson et al., 2008). The fragmentation mechanism in wet blow-out experiments is therefore not caused by high strain of the magma due to deformation of the melt plug, but by the process of MFCI, which is the main process of phreatomagmatic explosions (Zimanowski et al., 1997a, Zimanowski, 1998).

Only the inner part of the melt plug is fragmented during both dry and wet blow-out experiments, the melt at the crucible margin is left behind as the result of the cooling of the melt in the seven minutes, during which the thermal gradient between the inside and the margin of the melt is equalised.

Using a thermal granulation experiment as a comparative test run, the melt was poured directly from the crucible into water and quenched immediately, with cooling of the melt underneath the glass transition temperature within milliseconds. No explosive magma/water interaction occur, as the magma water interface is to small for any MFCI to occur. As a result the melt is only fragmented due to thermal stresses (Büttner et al., 1999, 2002, Austin-Erickson et al., 2008, Dürig et al., 2012b). These experiments are used as a equivalent to natural non-explosive magma/water interaction (Büttner et al., 1999).

The material of each experimental run was carefully collected after each experiment. Fragments of the ash fraction were separated for further investigations by hand-sieving of each sample. Ash sized material was used, because the particles are small enough to cool very fast during the ejection, but large enough to preserve enough information about included microlites. The clasts were set in epoxy and then polished from one side to

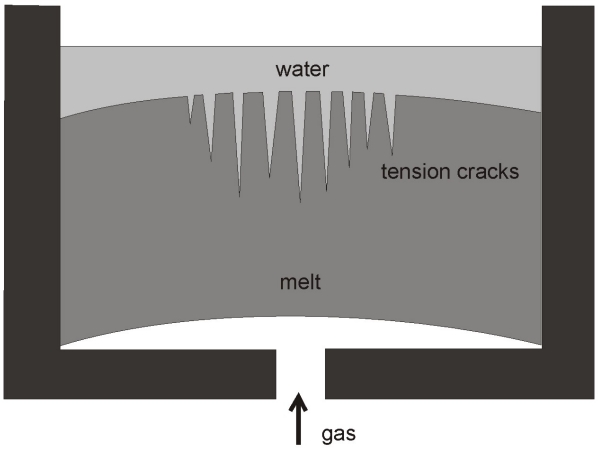

Figure 5.4: Process of melt water contact in the crucible. The water flows into the cracks occurring in the melt by deformation of the melt plug and interacts with the melt in the way of MFCI (modified after Austin-Erickson et al. (2008)).

produce a cross-section through the clasts. Back scattered electron (BSE) microscope images of the clasts were produced using the JEOL JSM-7001F FEG scanning electron microscope at the Monash University Centre for Electron Microscopy. The images were derived using 30 kV acceleration voltage and 10 mm working distance.

Clasts were separated from the natural Lake Purrumbete samples by sieving. BSE images were produced from polished thin sections of the coarse ash size fraction by using the JEOL 840a scanning electron microscope at the Monash University Centre for Electron Microscopy, with 15 kV acceleration voltage and 8 mm working distance.

5.4 Microlite textures

5.4.1 Natural juvenile clasts

Only fresh clasts without any signs of ash coating were considered to be fragments of the magma interacting with ground water and causing the eruptive event. Clasts with varying degrees of ash coating are considered to be recycled clasts, and to originate from earlier eruptive events (Houghton and Smith, 1993). The particles have a blocky shape and sharp and curvi-planar edges, indicating clast formation by brittle fragmentation. Fluidal clasts indicative of ductile fragmentation such as Pele's hair and tears are very rare in the Lake Purrumbete sequence (Jordan et al., 2013a, chapter 2) and were not observed in the analysed thin sections.

BSE images of juvenile ash particles show that the juvenile particles of the same sample contain various amounts of microlites ranging from microlite poor to microlite rich (Figure 5.5). The microlite population consists predominantly of plagioclase laths and minor pyroxenes, olivine and oxides. The juvenile clasts contain also larger phenocrysts such as olivine, pyroxenes and feldspars. Microlites are general randomly distributed over the entire clast area (Figure 5.5A-B), whereas the microlite abundance can vary between parts of the same clast. Some clasts show microlite alignments of the longest

axes (Figure 5.5D), whereby the alignment can again affect the whole clast or only parts of the clast. Vesicles within the clasts are often also elongated and oriented. However, there is no overall relationship between vesicle orientation and microlite orientation, as the following relationships were observed: both vesicle and microlites oriented in the same direction; orientation of microlites but no orientation of vesicles; and no orientation of vesicles and microlites.

The microlites are generally singular crystals with fully developed crystal shapes. Microlite rich clasts, however, can contain only a few singular, larger microlites, while the vast majority of microlites forms small clusters with a dendritic texture (Figure 5.5C).

5.4.2 Experimental particles

Microlite free clasts occur in both dry and wet blow-out experiments (Figure 5.6A-B). These clasts are sub-rounded to rounded in form or have elongated fluidal shapes typical of ductile fragmentation (Büttner et al., 2002).

Clasts containing microlites, differ in microlite abundance and microlites textures. These variations occur in clasts of both dry and wet blow-out experiments. All clasts containing microlites show signs of brittle fragmentation such as curvi-planar edges, angular shapes and fractures.

Microlite poor clasts contain larger cubic to rectangular, white microlites in BSE images and a few lath-like grey microlites in BSE images. The microlites are often accumulated along the clast margins and some clasts show first signs of a developing dentritic texture (Figure 5.6C-D).

Microlite rich clasts have a needle like texture (Figure 5.6E-F), with three different types of microlites, such as very small, white microlites in BSE images, often formed as needles; larger rectangular to subrounded light grey microlites in BSE images and lath-like dark grey microlites in BSE images, which can also occur as long needles.

BSE images of the thermal granulation clasts show that the clast interior consists of pure glass without any microlites or crystals, with a few vesicles preserved within these clasts. The clasts have sharp corners and the edges can be convex or concave (Figure 5.6G-H).

Figure 5.5 *(following page)*: Microlite textures in natural clasts from Lake Purrumbete. Microlites include plagioclase, olivine, pyroxenes (light grey), and oxides (white), set in a glass groundmass (dark grey) A)-B) microlite rich clasts with no preferred orientation of the microlites. C) Dendritic texture of very small microlites with uneven distribution over the clast. D) Orientation of larger microlites but no orientation of the vesicles. E) Parallel orientation of both vesicles and microlites, note concentration of microlites in a band through the clast. F) Almost microlite free clast in a very vesicular clast.

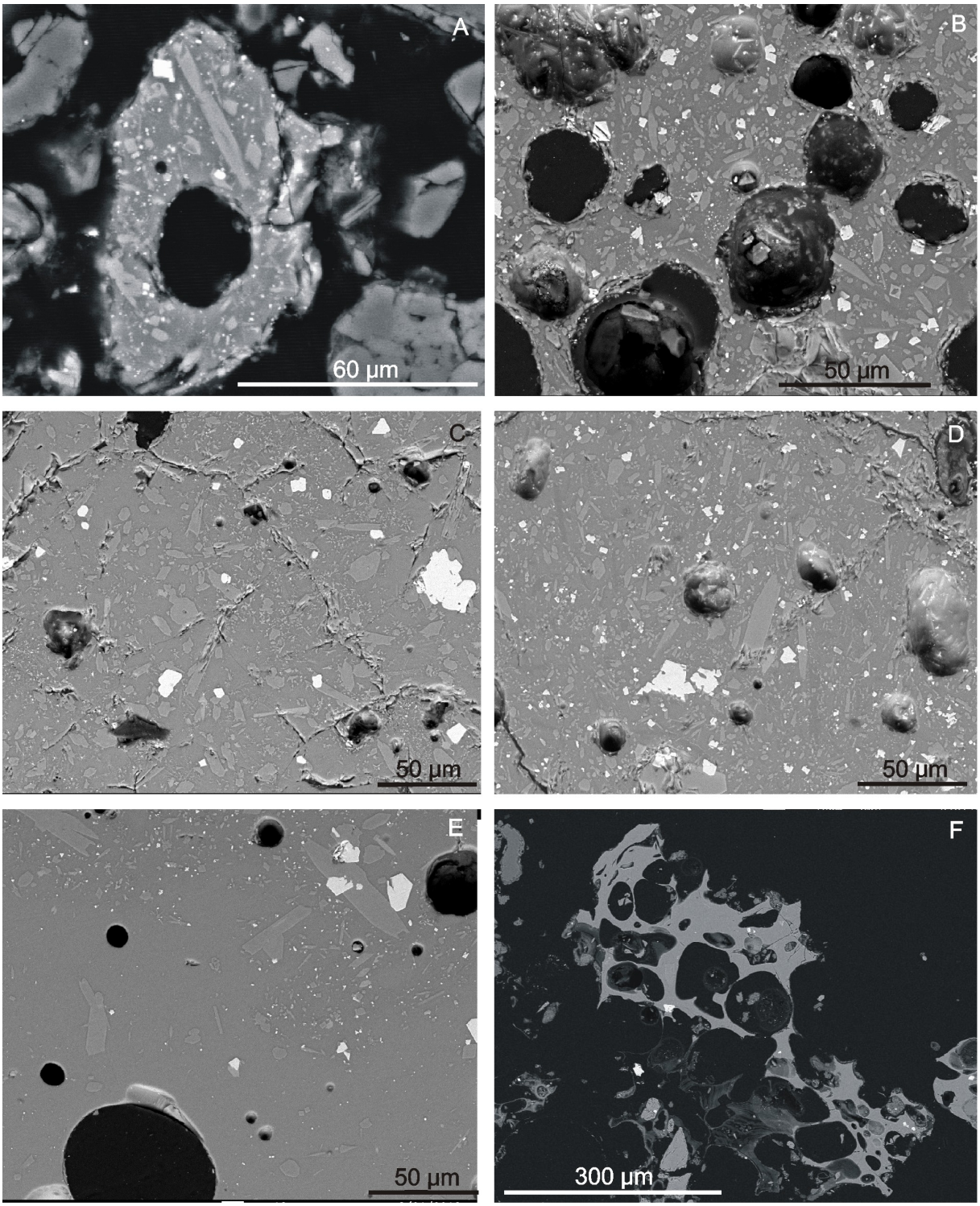
A
60 µm
B
50 µm
C
50 µm
D
50 µm
E
50 µm
F
300 µm

5.5 Discussion

5.5.1 Microlite Formation

The microlite free clasts of the thermal granulation experiment are evidence that the melt in the crucible was microlite free. The immediate cooling of the melt by pouring it into water led to instantaneous freezing of the melt, whereby the shapes of the clasts were fractured by brittle contractional cooling fractures. In the granulation experiment a significant amount of energy is released as kinetic energy due to steam expansion. The small contact area of magma and water in these experiments result in generation of only a small amount of mechanical energy (Büttner et al., 2002). As a result, the granulation clasts show the state of the melt in the crucible prior to the onset of the experiments, which was microlite and crystal free. However, the thermal gradient between the inner part of the melt plug and the melt at the crucible margin was not eliminated for the granulation experiments by switching of the induction heating seven minutes before the actual experiment, as described in the methods part. However, cooling of the melt occurred only along the crucible margin during these seven minutes to equalize the temperature between the inner part and the margin at a temperature around 1283 K. The melt at the margin, however, is neither fragmented nor ejected, but is staying within the crucible. As a result the microlites within the ejected ash particles cannot be the result of cooling during these seven minutes.

Therefore the microlites in the blow-out experiments can only have been formed during the experiment itself or afterwards by cooling of the clasts. Szramek et al. (2010) suggested that cooling of pumice clasts in the atmosphere will cause microlite formation. However, the clasts, used in their study, were small bombs, where cooling of the clast interior is much slower than for ash particles, which should freeze immediately. In addition, if cooling of the experimental clasts after ejection led to microlite formation, it would be expected that all clasts of the same experiment contain the same amount of microlites and the same textures, as all analysed clast were in the same size range and had the same starting temperature. Furthermore, clasts formed during wet blow-out experiments should contain less microlites or no microlites compared to the dry blow-out experiments, due to rapid cooling during melt/water interaction, which has not been observed. Therefore cooling can be excluded as a mechanism for microlite formation in these experiments.

The reaction of a saturated liquid to mechanical stress with immediate crystallization is a common phenomenon (VanHook, 1969) and is used in ultrasonic science for the creation of synthetic crystals (for example by Pal et al. (2013)). Experiments conducted

Figure 5.6 *(following page)*: Microlite textures in experimental derived clasts. A)-B) Pele's tears containing no microlites; C)-D) microlite poor clasts with concentration of microlites at the edges and minor dendritic textures in the clast interior; E)-F) microlite rich clasts with different microlite sizes; G)-H) microlite free angular clasts derived from thermal granulation experiments.

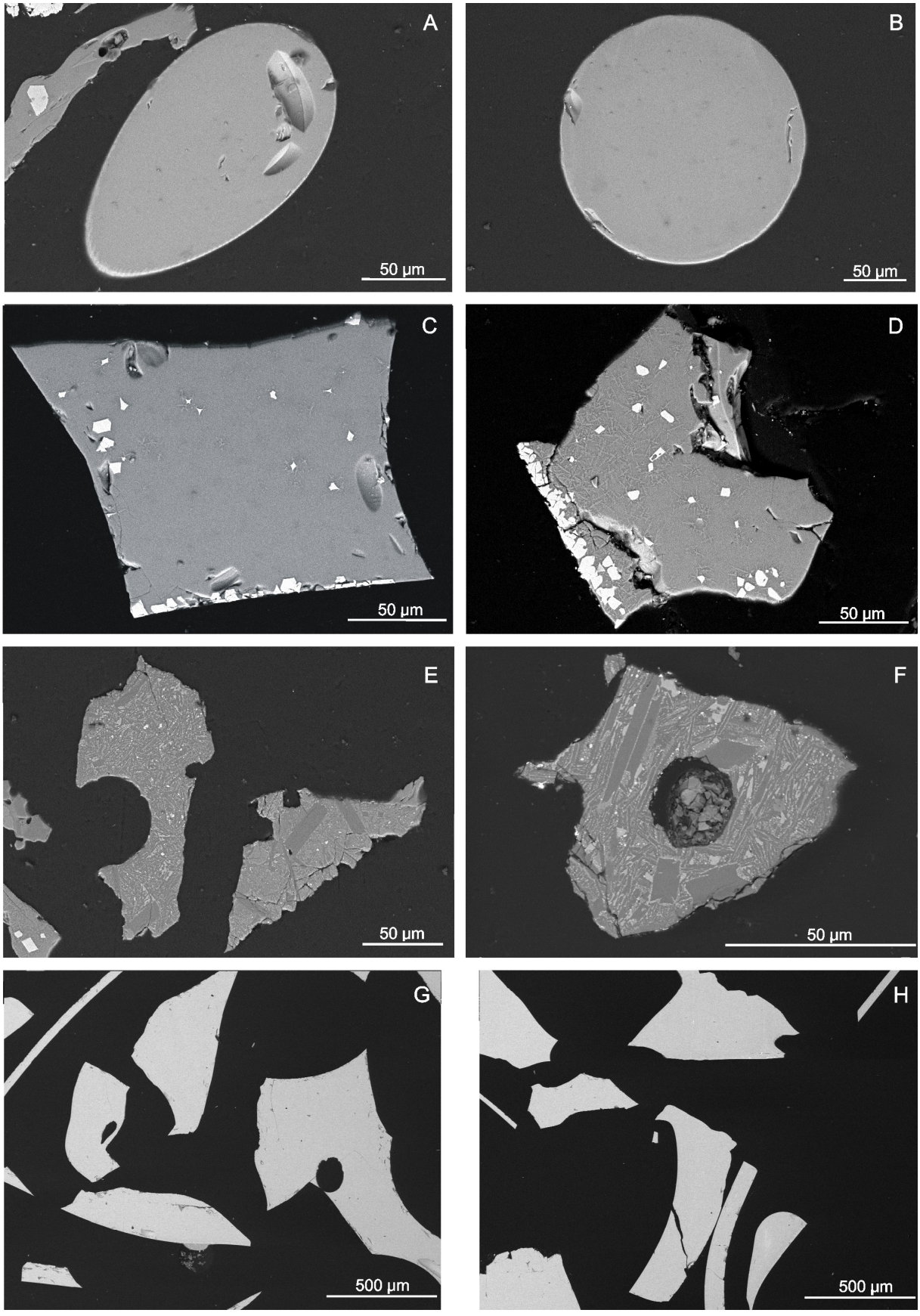
A
50 µm
B
50 µm
C
50 µm
D
50 µm
E
50 µm
F
50 µm
G
500 µm
H
500 µm

by Bartels and Furman (2002) showed that sonic and ultrasonic waves also enhance crystal number densities in basaltic melts. Acoustic waves are typically generated within volcanic explosions and did also occur during the experiments. However, these acoustic waves would propagate through the whole melt and therefore would initiate homogeneous microlite nucleation. Records of the acoustic signal from each experiment show that acoustic waves occurred after fragmentation and after the ejection of the clasts. As a result, it can be concluded, that the observed microlites were not caused by propagation of acoustic waves. However, stress waves released by fragmentation of the material could have a similar influence on microlite formation as acoustic waves.

The only possible mechanism responsible for the microlite formation during these experiments must be the fragmentation process in the crucible itself. The fact that clasts formed by ductile fragmentation are free of microlites suggests that microlite formation is caused by brittle fragmentation due to straining and shearing of the magma during fragmentation (Büttner et al., 2002). Brittle fragmentation can be caused by both high degrees of internal strain of the melt or melt/water interaction, where expansion of the water due to heating cause rapid deformation of the melt, resulting in brittle fragmentation (Büttner et al., 2002). Mechanical energy is released during brittle fragmentation and clasts formed by brittle fragmentation will have experienced high rates of internal mechanical stress. The melt may react to this stress not only with fracturing but also with rapid microlite nucleation and growth. Influence of mechanical stress on microlite formation has been suggested by Berkebile and Dowty (1982) for microlite formation within glass beads in dynamic cooling experiments. Microlite formation was only observed within the glass bead, in cases where the glass beads had been touched by hand during the experiment, otherwise the microlites formed only along the margin of the glass bead. Berkebile and Dowty (1982) assumed that either the mechanical stress or contamination caused the microlites to nucleate in the interior of the glass bead.

Fluidal shaped clasts, however, are formed by ductile deformation during expansion and fast acceleration of the melt surrounding the actual explosion locus. This process leads to liquid instabilities which result in ductile fragmentation without releasing mechanical energy (Büttner et al., 2002). The lack of mechanical stress may be the reason for the lack of microlites in the fluidal shaped clasts. The melt forming these clasts were not disturbed by any mechanical stress and therefore fast microlite nucleation could not happen.

5.5.2 Application to natural deposits from Lake Purrumbete

Microlite formation caused by decompression of the magma may have caused nucleation and growth of microlites in the Lake Purrumbete clasts. Two decompression events have been identified by vesicle nucleation, whereby the second happened fast during acceleration of the melt near the fragmentation surface (Jordan et al., 2013b, chapter 4). Decompression of the magma, however, would affect the whole magma body and trigger microlite formation laterally throughout the magma column, resulting in more homogeneous

microlite abundances within clasts of the same eruptive event. Valentine (2012) suggested that magma may rise into different depth of the diatreme before explosive interaction with ground water, which is indicated at Lake Purrumbete by the different vesicularities of the clasts (Jordan et al., 2013b, chapter 4). If magma rising into higher levels of the diatreme becomes more decompressed, as indicated by larger bubbles, the magma should also contain more microlites, if microlite growth is controlled by decompression. This is not the case at Lake Purrumbete, where microlite rich clasts are often vesicle poor and vesicle rich clasts are often microlite poor. The very different microlite textures and abundances observed in clasts from single eruptive events at Lake Purrumbete thus cannot only be explained with decompression induced microlite formation.

There is no evidence from the pyroclastic record that significant amount of cooling of the magma occurred prior to fragmentation, the geochemical data instead shows that magma ascent was relatively fast and direct from the mantle source (Jordan et al., 2013c, chapter 3), implying that the magma did not cool significantly prior to fragmentation. If cooling occurred within the diatreme, by magma rising into different depth, microlite nucleation may have been triggered by cooling. The time scale for cooling induced microlite growth, however, would have been extremely short, as fragmentation occurs as soon as the magma hits water within the diatreme.

The occurrence of the different microlite populations and textures may be best explained by stress induced microlite nucleation. Stress within the magma may not be uniform during the fragmentation process indicated by the different grain size of the material. The process of MFCI in phreatomagmatic explosions fragments the magma into fine ash particles (Büttner et al., 2002), while the larger clasts are formed by passive fragmentation during ejection of the material (Büttner et al., 2002) or by shockwaves caused by the phreatomagmatic explosions (Raue, 2004). These different processes will cause different internal stress, which may have caused the different microlite abundances observed in the Lake Purrumbete clasts. If internal mechanical stress of the magma causes microlite formation, this may already happen during magma ascent, as strain occurs within the magma due to different ascent velocities of the magma in the interior of the conduit and at the conduit margins. In addition acceleration of the melt, as indicated by the high BND values (Jordan et al., 2013b, chapter 4), will cause high strain within the magma (Papale, 1999). This high strain may be only local and result in also local microlite nucleation, which is supported by the different textures of aligned and randomly distributed microlites within the Lake Purrumbete clasts. In addition, the occurrence of elongated vesicles, which are aligned in the same direction as the microlites, indicates that both microlites and vesicles have experienced the same stress and support the theory of stress induced microlite formation during strain within the conduit.

5.5.3 Application to other natural deposits

The concept of stress induced microlite formation will change the perspective of using microlites as a measure for conduit processes as observed microlite populations in volcanic material may be not only the result of decompression and cooling in the conduit but also of stress during magma fragmentation. Therefore it will be difficult to differ between microlites generated by these different processes. The occurrence of different microlite populations and distributions in clasts of the same eruption may give evidence that microlite populations have been altered by the process of stress induced microlite formation. An example from the literature where microlites may have formed by stress during the fragmentation rather than cooling, is given by the 1959 fire-fountaining eruption of Kilauea Iki. The products of this eruption, of episode 15 and 16 in particular, have been described by Stovall et al. (2012) and Porritt et al. (2012). Microlite rich and microlite free scoria clasts have been observed by Stovall et al. (2012), whereby microlites in the microlite rich clasts have two different textures; microlite stringers and fasciculated textures. The microlite stringers occur predominantly in transitional to fluidal clasts. Microlite free clasts are interpreted to have originated from the erupting magma, while microlite rich clasts are suggested to originate from lava lake material that had time to cool before incorporation into the eruption. The different microlite textures are also interpreted as having been derived from different cooling rates. In Pele's hair and tears that originate from the same episodes, however, microlites were not observed (Porritt et al., 2012). If mixing of microlite rich lava lake material into the fresh erupting magma is the reason for the different microlite textures, it would be expected that also Pele's hair and tears should contain some of the microlite rich material, which is not the case. The occurrence of different microlite textures in the 1959 Kilauea Iki eruption may be explained by stress induced microlite formation. Pele's hair and tears are formed by ductile fragmentation and therefore did not experience the stress acting during brittle fragmentation, as a result no microlites were formed in these clasts, which is consistent with the microlite free tears produced during our experiments. The microlite stringers in transitional and more fluidal scoria clasts, observed by Stovall et al. (2012), may be the result of weaker stress during brittle fragmentation which is also reflected in the clast shape, whereas the fasciculated textures in microlite rich clasts may be the result of intense stress.

5.6 Conclusions

- Dry and wet blow-out experiments showed that microlites can also form in an extremely short time frame of seconds and during the fragmentation process.
- Traditional models of microlite formation due to decompression or cooling of the magma cannot be applied to the observed phenomenon of microlite formation during fragmentation experiments.

- Rapid crystallisation of saturated liquids and melts due to mechanical stress is a common phenomenon and must be considered for magmatic melts.
- The observed relationship of microlite formation and clasts, formed by brittle fragmentation, suggests that the same internal stress, which forces the break up of the magma, triggers microlite formation.
- Stress induced microlite formation during the fragmentation of the melt has to be considered when using microlite number densities and structures to model magma ascent rates and conduit processes, as microlite populations may have been modified by this process, overprinting the microlite textures originating from decompression in the conduit.
- The difference in microlite abundance and textures observed in the Lake Purrumbete clasts are similar to the observed microlite textures and abundances in the experimentally derived clasts and can be well explained with stress induced microlite formation.
- The amount of microlites within the clasts may reflect the intensity of the internal stress a clast has experienced during fragmentation.
- The process of rapid microlite formation has to be further investigated, in particular the relationship between microlite abundance and stress rate.
- Study of the morphology and textures of microlites related to fragmentation mechanisms of host pyroclasts from different types of pyroclastic and autoclastic deposits should be undertaken to develop a better understanding of the conditions of microlite formation and pyroclast formation.

6

Experimental fragmentation of vesiculated basaltic melt in dry and wet blow out experiments; analogy to magmatic and phreatomagmatic explosions

S.C. Jordan, T. Dürig and R.A.F. Cas

Abstract

The Pleistocene eruption of the Lake Purrumbete Maar, southeastern Australia, produced a complex pyroclastic sequence with deposits varying from magmatic to wet phreatomagmatic. To gain better understanding of the fragmentation processes during the eruption, dry and wet blow-out fragmentation experiments were conducted using a comparable melt, with variable degrees of vesiculation. The experimental results show that the melt had a low viscosity and that phreatomagmatic explosions in the way of molten fuel coolant interaction can occur in the vesiculated melt if fractures form within the melt prior to fragmentation. Furthermore, natural and experimental fine ash particles were compared using high resolution scanning electron microscope images, image particle analysis and statistical methods. The results show that the natural samples have an overall similarity to each other, while experimental samples differ a little from each other and from the natural samples. These small differences may be explained by the development of the particle shape being mainly controlled by pre-stress of the melt prior to fragmentation, which will be different in the melt in an experimental crucible compared to the magma in the conduit.

6.1 Introduction

Phreatomagmatic deposits are generally characterised by very low vesicle content and dense, blocky clasts (Dellino et al., 1990, Dellino and La Volpe, 1995, Dellino et al., 2001, Büttner et al., 1999). It has been suggested that phreatomagmatic eruptions may be prevented by a high vesicle content in the melt, if the exsolving gas is a non-condensible gas like CO_2 (Zimanowski et al., 1991, Zimanowski, 1998). Jordan et al. (2013a, chapter 2) showed that the fragmentation level in maar volcanoes can be located very close to the surface where vesiculation of the melt should occur. For magmatic type fragmentation many authors (Spieler et al., 2004, Büttner et al., 2006, Dürig et al., 2012a) suggested that an increase in the vesicularity of the melt decreases the strength of the melt. As a result more vesicular melts are more prone to fragmentation then less vesicular melts, leading to the question of whether a vesicular melt would increase the fragmentation efficiency of phreatomagmatic eruptions.

The Lake Purrumbete Maar, in the Newer Volcanics Province in southeastern Australia, is the perfect field area to investigate the influence of the melt vesicularity on the phreatomagmatic eruption style. A variety of deposits ranging from magmatic influenced dry phreatomagmatic to wet phreatomagmatic indicates that different fragmentation processes may have been active during the eruption of the maar, while the very shallow fragmentation level, determined by country rock lithics, resulted in a relatively high vesicle content of the pyroclasts (Jordan et al., 2013a, chapter 2). Phreatomagmatic activity has been identified at Lake Purrumbete by the presence of the maar, the depositional structures of the pyroclastic sequence, which shows characteristic features of base surge deposits, as well as the presence of abundant accretionary lapilli (Jordan et al., 2013a, chapter 2), which are all typical for maar eruptions. Therefore it is of major interest to quantify the fragmentation processes at Lake Purrumbete using ash particles, as ash particles show characteristic features depending on the fragmentation style (Büttner et al., 1999, Dellino et al., 2001).

The processes of magmatic fragmentation and molten fuel coolant interaction (MFCI) type phreatomagmatic fragmentation have been investigated in several previous studies (Zimanowski et al., 1991, Alidibirov and Dingwell, 1996, Zimanowski et al., 1997b, Büttner et al., 2002, 2006, Austin-Erickson et al., 2008) using different experimental set-ups. In addition, it also has been shown by these authors, that the experimental derived particles are similar to particles originating from natural deposits and therefore can be used to infer the fragmentation processes, leading to the formation of natural deposits.

6.2 Geological setting of Lake Purrumbete and Mount Rouse

Lake Purrumbete is located in the monogenetic, basaltic, intraplate Newer Volcanics Province (NVP) in southeastern Australia. Volcanism in the NVP started in the early Pliocene (Price et al., 1997), and the youngest eruption of Mount Gambier occurring ca. 5 ka ago. The province comprises over 400 eruption points and covers an area of over 25000 km^2 (Joyce, 1975, Cas and van Otterloo, 2011) .

Lake Purrumbete is a very large maar complex (>3 km) with multiple coalesced craters formed by predominantly phreatomagmatic eruptions and only minor more magmatic phases (Figure 6.1, Jordan et al., 2013a; chapter 2). The eruption took place in three stages, with a significant volcanic hiatus between the second and third stage (Jordan et al., 2013a, chapter 2). The at least 40 m thick pyroclastic sequence consists of wet phreatomagmatic fine ash lithofacies, dry phreatomagmatic lapilli ash lithofacies and few intercalated magmatic influenced scoriaceous lapilli lithofacies (Figure 6.2), which have been described in detail by Jordan et al. (2013a, chapter 2). The differences in the lithofacies types are caused by changes in the water supply, which was restricted in some of the coalesced craters.

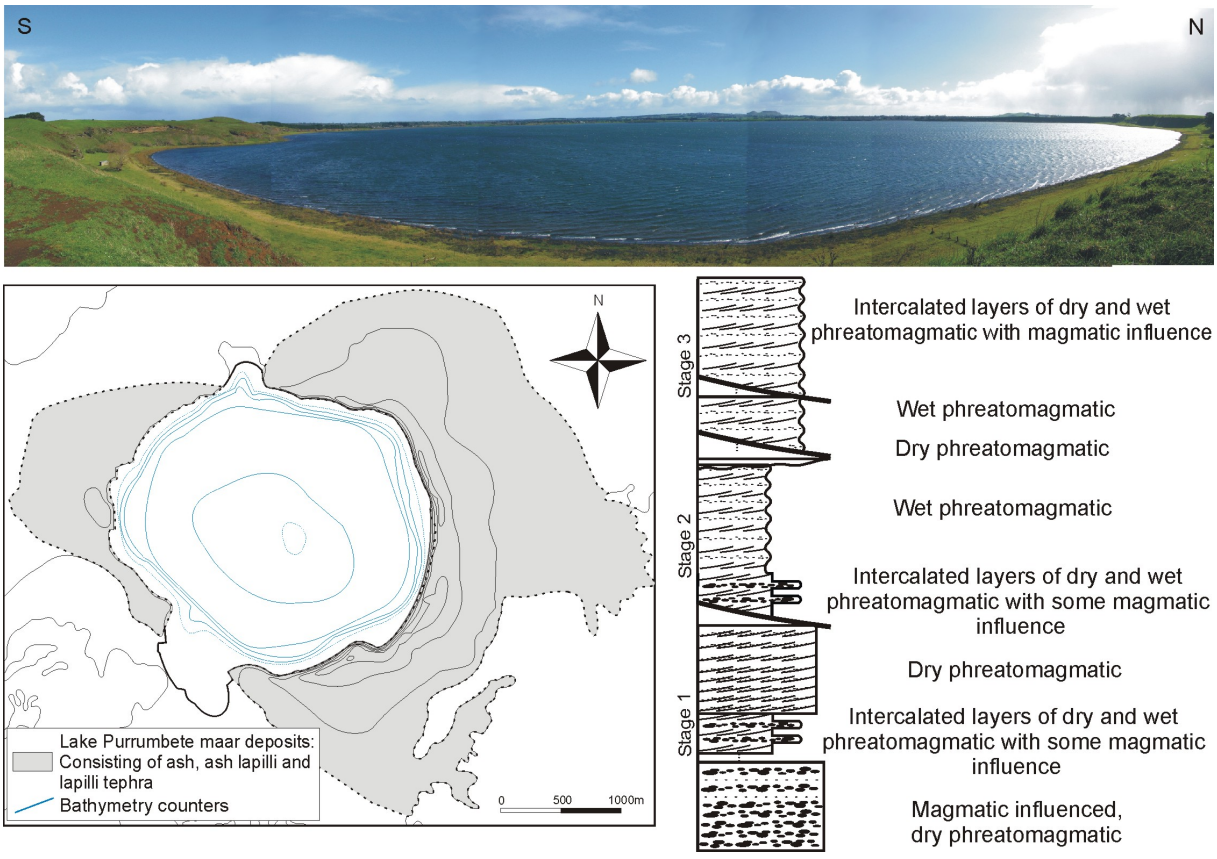

Figure 6.1: View of Lake Purrumbete from the eastern crater rim. The geological ma shows the distribution of the pyroclastic material around Lake Purrumbete. The composite stratigraphic log reflects the fluctuations in the eruption.

Figure 6.2: Deposit types of the Lake Purrumbete pyroclastic sequence. A) outcrop along the crater wall comprising fine wet phreatomagmatic ash deposits at the bottom and magmatic influenced dry phreatomagmatic scoria deposits at the top. B) Quarry cross section through the crater rim showing dry phreatomagmatic lapilli-ash deposits with characteristic base surge cross bedding.

6.3 Experimental setup

The Lake Purrumbete pyroclastic material is relatively fine grained (lapilli to ash size) and ash coating of lapilli clasts is common. Together with a relatively high ash content, this makes it impossible to separate a representative amount of clean juvenile material to use in fragmentation experiments. As a solution to this problem scoria material from Mount Rouse with a similar geochemistry than the Lake Purrumbete material was used for the experiments (Table 6.1). Large clean scoria clasts were crushed in a rock mill and sieved afterwards to separate the grain size fraction between 0.5-4 mm, which is best for homogeneous melting.

Table 6.1: General geochemistry of Lake Purrumbete and the Mount Rouse material.

	SiO_2	TiO_2	Al_2O_3	Fe_2O_3	MnO	MgO	CaO	Na_2O	K_2O	P_2O_5	LOI
Mt Rouse											
2208-590	47.62	2.4	13.99	12.2	0.16	8.68	8.19	3.59	1.65	0.66	0.4
Lake Purrumbete											
514	46.5	2.74	14	12.3	0.16	5.68	7.95	4.26	2.72	1.14	2.3
WQ5a	46.1	2.89	13.8	13	0.16	6.99	6.71	3.08	2.4	1.04	3.52

Mount Rouse is a volcanic complex located 90 km to the west of Lake Purrumbete. Material of a scoria fallout deposit was used for the experiments. The scoria clasts contain 5-10 % crystals, including olivine, clino- and ortho-pyroxene and K-feldspar, and at least 50 % vesicles, with microlites occuring in various amounts within the glassy groundmass.

The melting behaviour of the material was tested during the run of a thermal granulation experiment, where the melt is poured into water and fragmented by thermal quenching of the material. This experiment can be used as an analogue for the natural process of magma entering a waterbody and being fragmented by quenching.

Figure 6.3 shows the experimental setup of the blow-out experiments, which follow the

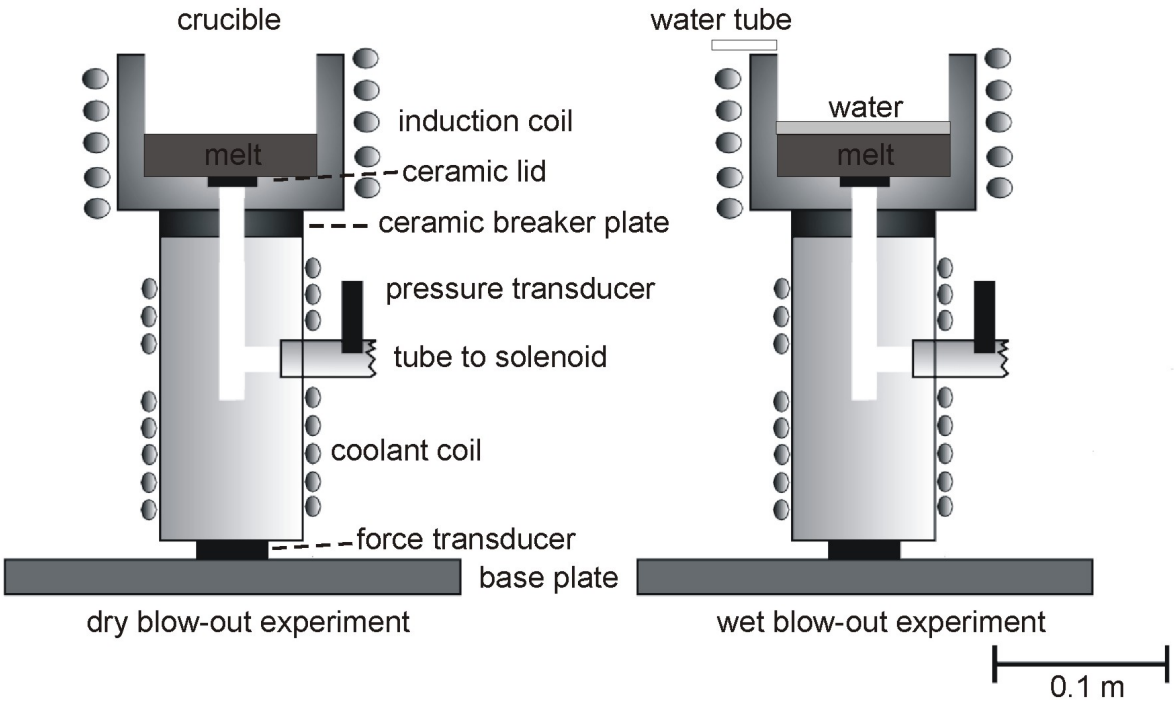

Figure 6.3: Experimental setup of dry and wet blow-out experiments (modified after Büttner et al. (2006) and Austin-Erickson et al. (2008)).

experimental setup used by Büttner et al. (2006) for dry blow-out experiments and by Austin-Erickson et al. (2008) for wet blow-out experiments and described in chapter 5. The material was melted in a steel crucible using heating by an induction coil. A gas tube was connected to the crucible by a hole in the crucible bottom and closed by a ceramic lid, which was used for the injection of pressurized gas (driving pressure of 10 MPa). The gas injection was controlled over a valve, while the pressure created by the gas injection is measured by a pressure transducer. A ceramic breaker plate was used for insulation of the hot top part of the setup from the cool bottom part. In addition, a coolant coil was used to cool the lower part of the setup, as both pressure and forces transducer are heat sensitive. The latter was used to record the repulsive force of the system.

Three hundred grams of material are used to create a melt plug inside a steel crucible. The relatively fast melting of the material using inductive heating (few hours) preserved vesicles originating from the scoria clasts. The amount of preserved vesicles within the melt was decreased between each experiment to evaluate the influence of vesicles on the fragmentation process. This was done by heating the melt for a longer time leaving more time for the vesicles to escape from the melt. The melt temperature was adjusted to 1283-1293 K. By heating the melt to the desired temperature and cooling over a short time interval of the seven minutes, thermal gradient was removed between the interior of the melt and the melt at the crucible margin.

The experiments began with the injection of gas underneath the melt plug, causing the melt to bulge and deform. As a result micro cracks formed in the melt plug. Brittle fragmentation of the melt was caused by the high strain rate during deformation within the crucible, with further fragmentation by acceleration of the whole system during ejection

out of the crucible, which is driven by the gas pressure (Büttner et al., 2002, 2006).

The experimental process was the same during wet blow-out experiments, except that water was poured onto the melt plug at the moment of opening the gas valve and therefore shortly before the onset of deformation. With the melt bulging due to the injection of gas and the formation of micro cracks, the water than flowed into these micro cracks (Austin-Erickson et al., 2008). This enhanced the contact area of magma and water leading to explosive magma/water interaction in the way of MFCI, in which the external water is explosively superheated by the magma (Austin-Erickson et al., 2008, Büttner and Zimanowski, 1998, Büttner et al., 2002).

During the experiments the following signals were recorded: acoustic signal caused by acoustic waves using a microphone, repulsion force of any accelerating material using a force transducer and pressure of the gas underneath the melt plug using a pressure transducer. The experiments were videotaped with two high speed cameras differing in resolution (5000 and 300 frames per minute). Acoustic waves are released at the end of the fragmentation and indicate the opening of the system and the ejection of material. The pressure signal is used to clarify if true fragmentation occurred, as the pressure signal should drop after complete fragmentation of the melt plug. The signal of the repulsion force allows to determine the energies released during fragmentation and is also indicating the onset of fragmentation (Appendix 7).

6.4 Results of the experiments

The fragmentation process can be analysed using the different recorded signals, in particular the signals of the pressure and the force transducer, where the pressure transducer recorded the pressure underneath the melt plug and the force transducer measures the repulsion force of particles breaking out of the melt plug and being ejected out of the crucible. The diagrams of the signal plots of the different experimental runs (Figure 6.4) show that during the dry blow-out series the melt reacted differently to the applied pressure. Experiment Bl5 was the only well-functioning dry blow-out experiment, both experimental runs Bl6 and Bl7 are characterised by two fragmentation events, an early failure of the melt plug with gas release and ejection of a small volume of fragments, followed by closure of the system and a second pressure build-up before the second fragmentation event. The second fragmentation event is the actual fragmentation event, but as a result of the gas release during the first event the fragmentation energy during the second event is relatively small.

The graphs of the signal plots of the wet blow-out experiments (Figure 6.4) show that fragmentation started before the pressure reached the maximum and therefore was not driven by pressurisation and deformation of the melt plug, instead explosive magma/water interacting caused the fragmentation of the melt. The signals are in agreement with the lay out of the experiments, in which the deformation of the melt plug is only used to form micro cracks in the melt plug, to increase the interface for magma/water interaction. The

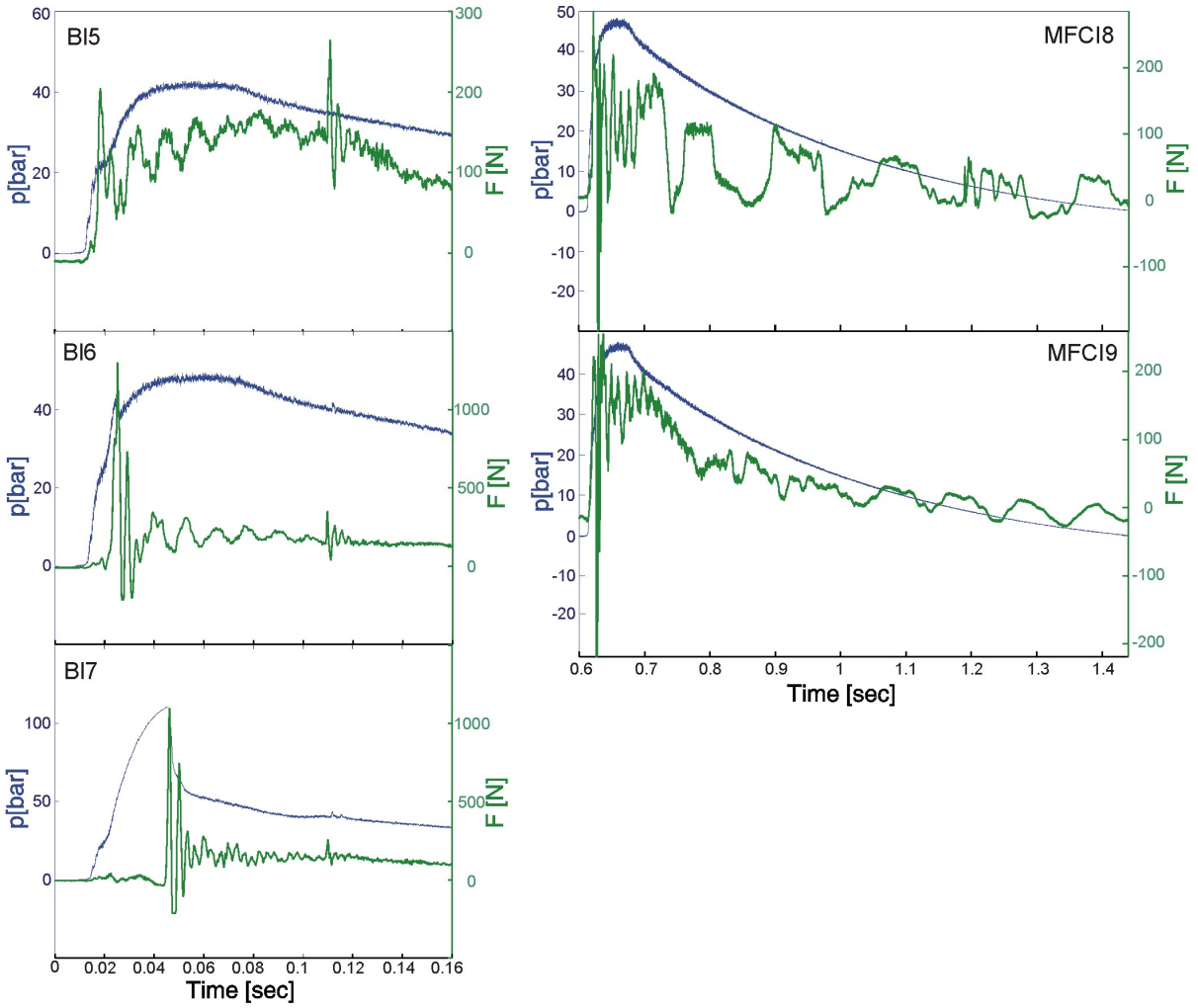

Figure 6.4: Diagrams of the plotted data recorded by the force and pressure transducers. Experimental run Bl5 shows acceleration of the melt plug failed at the beginning with further pressure built up and fragmentation, indicated by second peak of the force graph. Both experimental runs Bl6 and Bl7 show a first fragmentation event indicated by the first peak in the force graph, followed by closure of the system and a later second fragmentation event (second peak in the force graph). Early fragmentation due to magma/water inter action is indicated for both experimental runs MFCI8 and 9 by the strong peaks in the force graph prior to the peak in the pressure graph.

actual fragmentation process is MFCI like magma/water interaction, where fragmentation is caused by explosive superheating of the water. MFCI will take place as soon as micro cracks open and therefore before the maximum of the pressure is reached.

6.5 Particle analysis

6.5.1 Methods

Particles actively produced by the explosive magma/water interaction are smaller than 130 μm (Büttner et al., 2002) and therefore only particles in this size range have been used for the analysis. Scanning electron microscope (SEM) images were taken of the ash

particles, using the JEOL 7001 electron microscope of the Monash Centre of Electron microscopy with a working distance of 10 mm and an acceleration voltage of 15 kV. Afterwards the 2 dimensional SEM images were converted into binary images for further analysis. The analysis of the particle shapes follows the method of image particle analysis (IPA) proposed by Dellino and La Volpe (1996) and used by Zimanowski et al. (2003) and Dürig et al. (2012b) for comparison of natural and experimentally derived ash particles. Four adimensional IPA parameters are used for the statistical analysis of the particles, including compactness, rectangularity, elongation and circularity (Appendix 8).

Compactness is the ratio of the cross-section area A and the product of breadth b and width w of the bounding box circumscribing the particle (Figure 6.5):

$$compactness = \frac{A}{b * w} \tag{6.1}$$

Values for compactness range between 0 and 1, with values close to 1 indicating a particle shape similar to a rectangular.

The rectangularity of a particle shape is defined by the ratio of the particle perimeter p and the perimeter of the bounding box written as:

$$rectangularity = \frac{p}{2 * b + 2 * w} \tag{6.2}$$

where b is the breadth and w is the width of the bounding box. Values close to 1 again indicate a particle shape close to a rectangle.

Elongation is specified by:

$$elongation = \frac{a}{m} \tag{6.3}$$

with a being the maximum Feret diameter of the particle and m being the mean length of the line segments perpendicular to the maximum intercept, which is equal to particle area/maximum intercept. More elongate particles will have higher elongation values than non-elongated particles. The circularity is defined by:

$$circularity = \frac{p}{c} \tag{6.4}$$

with c being the perimeter of a circle with the same area than the particle itself. As a result, particles with a circularity of 1 are round while more irregular particles will have higher circularity values.

The shape parameters of the samples were compared by using different statistical methods applicable for IPA analysis (Dellino et al., 2001, Büttner et al., 2002, Mele et al., 2011, Dürig et al., 2012c). The samples were first compared by means using a t-test (test of equality of means), where the results show if samples are significantly different to each other. Afterwards, samples which showed no significant differences, were further analysed to determine significant similarities, using equivalent tests (Dürig et al., 2012b).

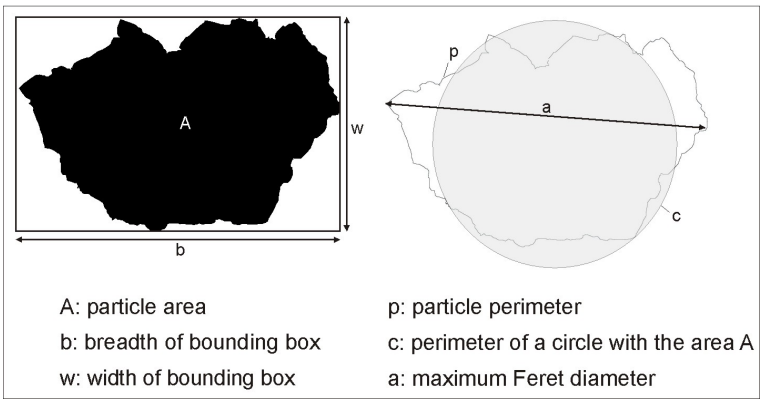

Figure 6.5: Particle parameters determined by ImageJ to use for the calculation of the IPA parameters.

6.6 Natural particle morphology

Figure 6.6A shows a bulk SEM image of a natural Lake Purrumbete ash sample. The most common particle type in the pure phreatomagmatic ash samples of Lake Purrumbete Maar consists of subrounded particles with an irregular outline and a rough surface, which is the result of brittle fragmentation (Büttner et al., 2002). Less common are angular and curvi-planar fragments, with a smooth surface and products of brittle fragmentation as well as blocky particles with a rough surface. Rounded particles similar to Pele's tears are very rare. Typical structures of magma/water interaction such as quenching cracks and stepped surfaces occur only in minor amounts. Many clasts have a distinct foam like surface texture, which is more predominant in samples of wet phreatomagmatic deposits than in dry phreatomagmatic (Figure 6.7). This foam like texture is similar to the chemical pitting textures described by Dellino et al. (2001) and therefore may have been caused by the contact of fluids and hot glass particles. The majority of clasts have smaller particles adhering to the surface, which is characteristic for phreatomagmatic derived particles (Dellino et al., 2001).

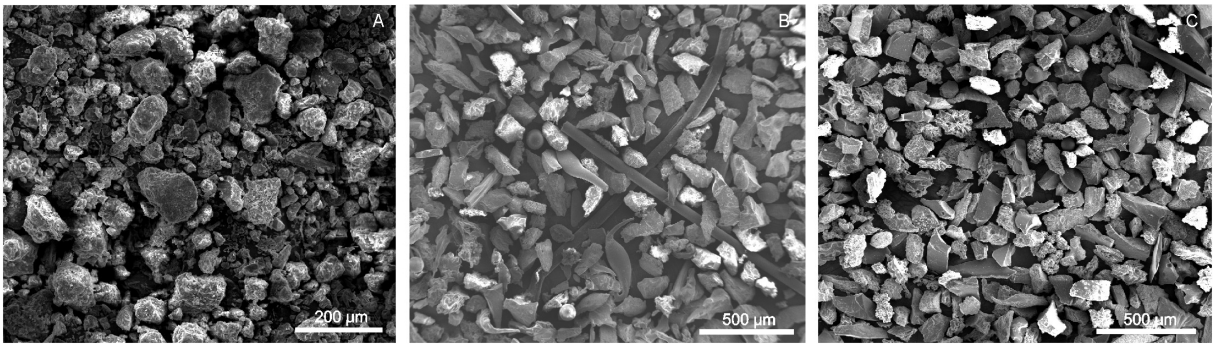

Figure 6.6: Bulk SEM images of A) natural Lake Purrumbete, B) dry blow-out and C) wet blow-out ash samples.

In samples of magmatic influenced dry phreatomagmatic deposits the same clast types occur as in pure phreatomagmatic deposits, but in different abundances. Subrounded particles with an irregular outline and a rough surface are as abundant as angular and

curvi-planar fragments. Many particles have abundant vesicle textures on the surface. In addition, Pele's hair are also common and some elongated particles in the form of Pele's hair have been observed (Figure 6.7). However, textures such as quenching cracks, chemical pitting and adhering particles are also common, indicating some magma/water interaction.

6.7 Experimental particle morphology

The samples of dry blow-out experiments contain abundant particles with a fluidal shape, including stretched, flexed and contorted structures, and elongated or spherical shapes (Figures 6.6B and 6.7), indicating ductile fragmentation (Büttner et al., 2002). Other particles are angular with a smooth surface and can show vesicle imprints or curvi-planar shape. Less abundant are sub-rounded to sub-angular particles with a rough surface. Particles with a cubically surface structure are also common, while particles with a stepped surface occur only in minor amounts. Samples of the wet blow-out experiments contain the same range of particle shapes and surface structures than the dry blow-out samples, but fluidal shaped particles are less abundant (Figure 6.6C). Textures such as chemical pitting or adhering particles are absent, but quenching cracks occur.

Particles formed during the thermal granulation experiment are exclusively angular with sharp edges and a very smooth, glassy surface (Figure 6.8). Concentric fracture marks are a common feature indicating brittle fragmentation.

6.8 IPA results

The mean shape parameters for each sample are given in Table 6.2 together with the standard deviation. The diagram of a plot of the circularity and elongation values versus the rectangularity and compactness values (Figure 6.9) shows that the IPA values are relatively similar. This plot can be generally used as a basic instrument to determine clusters of particles with similar shape characteristics (Büttner et al., 2002, Dürig et al., 2012a). The results of the t-test (Table 6.3), however, show that the majority of samples are significantly different in at least one parameter and can be excluded from further analysis. For the remaining samples the data of the equivalence test is listed in Table 6.4. The results show that particles of the thermal granulation experiment (sample GT) have different shape parameters to all other samples, where the difference to natural samples, in particular, indicates that fragmentation by thermal granulation alone did not occur during the Lake Purrumbete Maar eruption. Furthermore the natural ash particles are predominantly similar to each other, reflecting similar fragmentation processes during the entire Lake Purrumbete Maar eruption. However, the natural samples also show small differences to the experimental derived samples of both dry and wet blow-out experiments, reflecting differences between the natural environment and the experimental setup. Small

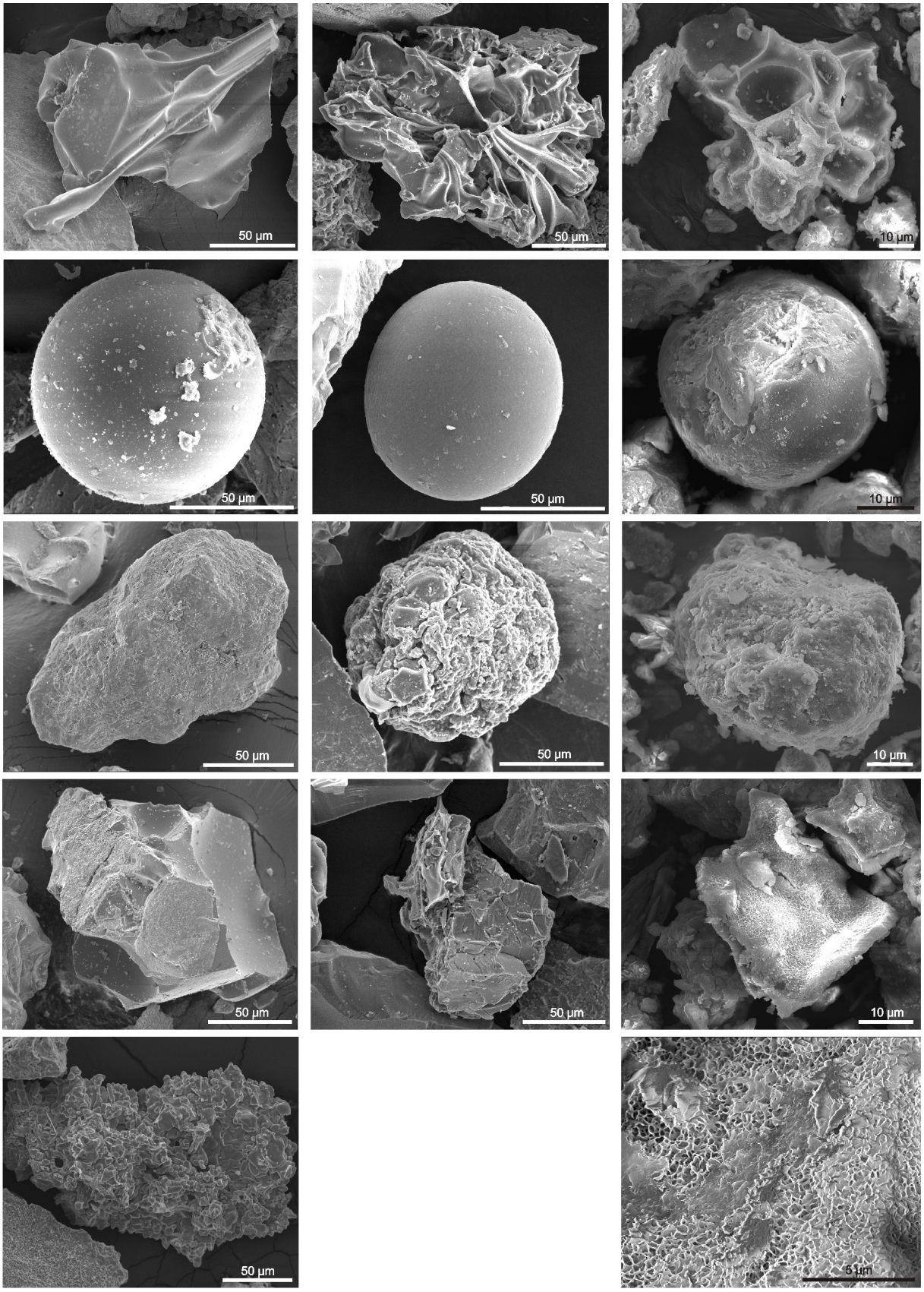

Figure 6.7: SEM images of natural and experimental ash particles. First column: particles derived from dry blow-out experiments; second column: particles from wet blow-out experiments; last column: natural ash particles, with high resolution image of chemical pitting (last image).

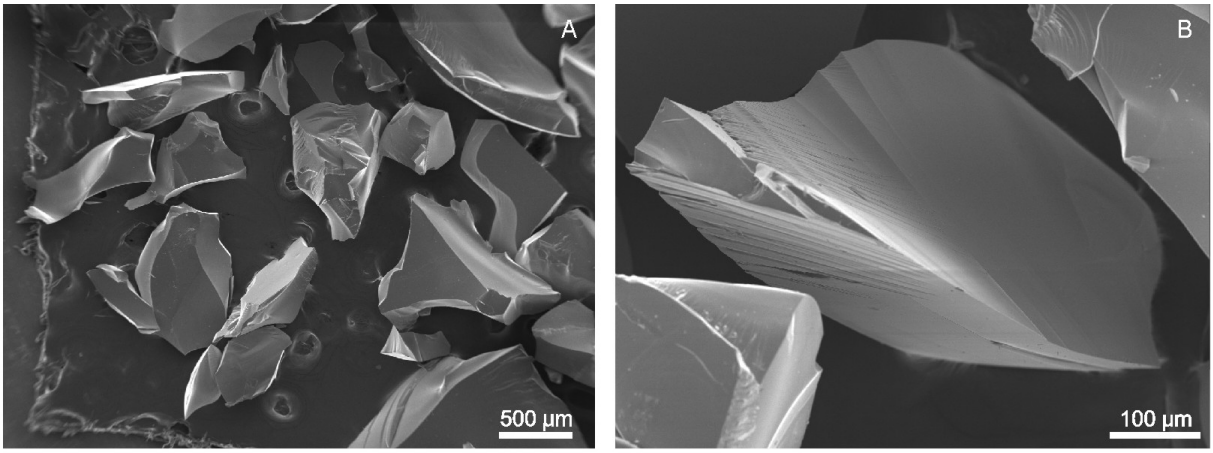

Figure 6.8: SEM images of ash particles derived from thermal granulation experiments, with typical angular shape and fracture marks on the smooth surface.

Table 6.2: Mean value of IPA parameter and standard diviation (std) of both natural and experimental samples.

sample	Rectangularity		Compactness		Elongation		Circularity	
	mean	std	mean	std	mean	std	mean	std
Bl5	0.91	0.07	0.55	0.14	3.68	2.77	1.49	0.38
Bl6	0.94	0.12	0.56	0.12	3.19	2.14	1.49	0.33
Bl7	0.92	0.08	0.65	0.07	1.2	0.28	1.31	0.15
MFCI8	0.89	0.07	0.56	0.15	3.23	2.39	1.41	0.25
MFCI9	0.93	0.08	0.61	0.12	3.15	1.76	1.42	0.22
GT	0.87	0.04	0.55	0.1	3.2	1.30	1.37	0.17
514	0.96	0.07	0.59	0.12	2.86	2.7	1.46	0.3
559	0.94	0.08	0.63	0.08	2.24	0.56	1.36	0.19
A6	0.93	0.08	0.61	0.11	2.59	0.93	1.37	0.15
Ba	0.95	0.08	0.63	0.08	2.26	1.4	1.37	0.16
ash1	0.98	0.06	0.62	0.09	1.14	0.19	1.44	0.14
ash4	0.98	0.14	0.60	0.11	2.5	0.89	1.46	0.31
M-ash	0.9	0.05	0.58	0.11	2.69	0.91	1.36	0.15

variations in the experimental setup are also indicated by the small differences in the IPA parameters between experimental samples of the same experimental series.

Table 6.3: Results of the t test. Comparison of the sample pairs is done for each IPA parameter, with values smaller 0.05 being significantly different and values smaller 0.01 being highly significantly different. The status of difference is given in column Dif.

set 1	set 2	Rectangularity	Compactness	Elongation	Circulation	Dif
Bl5	Bl6	0.229	0.784	0.453	0.983	no
Bl5	Bl7	0.767	0.002	0	0.015	yes
Bl5	MFCI8	0.35	0.812	0.505	0.355	no
Bl5	MFCI9	0.29	0.115	0.393	0.393	no
Bl5	GT	0.013	0.929	0.386	0.12	yes
Bl5	514	0.009	0.236	0.254	0.768	yes

Continued on next page

Table 6.3: Results of the t test. Comparison of the sample pairs is done for each IPA parameter, with values smaller 0.05 being significantly different and values smaller 0.01 being highly significantly different. The status of difference is given in column Dif.

set 1	set 2	Rectangularity	Compactness	Elongation	Circulation	Dif
Bl5	559	0.182	0.026	0.029	0.154	yes
Bl5	A6	0.323	0.093	0.043	0.118	yes
Bl5	BA	0.055	0.01	0.008	0.1	yes
Bl5	ash	0.003	0.037	0.001	0.59	yes
Bl5	mash	0.664	0.525	0.244	0.271	no
Bl6	Bl7	0.356	0.003	0	0.01	yes
Bl6	MFCI8	0.073	0.985	0.951	0.329	no
Bl6	MFCI9	0.734	0.168	0.935	0.363	no
Bl6	GT	0.006	0.673	0.985	0.103	yes
Bl6	514	0.42	0.338	0.617	0.772	no
Bl6	559	0.968	0.03	0.032	0.085	yes
Bl6	A6	0.694	0.139	0.173	0.101	no
Bl6	BA	0.785	0.016	0.034	0.085	yes
Bl6	ash	0.159	0.068	0.004	0.586	yes
Bl6	mash	0.147	0.635	0.451	0.218	no
Bl7	MFCI8	0.25	0.008	0	0.05	yes
Bl7	MFCI9	0.474	0.149	0	0.023	yes
Bl7	GT	0.01	0	0	0.108	yes
Bl7	514	0.029	0.045	0.003	0.012	yes
Bl7	559	0.32	0.573	0	0.297	yes
Bl7	A6	0.514	0.11	0	0.087	yes
Bl7	BA	0.128	0.443	0	0.132	yes
Bl7	ash	0.009	0.113	0	0.006	yes
Bl7	mash	0.537	0.031	0	0.284	yes
MFCI8	MF9	0.062	0.2	0.888	0.907	no
MFCI8	GT	0.171	0.719	0.956	0.485	no
MFCI8	514	0.001	0.37	0.594	0.48	yes
MFCI8	559	0.039	0.052	0.043	0.404	yes
MFCI8	A6	0.072	0.171	0.187	0.483	no
MFCI8	BA	0.007	0.029	0.046	0.414	yes
MFCI8	ash	0	0.087	0.007	0.542	yes
MFCI8	mash	0.758	0.665	0.465	0.525	no
514	559	0.324	0.196	0.323	0.165	no
514	A6	0.128	0.625	0.611	0.154	no
514	BA	0.483	0.167	0.249	0.129	no
514	ash	0.462	0.482	0.028	0.814	yes
514	mash	0.016	0.78	0.834	0.277	yes
514	MFCI9	0.146	0.652	0.646	0.529	no
514	GT	0	0.129	0.549	0.158	yes
559	A6	0.689	0.366	0.145	0.721	no
559	BA	0.717	0.902	0.879	0.832	no
559	ash	0.157	0.405	0.123	0.148	no
559	mash	0.145	0.139	0.105	0.934	no
559	MFCI9	0.732	0.408	0.017	0.305	yes
559	GT	0	0.002	0.004	0.746	yes

Continued on next page

Table 6.3: Results of the t test. Comparison of the sample pairs is done for each IPA parameter, with values smaller 0.05 being significantly different and values smaller 0.01 being highly significantly different. The status of difference is given in column Dif.

set 1	set 2	Rectangularity	Compactness	Elongation	Circulation	Dif
A6	BA	0.395	0.36	0.118	0.867	no
A6	ash	0.043	0.874	0.002	0.151	yes
A6	mash	0.259	0.488	0.76	0.821	no
A6	MFCI9	0.948	0.998	0.151	0.369	no
A6	GT	0.001	0.032	0.046	0.983	yes
BA	ash	0.184	0.403	0.052	0.121	no
BA	mash	0.062	0.126	0.171	0.924	no
BA	MFCI9	0.434	0.399	0.019	0.303	yes
BA	GT	0	0.001	0.001	0.889	yes
ash	mash	0.023	0.386	0.011	0.263	yes
ash	MFCI9	0.053	0.88	0.001	0.614	yes
ash	GT	0	0.011	0	0.154	yes
mash	MFCI9	0.228	0.529	0.412	0.417	no
mash	GT	0.073	0.349	0.235	0.843	no
MF9	GT	0.001	0.047	0.899	0.369	yes

Table 6.4: Results of the equivalent test. Comparison of the sample pairs is done for each IPA parameter, using threshold limits defined by Dürig et al. (2012b). Significant similarity of samples is indicated with 'yes', no similarity is shown by 'no' and () means no statement can be made about the similarity of the samples, as the variations within each sample are not comparable.

set 1	set 2	Rect = 0.7	Comp =0.11	Elong = 0.9	Circ = 0.13
Bl5	Bl6	()	yes	no	no
Bl5	MFCI8	yes	yes	no	()
Bl5	MFCI9	yes	no	()	()
Bl5	mash	yes	yes	()	()
Bl6	MFCI8	()	yes	no	no
Bl6	MFCI9	yes	yes	no	()
Bl6	514	()	yes	no	no
Bl6	A6	yes	yes	()	()
Bl6	ash4	yes	yes	()	no
Bl6	mash	()	yes	()	()
MFCI8	MFCI9	yes	yes	no	()
MFCI8	GT	()	()	()	()
MFCI8	A6	yes	yes	()	()
MFCI8	mash	yes	yes	()	no
514	559	yes	yes	()	()
514	A6	yes	yes	()	()
514	BA	yes	yes	()	()
514	MFCI9	yes	yes	()	no
514	ash4	()	yes	()	no
559	A6	yes	yes	()	yes

Continued on next page

Table 6.4: Results of the equivalent test. Comparison of the sample pairs is done for each IPA parameter, using threshold limits defined by Dürig et al. (2012b). Significant similarity of samples is indicated with 'yes', no similarity is shown by 'no' and () means no statement can be made about the similarity of the samples, as the variations within each sample are not comparable.

set 1	set 2	Rect = 0.7	Comp =0.11	Elong = 0.9	Circ = 0.13
559	BA	yes	yes	yes	yes
559	ash4	()	yes	yes	()
559	mash	yes	no	no	yes
A6	BA	yes	yes	()	yes
A6	MFCI9	yes	yes	()	yes
A6	ash4	()	yes	yes	()
A6	mash	yes	yes	yes	yes
BA	ash4	()	yes	()	()
mash	MFCI9	yes	yes	()	no
mash	GT	yes	yes	no	yes

6.9 Discussion

Comparison of the surface textures of natural and experimental derived particles show that there are two major differences. The natural particles have a more "dirty" surface, showing chemical pitting textures, abundant adhering particles and a rough surface, while experimental particles have typically clean glassy surfaces. Experimental particles, however, more often have a fluidal shape, where stretched and contorted shapes in particular are very common. These are absent in natural samples and only a few Pele's hair and tears occur. These differences may be the result of differences in the environment of the fragmentation process. While fragmentation takes place in an open crucible in the experimental run, fragmentation in a maar volcano occurs typically somewhere within the diatreme, surrounded by the material of the diatreme infill. As a consequence, the material in the experiment is ejected immediately after fragmentation and has no further contact with other particles or water. The natural particles instead are ejected into and through the diatreme infill (Valentine, 2012) and therefore come in contact with other particles and water. The increased occurrence of chemical pitting in the wet phreatomagmatic deposits indicates that the abundance of water may also play a major role in the formation of this texture. The surrounding water bearing diatreme infill on the other hand may prevent a fast acceleration of the fragmented material and therefore may prevent the occurrence of ductile fragmentation, explaining the absence of fluidal shaped particles in the majority of the Lake Purrumbete deposits.

Fluidal shaped particles are usually more common in magmatic deposits (Dellino et al., 2001), but can also occur in phreatomagmatic deposits (Büttner et al., 2002). In the experimental series presented here, they occur in both dry and wet blow-out experiments, where they are a dominant particle type in dry blow-out experiments, but still relatively

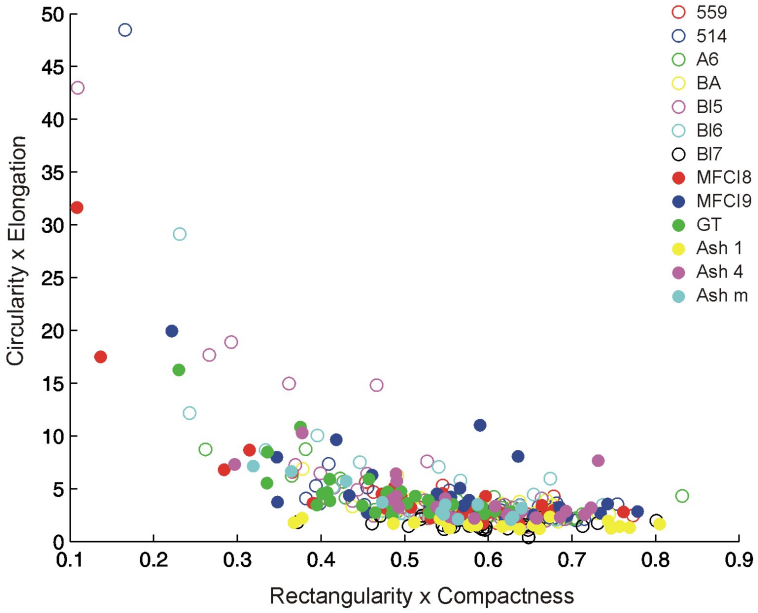

Figure 6.9: Comparative plot of the IPA values of all analysed particles. The majority of particles plot in the same field, indicating an overall similarity if the clasts.

abundant in wet blow-out experiments. The abundant fluidal shaped particles in the wet blow-out samples may be explained by a relatively low viscosity of the melt and the absence of a post-fragmentation environment, which enhances the formation of these particles (Shimozuru, 1994, Büttner et al., 2002). A low viscosity of the melt is also indicated by the experimental runs Bl6 and Bl7, where the re-closure of the system during the experiment may be the result of low melt viscosity, which may have also influenced the process of phreatomagmatic eruptions at Lake Purrumbete Maar. A low viscosity of the melt enhances the ability of magma and water to mix (Morrissey et al., 2000, Zimanowski et al., 2004, Austin-Erickson et al., 2008), resulting in more efficient phreatomagmatic eruptions.

The experimental results presented here show that MFCI-type magma/water interaction is possible in vesicular melts, if the magma water interface is enhanced by fracturing of the melt prior to fragmentation in a similar way as being described by Austin-Erickson et al. (2008) for phreatomagmatic explosion of high silica magma. The vesicles in the experimental melt, however, were filled with air, as they have been the vesicle remnants within the used scoria clasts and therefore did not contain any gas phases which exsolve during magma ascent. Work on vesicle textures and bubble number densities of phreatomagmatic pyroclasts (Murtagh et al., 2011, Ross and White, 2012, Jordan et al., 2013b, chapter4) shows that the vast majority of the vesicles in these deposits are very small and therefore can be interpret as being formed shortly before fragmentation in the upper part of the conduit, where the exsolving gas phase is H_2O rather then CO_2. Therefore magma/water interaction should be not prevented by the presence of a compressible gas. The exsolution of the H_2O will lead to acceleration of the melt near the fragmentation level (Massol and Koyaguchi, 2005, Shimano and Nakada, 2006, Polacci et al., 2009) resulting in a higher strain rate of the melt and potential fracturing of the melt, which will enhance the

magma/water interface, similar to the micro cracks in the experiments.

Although the vesicle content of the melt was changed for each experimental run, the experimental samples look very similar to each other and the results of the IPA analysis show only very small differences between the samples. It would be expected that fragmentation of a vesicular melt would produce a large amount of curvi-planar particles and particles with vesicles visible on the surface, whereas samples of a low vesicular melt should contain only a few of these particles, resulting in more distinctive differences. This is supported by the IPA results of the natural samples, which show that they are predominantly similar to each other, although the vesicularity of the different deposit types is very variable (Jordan et al., 2013b, chapter 4).

The very small differences in the IPA values of the experimental clasts can be also explained by differences in the intensity of pre-stress prior to the fragmentation of the melt (Dürig et al., 2012a). Dürig et al. (2012a) suggested that the formation of the particle shape is highly influenced by pre-stresses within the melt. In the experimental runs pre-stress is the result of the bulging of the melt in the crucible, whereby the geometry and the intensity of the pre-stress is generally comparable in experiments with the same starting conditions. However, both pre-stress geometry and intensity are dependent on the material response to the applied deforming force, which varies with different material properties such as vesicularity of the melt. The small variation in the IPA between experimental samples therefore may be the result of different pre-stress caused by different degrees of vesicularity. Pre-stress also occurs in the melt in the conduit, where the magma is strained during ascent. The strain may be heterogeneously distributed through the magma column, as indicated by stretched vesicles observed in the Lake Purrumbete pyroclasts by Jordan et al. (2013b, chapter 4), which may influence the development of the particle shape. This may explain the differences between particles of the natural samples and the experimental samples, in particular samples derived from wet blow-out experiments, as the pre-stress will be different for a setup in a crucible and the conduit.

6.10 Conclusions

- A vesiculated melt can be fragmented by MFCI like magma/water interaction, when the magma/water interface is enhanced by fracturing of the melt before fragmentation.
- The mixing of magma and water may have been further enhanced by the low viscosity of the melt.
- Changes in the vesicularity of the melt do not appear in differences in the particle morphology and shape.
- The differences in the conditions between natural conduits and experimental setup result in detectable small difference in the particle shape of natural particles and

experimental derived particles.

- The shape of the particles is predominantly influenced by pre-stress in the melt before fragmentation, whereby weak zones formed by strain localisation may play an important role.

7

Conclusions and Discussion

7.1 Conclusions

The following conclusions can be drawn from this research project:

From chapter 2:

- Lake Purrumbete Maar volcano is characterised by a typical maar rim sequence consisting predominantly of dry and wet phreatomagmatic deposits sourced from low density base surge currents and minor interbedded magmatic influenced dry phreatomagmatic scoriaceous deposits.
- Based on xenolith clast populations the maar crater has a shallow bowl shaped subsurface structure. The large diameter to depth ratio is caused by shallow aquifers and multiple vent migration events, leading to a coalesced shallow vent complex.
- Vent migration was probably mainly caused by clogging of the original vent by wall rock collapse and crater infill, but processes including activity on fault structures and a new magma influx and its lateral migration along basement structures controlled fissure conduits.
- The evidence for at least one volcanic hiatus and reactivation of the system afterwards raises the question if the Lake Purrumbete Maar volcano is strictly monogenetic.
- The location of each major vent has been determined using transport direction of base surges, determined by cross bed measurements, and ballistic ejecta data.
- Each vent has a unique eruption pattern corresponding to characteristic deposits. The eruptions were strongly influenced by the underlying aquifers of the fractured Gellibrand Marl and the porous Black Rock Sandstone.

From chapter 3:

- The geochemistry of samples from the Lake Purrumbete Maar indicate that the maar formed in an eruption sequence where the most evolved melt was erupted first and the most primitive melt was ejected last.

- The observed trace element variations cannot be explained by assimilation of crustal material, primarily as all samples from Lake Purrumbete have relatively constant SiO_2 concentrations. In addition, observed trends in (La/Sm)/Sm ratios cannot be generated by crystal fractionation. It is likely that partial melting of a fertile mantle generated the magmas that formed the Lake Purrumbete Maar, although it should be noted that partial melting is a long-lived process compared to the very short-lived eruption of this single monogenetic volcano.

- Melt extraction via high porosity channels in the mantle (Spiegelman and Kelemen, 2003) can explain the distinctive geochemical variations evident at Lake Purrumbete.

- These variations were preserved by fast ascent of the magma through the crust, reducing the time for further differentiation by assimilation of crustal material and/or crystal fractionation.

- The magma remaining in the conduit system was modified by crystal fractionation during quiescence, with subsequent ejection together with fresh melt from the mantle, as indicated by the presence of mantle xenolith fragments.

From chapter 4:

- The comparison of BND values and BSD of fine ash deposits with coarser deposits is possible if different size classes of pyroclasts are analysed and compared carefully for all samples.

- Similar BND values and BSD profiles of all Lake Purrumbete deposit types indicate that the eruption style has not been influenced by the vesicularity of the melt.

- BND values and BSD profiles indicate that bubble nucleation occurred in two steps. The first bubble population formed deep in the conduit/ or magma chamber while the second population nucleated in the shallow conduit near the fragmentation level due to supersaturation and acceleration of the melt (Massol and Koyaguchi, 2005, Shimano and Nakada, 2006).

- The initial ascent rate of the magma changed over the course of the eruption. It was slower at the beginning, causing a higher degree of supersaturation of the magma and larger BND values of the second vesicle population. With increasing ascent rate of the magma the degree of supersaturation decreased resulting in smaller BND values due to smaller amounts of vesicles of the second vesicle population.

- The large number of vesicles of the second vesicle population is caused by acceleration of the melt near the fragmentation level and rapid decompression. The high BND values are similar to those observed in pyroclasts of the Etna 122 BC eruption, indicating fast magma ascent rates prior to fragmentation.

From chapter 5:

- Dry and wet blow-out experiments showed that microlites can form in an extremely short time frame of seconds and during the fragmentation process.
- Traditional models of microlite formation due to decompression or cooling of the magma cannot be applied to the observed experimental phenomenon.
- Rapid crystallisation of saturated liquids and melts due to mechanical stress is a common phenomenon and is widely used in ultrasonic science and therefore must be considered for magmatic melts.
- The observed relationship of microlite formation and clasts, formed by brittle fragmentation, suggests that the same internal stress, which forces the break up of the magma, triggers microlite formation.
- Stress induced microlite formation during the fragmentation of the melt has to be considered when using microlite number densities and structures to model magma ascent rates and conduit processes, as some or most of the microlites in the clasts may have been formed by this process, instead of being formed by decompression in the conduit.
- The difference in microlite abundances and textures observed in the Lake Purrumbete clasts are similar to the observed microlite textures and abundances in the experimentally derived clasts and can be well explained with stress induced microlite formation during fragmentation.
- The amount of microlites within the clasts may reflect the intensity of the internal stress a clast has experienced during fragmentation.
- The process of rapid microlite formation has to be further investigated, in particular the relationship between microlite abundance and stress rate.

And from chapter 6:

- A vesiculated melt can be fragmented by MFCI like magma/water interaction, when the magma/water interface is enhanced by fracturing of the melt before fragmentation.
- The mixing of magma and water may have been further enhanced by the low viscosity of the melt.
- Changes in the vesicularity of the melt do not appear in differences in the particle morphology and shape.
- The differences in the conditions between natural conduits and experimental setup result in detectable small difference in the particle shape of natural particles and experimental derived particles.

- The shape of the particles is predominantly influenced by pre-stress in the melt before fragmentation, whereby weak zones formed by strain localisation may play an important role.

7.2 Discussion

The implications of these conclusions on the general research on maar volcanoes and the phreatomagmatic eruption style are further discussed in detail in the following discussion part. Each of the five research chapters highlights a different aspect of research on small basaltic volcanic systems such as maar volcanoes. This part will bring together the different aspects and discus them with regards to the aims of this research project.

7.2.1 Determining of the process of large maar formation, such as Lake Purrumbete and the controlling factors

Maar volcanoes have a typical diameters of 100 m to 1500 m (Lorenz, 1986) but can range to over 3000 m (Cas and Wright, 1987, Németh et al., 2001). As mentioned in chapter 2, the general accepted model of maar formation is by downwards growth of the maar diatreme due to deepening of the explosion point (Lorenz, 1986). It has been discussed in chapter 2 that this model is inapplicable for the formation of the Lake Purrumbete Maar, as the explosion point was located relatively close to the surface, within the first 100 m. In general it can be questioned if large maar volcanoes consist of only one main diatreme, which has been formed by deepening of the explosion point. Lorenz (1986) suggested in some of his figures that the width of the maar may be equal to the depth of its diatreme. This would mean for large diatremes that they would reach over kilometres deep into the ground. Phreatomagmatic explosions might be impossible at this depth, due to the high pressure of the overlying diatreme infill. Lorenz (1986) suggested a pressure barrier for phreatomagmatic explosions of 20-30 bar. The maar diatreme infill may be less dense than the surrounding country rock, but at a depth of 2-3 km the pressure of the overlying diatreme infill may overcome this threshold and therefore not allow explosive interaction between magma and water. It is suggested in chapter 2 that the large size of Lake Purrumbete Maar is the result of coalescence of multiple vents. Vent migration has been observed before at different locations world wide such as the Tihany Maar Volcanic Complex, Hungary (Németh et al., 2001), the Coombs Hills, Antarctica (White and McClintock, 2001), the Fekete-hegy volcanic complex, Hungary (Auer et al., 2007) and the Atexcac maar, Mexico (Carrasco-Núñez et al., 2007). However, all of these volcanic structures have either elongated or lobate shapes typical for vent migration. It has been discussed that any lobate structure at Lake Purrumbete has been blurred by mass flow of the soft sediment into the vent. Furthermore the soft sediment substrate would prevent the formation of separated diatremes and a lobate shape, as saddles of country rock between these diatremes would collapse due to the weak strength of the soft sediment.

The elongation of maar structures is often caused by vent migration along pre-existing tectonic structures, as observed for example at Atexcac maar (Carrasco-Núñez et al., 2007). At Lake Purrumbete, however, the vents migrated along two fault structures almost perpendicular to each other, preventing the formation of an elongated shape. In addition, the pyroclastic sequence (chapter 2) and the geochemistry (chapter 3) give evidence for at least three eruption phases caused by single magma pulses. Each eruption phase started out at the same location, with later migration along one of the fault lines. The direction of migration may have been influenced not only by the stress field of the region or the weakness along the fault lines, but also by blockage of the pathways by cooled magma from a previous eruption phase.

The occurrence of multiple eruption phases is uncommon for monogenetic volcanoes, such as maars, which are considered to have been formed by a single short lived eruption of one magma pulse (Walker, 1993, Risso et al., 2008, Németh, 2010, White and Ross, 2011). The reactivation of these small volcanic systems is considered to be prevented by sealing of the former pathways through the crust by cooled magma (Mazzarini et al., 2010). The eruption of multiple magma batches has been observed for other small volcanic centres including the Rangitoto volcano in the Auckland volcanic field (Needham et al., 2011), and other volcanic centres in the NVP, such as Mount Rouse (Boyce, 2011) and Mount Gambier (van Otterloo and Cas, 2011). In addition, reactivation of maar volcanoes have also been recorded by Bradshaw and Smith (1994), Freda et al. (2006) and Jordan et al. (2013a, chapter 2). At Lake Purrumbete at least three magma pulses rose through the crust to the surface along the same path. The question is why was the system reactivated.

Many studies have shown that the spatial distribution of volcanoes in monogenetic volcanic fields is dependent on pre-existing tectonic structures in the region (Alaniz-Alvarez et al., 1998, Lesti et al., 2008, Németh, 2010, Cebriá et al., 2011). These structures are zones of weakness in the crust, along which magma will ascend preferentially. The formation of small volcanoes in a volcanic field is thought to be the result of the rise of a single magma batch, released from the source. Németh (2010, and references therein) suggested a model in which small magma volumes are generated by tapping of a melt channel within the mantle. The melt would flow into the conduit until the region around the conduit entrance is exhausted. Shifts sideways to more melt rich regions may result in the formation of a new conduit or if the shift takes place in a short time the former conduit may be still warm and available for magma transport, with the time scale of these shifts being dependent on the ability of fracture formation within the crust (Németh, 2010, and references therein). This process of tapping a melt channel can explain the three magma pulses at Lake Purrumbete very well and is supported by the geochemical variations recorded in the Lake Purrumbete pyroclastic sequence. As mentioned in chapter 3 these geochemical variations are best explained with magma differentiation due to melt transport through highly porous melt channels within the mantle.

The formation of a volcanic complex is therefore dependent on the tapping process of melt channels within the mantle (Németh, 2010, and references therein), whereby the type

of volcanic complex is influenced by properties of the near surface stratigraphy and the environment, including factors, such as availability of ground or surface water, fault lines and fractures and strength of the substrate.

7.2.2 Understanding the role of melt vesicularity and microlite content in phreatomagmatic eruptions

Role of melt vesiculation

In volcanic fields a whole variety of dry magmatic eruption types can be observed, ranging from effusive lava flows to Strombolian scoria cones and Hawaiian spatter cones (Németh, 2010). The type of eruption style is mainly controlled by the magma rise speed and the vesiculation and degassing of the melt (Parfitt, 2004). Vesiculation of the melt is considered to have no control on the phreatomagmatic eruption style, as phreatomagmatic explosions occur whenever mixing of magma and water is efficient enough to create a large enough interface for magma/water interaction (Zimanowski et al., 1997a). The level of phreatomagmatic explosions at Lake Purrumbete was relatively close to the surface, as mentioned in chapter 2, therefore it can be assumed that vesiculation of the melt had started prior to magma/water interaction. Zimanowski (1998) suggested that vesiculation of the magma may prevent explosive magma/water interactions, in the case of the degassing phase being CO_2. In contrast to H_2O, CO_2 is a compressible gas and may buffer explosive magma/water interactions. It has been shown in chapter 4 that the erupting magma at Lake Purrumbete was vesiculated to different degrees and that the majority of vesicles formed shortly before fragmentation high in the conduit, where the degassing phase is typically H_2O. As a result, magma/water interaction was not prevented by the occurrence of CO_2. In addition, the fragmentation experiments, described in chapter 6, showed that molten fuel coolant interaction can occur in vesiculated melts, when deformation of the melt causes the formation of micro fractures, enhancing the magma/water interface, as described for high silica melts by Austin-Erickson et al. (2008).

As mentioned in chapter 4 no relationship between Bubble number density (BND) and eruption style were found for the Lake Purrumbete pyroclasts, implying that the variations within the phreatomagmatic eruption style are not influenced by the vesicularity of the melt. The high BND values observed in the Lake Purrumbete clasts are in the same range as BND values found in pyroclasts of other phreatomagmatic centres, such as the Ilchulbong tuff cone, Jeju Island, South Korea (Murtagh et al., 2011) and the Coombs Hill, Antarctica (Ross and White, 2012) and are similar to BND values found in clasts from Plinian deposits (Shea et al., 2010). In addition, these values are too high for Strombolian or Hawaiian eruption styles (Murtagh et al., 2011). But with the phreatomagmatic eruption style being the wet equivalent of both Hawaiian and Strombolian eruption types, the BND values should be in the range of these eruption types. It could be argued, that the late stage of vesiculation and the interruption of further vesicle growth by phreatmagmatic explosions in the conduit may preserve the state of the vesicle population shortly after nucleation,

indicated by the small vesicle size, whereas in Stombolian and Hawaiian eruption types the magma ascends further up in the conduit, resulting in a longer time scale available after nucleation for the vesicles to grow. Due to the large number of nucleated vesicles many of these vesicles will coalesce if they have enough time for expansion, which may lead to a decrease in the BND values in Strombolian and Hawaiian eruptions. But this should be also the case if the external water is near the surface, as it is in the case of the Lake Purrumbete Maar (Jordan et al., 2013a, chapter 2). Studies of BND values have been made, to our knowledge, so far, predominantly on large composite volcanoes, such as Stromboli and Kilauea (Lautze and Houghton, 2007, Stovall et al., 2011) and not on small Strombolian scoria cones or Hawaiian spatter cones, which are the dry equivalent to phreatomagmatic centres such as Lake Purrumbete and Illchulbong. It would be of great interest if clasts from these small cones show the same BND values as the large composite volcanoes or if their BND values are more similar to the phreatomagmatic centres. However, Coombs Hill is not a small phreatomagmatic centre but the wet equivalent to flood basalt vent systems (White and McClintock, 2001), indicating that the late nucleation of a large amount of vesicles is not exclusive to ascent of small magma batches, as those of small volcanic complexes.

Role of microlites

Although much work has been done on microlite number densities and structures in volcanic material of large composite volcanoes with a more felsic composition, for example by Cashman and McConnell (2005) and Cichy et al. (2011), only a little work has been done on microlite populations occurring in pyroclasts of small volcanic centres, such as maars, tuff rings and scoria cones (Mattsson, 2010, Murtagh et al., 2011, for example). The formation of microlites may have a large influence on the generation of phreatomagmatic eruptions, as nucleation and growth of microlites increase the viscosity of the melt, making it more difficult for magma and water to mix (Morrissey et al., 2000), and resulting in less efficient explosive magma/water interaction. However, the occurrence of phreatomagmatic deposits with a rhyolitic composition, recognised for example by Self and Sparks (1978) and Austin-Erickson et al. (2008), shows that explosive magma/water interaction can occur in more viscous melts. Austin-Erickson et al. (2008) suggested a different mixing process for viscous melts with water, whereby water is intermingled with the melt by filling in micro cracks, that are formed by the strain of the melt during magma ascent. The relatively high abundance of microlites in the Lake Purrumbete clasts is evidence that microlite formation did not prevent phreatomagmatic eruptions (chapter 5). However, microlite abundances vary a lot between clasts of the same eruptive event, indicating that microlite formation was not homogeneous throughout the magma column.

As mentioned in chapter 5 much work has also been done on the process of microlite formation within the conduit (Berkebile and Dowty, 1982, Hammer and Rutherford, 2002, Couch et al., 2003, Cichy et al., 2011), using material with a more felsic composition than basalt. These studies show that microlite formation is triggered by decompression of the

melt during ascent. The process of microlite nucleation and growth is considered to be relatively slow and microlites are therefore an indicator for slow magma ascent (Brugger and Hammer, 2010). The small size of microlites further indicate that they were formed in the upper part of the conduit and had not enough time to grow to larger crystal sizes. The high BND values found in studies of phreatomagmatic pyroclast (Murtagh et al., 2011, Ross and White, 2012, and chapter 4) show that magma ascent was fast in the upper part of the conduit due to degassing of H_2O (chapter 4), leaving only a short time frame for microlite formation, which may be enough for microlites to form, as basaltic melts can crystallize more rapidly then more felsic melts (Szramek et al., 2010). It has been discussed in chapter 5 that the large variations in the microlite abundances between clasts of the same eruptive event are difficult to explain by generation due to decompression in the conduit, which should affect the whole magma body more homogeneously. The experiments which have been conducted to evaluate other microlite formation processes, have shown that microlites can also be formed by internal mechanical stress of the magma (chapter 5). Mechanical stress within the magma can occur anywhere in the volcanic system during fragmentation or strain of the magma during ascent. Therefore microlites have to be used with caution for interpretations of conduit processes, as there is no certainty that all the observed microlites were truly formed by decompression in the conduit and not by internal mechanical stress during ascent or fragmentation.

The process of stress induced microlite formation is a new observation and no other work has been done so far on this topic in volcanology, although it is known to be a phenomenon in material science and widely used in ultrasonic science for the synthesis of materials such as zeolite (Pal et al., 2013). Therefore there are many questions which could not be answered in this study, such as the dependence of microlite textures on the formation process, the dependence of microlite abundance on the internal stress rate and the exact parameters for stress induced microlite formation. In addition, as the presented experiments were conducted with basaltic melt, further experiments have to be done to investigate if stress induced microlite formation can also happen in melts with a more felsic composition.

7.2.3 Influence of strain

Austin-Erickson et al. (2008) showed that phreatomagmatic explosions are possible in viscous high silica melts if the magma/water interface is enhanced by micro crack formation caused by strain deformation of the melt prior to fragmentation. This is also the case for vesiculated melts, as shown by the results of the experimental work, presented in this study (chapter 5 and 6). As a result, the strain rate in the magma may influence the onset of phreatomagmatic explosions. Acceleration of the melt near the fragmentation level, which is indicated by the high BND values (chapter 4), will result in a high strain of the magma and may change the rheological behaviour of the magma from ductile to brittle (Papale, 1999, Büttner et al., 2002). This change in the rheological behaviour of

the magma may result in fracturing of the melt, leading to an increase in the surface area available for magma water interaction. However, Rust and Manga (2002) suggested that magmas containing a large amount of vesicles may be shear thinning, as the reaction of the vesicles to the strain during deformation will reduce the viscosity of the magma. This behaviour would counter act the change to brittle behaviour. The experimental work presented in chapter 5, however, indicates that strain may result in microlite formation, which would again increase the viscosity of the melt. The variations in the vesicle textures, such as stretched vesicles and rounded vesicles, as well as the differences in microlite content (chapter 4 and 5) show that strain was very localised within the magma column. This localization of strain may also explain how pre-stress within the magma can control the shape of the resulting fragments, which was indicated by the experimental work in chapter 6, as fragmentation of the magma may occur along these zones of high strain.

It is most likely that the strain caused by the acceleration of the melt causes some fracturing of the magma, which will lead to an increase in the magma/water interface and cause phreatomagmatic explosions. Explosive magma/water interaction has been suggested to be a cyclic process with mixing of magma and water due to instabilities at the magma/water interface, collapse of the insulating vapour films and explosive fragmentation of the magma by quenching and steam expansion (Wohletz, 1983, Kokelaar, 1986, Zimanowski et al., 1997a). The cyclicity of this process is thought to create the typical pulsating character of the phreatomagmatic eruption style, as there is a pause in fragmentation each time a new pre-mix has to form. More sustained phreatomagmatic eruptions, however, may be the result of magma/water interaction along a fracture enhanced interface, where water may run more continuously into new forming fractures, only controlled by the aquifer dynamics.

7.3 Hazard implications of large maar formation

The main hazards from the eruption of a large maar volcano is the production of a large volume of fine ash, which can affect a large area around the volcano and have a big impact on the air traffic not only in vicinity of the volcano but also regionally, due to ash dispersal by wind, as the world experienced during the eruption of Eyjafjallajökull (2010) and Puyehue-Cordón Caulle (2011). The important question is how much ash is formed and on what time scale. The formation of a large maar volcano like Lake Purrumbete will have a bigger impact if it is formed in one major event in a very short time scale of a few days to weeks than if it is formed over a longer time scale of years to hundred of years. The research at Lake Purrumbete has shown that these large maar volcanoes may form in a longer time frame and with periods of repose in the range of a couple of years, as indicated by volcanic hiatus in the Lake Purrumbete eruption, that was long enough for the crater to fill up with water and for the formation of a rounded beach sand deposit (Jordan et al., 2013a, chapter 2). The distribution of the volcanic material further indicates that each eruption was relatively small and similar to eruptions of small maars.

The immediate impact on society will be therefore similar to the impact of other maar eruptions experienced in modern times (for example Ukinrek 1977). These eruptions, however, did not take place in densely populated areas. Many volcanic fields, such as the Auckland volcanic field, New Zealand and the Eifel, Germany are located in densely populated areas or in the case of the NVP, close to large cities. In these areas even the eruption of a small maar volcano will have a major impact on the population and may cost many lives.

The geochemical data (chapter 3) has shown, that the magma ascended directly from the mantle, with acceleration near the fragmentation level and has not been stored in a magma chamber on its way through the crust. Cliff and Shaw (2004) found ascent velocities of 3-15 km/h for two maars in the Eifel volcanic field. Fast magma ascent rates like these will make it difficult to warn and evacuate the population in time and therefore will create a big risk for the population. These small volcanoes were generally considered to be monogenetic and therefore only active once. As a result these volcanic centres are of no danger to the population and any new activity will create a new volcanic centre somewhere else. However, the new research presented here (chapter 2 and 3) and other studies (Freda et al., 2006, White and Ross, 2011, Boyce, 2011, van Otterloo and Cas, 2011) show that these small volcanoes may have several eruption phases and can be reactivated several times. But the dependence of the activity of the volcanic centre on the tapping processes of mantle channels, as mentioned before, shows that reactivation of these systems can only happen in a specific time frame, in which the pathways through the crust are still warm and not blocked with cooled magma.

The current research on volcanic centres in the NVP shows that the formation of a volcanic complex with several vent locations, such as Lake Purrumbete is very common (Boyce, 2011, van Otterloo and Cas, 2011). The formation of a volcanic complex as a large maar volcano is mainly dependent on the availability of water. Lake Purrumbete was formed at a time where the groundwater table was higher than today and in a swampy area where there might have been also surface water available (chapter 2). With a drier climate today and decreased groundwater levels an active volcanic event would most likely result in the formation of a composite volcanic complex with all different types of volcanic landforms including scoria cones and maars. The formation of volcanic landforms by dry magmatic processes is less dangerous and will affect only the area in the vicinity of the volcanic centre, as these eruptions do not produce large volumes of fine ash, which can be distributed over a wide area.

7.4 Perspectives for future work

This research project has touched many important aspects of research on small monogenetic volcanism and maars in particular, with many new results and aspects to consider for future work. The project showed that small volume volcanoes detailed stratigraphic work and sampling for geochemical analysis can be used to examine mantle processes, as the melts of

these volcanoes rise fast from the mantle source often without further differentiation. This should be used in future to further investigate the model of highly porous melt channels within the mantle, which may be the reason for the formation of volcanic provinces. It would be great to further investigate this model at Lake Purrumbete by using isotope data. Furthermore, using BND values and BSD profiles has shown that acceleration of the melt near the fragmentation level is common in small volume phreatomagmatic volcanoes, such as maars and tuff cones and comparable to plinian eruptions, and may enhance phreatomagmatic explosions. The question is if these high BND values are exclusive to phreatomagmatic centres or do they occur in all small volcanic centres. To answer this question, the BND values of magmatic centres such as scoria cones should be investigated in addition to other phreatomagmatic centres. Furthermore the comparison of these BND values to BND values of other basaltic composite volcanoes would be of great interest.

The model of stress induced microlite formation will need further investigation with more experimental work to be done. It should be investigated if the microlite textures and/or abundances are dependent on the degree of stress. Further experiments are needed to investigate the process of strain induced microlite formation. In addition, more experimental work is needed to investigate the influence of pre-stress on the fragmentation and the resulting clast shapes. Our research showed that phreatomagmatic explosion can occur in vesiculated melts but the experimental series in this project could not answer the question if melt varying in the degree of vesiculation behave differently during phreatomagmatic explosions. To answer this question a large series of experiments is needed to be conducted in the future.

Bibliography

Alaniz-Alvarez, S. A., Nieto-Samaniego, A. F., Ferrari, L., 1998. Effect of strain rate in the distribution of monogenetic and polygenetic volcanism in the Transmexican volcanic belt. Geology 26, 591–594.

Alidibirov, M., Dingwell, D. B., 1996. Magma fragmentation by rapid decompression. Nature 380, 146–148.

ANRA, 2002. Australian natural resources atlas.
URL `www.anra.gov.au/topics/water/overview/vic/gmu-glenormiston.html`

Aranda-Gomez, J. J., Luhr, J. F., 1996. Origin of the Joya Honda maar, San Luis Potosi, Mexico. Journal of Volcanology and Geothermal Research 74, 1–18.

Auer, A., Martin, U., Németh, K., 2007. The Fekete-hegy (Balaton Highland Hungary) "soft-substrate" and "hard-substrate" maar volcanoes in an aligned volcanic complex - implications for vent geometry, subsurface stratigraphy and the palaeoenvironmental setting. Journal of Volcanology and Geothermal Research 159, 225–245.

Austin-Erickson, A., Büttner, R., Ort, M. H., Zimanowski, B., 2008. Phreatomagmatic explosions of rhyolitic magma: Experimental and field evidence. Journal of Geophysical Research 113, B11201.

Ban, M., Sagawa, H., Miura, K., Hirotani, S., 2008. Evidence for a short-lived stratified magma chamber: petrology of the Z-To5 tephra layer (c. 5.8ka) at Yao volcano, NE Japan. Geological Society, London, Special Publications 304, 149–168.

Bartels, K. S., Furman, T., 2002. Effect of sonic and ultrasonic frequencies on the crystallization of basalt. American Mineralogist 87, 217–226.

Berkebile, C. A., Dowty, E., 1982. Nucleation in laboratory charges of basaltic composition. American Mineralogist 67, 886–899.

Blondes, M. S., Reiners, P. W., Ducea, M. N., Singer, B. S., Chesley, J., 2008. Temporal - compositional trends over short and long time-scales in basalt of the Big Pine Volcanic Field, California. Earth and Planetary Science Letters 269, 140–154.

Blower, J. D., Keating, J. P., Mader, H. M., Phillips, J. C., 2002. The evolution of bubble size distributions in volcanic eruptions. Journal of Volcanology and Geothermal Research 120, 1–23.

Boult, P. J., White, M. R., Pollock, R., Morton, J. G. G., Alexander, E. M., Hill, A. J., 2002. Lithostratigraphy and environments of deposition. In: Boult, P. J., Hibburt, J. E. (Eds.), Otway Basin, 2nd Edition. Vol. 1 of The petroleum geology of South Australia. South Australia. Department of Primary Industries and Resources, Ch. 6.

Boyce, J., 2011. Mount Rouse volcano. In: IUGG Field Trip Guide. IUGG Melbourne Australia, pp. 46–54.

Bradshaw, T. K., Smith, E. I., 1994. Polygenetic quaternary volcanism at CraterFlat, Nevada. Journal of Volcanology and Geothermal Research 63, 165–182.

Brown, R. J., Branney, M. J., Maher, C., P., D.-H., 2010. Origin of accretionary lapilli within ground-hugging density currents: Evidence from pyroclastic couplets on Tenerife. Geological Society of America Bulletin 122, 305–320.

Brugger, C. R., Hammer, J. E., 2010. Crystallization kinetics in continuous decompression experiments: Implications for interpreting natural magma ascent processes. Journal of Petrology 51 (9), 1941–1965.

Büttner, R., Dellino, P., La Volpe, L., Lorenz, V., Zimanowski, B., 2002. Thermohydraulic explosions in phreatomagmatic eruptions as evidenced by the comparison between pyroclasts and products from Molten Fuel Coolant Interaction experiments. Journal of Geophysical Research 107 (B11).

Büttner, R., Dellino, P., Raue, H., Sonder, I., Zimanowski, B., 2006. Stress-induced brittle fragmentation of magmatic melts: Theory and experiments. Journal of Geophysical Research 111.

Büttner, R., Dellino, P., Zimanowski, B., 1999. Identifying magma-water interaction from the surface features of ash particles. Nature 401, 688–690.

Büttner, R., Zimanowski, B., 1998. Physics of thermohydraulic explosions. Physical Review E 57 (5), 5726.

Carey, S., Bursik, M., 2000. Volcanic plumes. In: Sigurdsson, H. (Ed.), Encyclopedia of Volcanoes. Academic Press, Ch. IV, pp. 527–544.

Carn, S. A., 2000. The Lamongan volcanic field, East Java, Indonesia: physical volcanology, historic activity and hazards. Journal of Volcanology and Geothermal Research 95, 81–108.

Carrasco-Núñez, G., Ort, M. H., Romero, C., 2007. Evolution and hydrological conditions of a maar volcano (Atexcac crater, Eastern Mexico). Journal of Volcanology and Geothermal Research 159, 179–197.

Cas, R., Simpson, C., Sato, H., 1993. Newer Volcanics Province - processes and products of phreatomagmatic activity. In: IAVCEI Canberra 1993 Exkursion Guide. IAVCEI, Australian Geological Survey Organisation.

Cas, R., van Otterloo, J., 2011. Introduction to the IUGG Excursion Guide. In: IUGG Field Trip Guide. IUGG Melbourne Australia, pp. 6–31.

Cas, R. A. F., Wright, J. V., 1987. Volcanic successions. Allen and Unwin, London.

Cashman, K. V., McConnell, S. M., 2005. Multiple levels of magma storage during the 1980 summer eruptions of Mount St. Helens, WA. Bulletin of Volcanology 68, 57–75.

Cebriá, J. M., Martín-Escorza, C., López-Ruiz, J., Morán-Zenteno, D. J., Martiny, B. M., 2011. Numerical recognition of alignments in monogenetic volcanic areas: Examples from Michoacán-Guanajuato Volcanic Field in Mexico and Calatrava in Spain. Journal of Volcanology and Geothermal Research 201, 73–82.

Cichy, S. B., Botcharnikov, R. E., Holtz, F., Behrens, H., 2011. Vesiculation and microlite crystallization induced by decompression: a case study of the 1991-1995 Mt Unzen eruption (Japan). Journal of Petrology 52 (7&8), 1469–1492.

Cliff, S. J., Shaw, 2004. The temporal evolution of three magmatic systems in the West Eifel volcanic field, Germany. Journal of Volcanology and Geothermal Research 131, 213–240.

Condie, K. C., 2005. High field strength element ratios in Archean basalts: a window to evolving sources of mantle plumes? Lithos 79, 491–504.

Couch, S., Sparks, R. S. J., Carroll, M. R., 2003. The kinetics of degassing-induced crystallization at Soufríere Hills Volcano, Montserrat. Journal of Petrology 44 (8), 1477–1502.

Cupper, M. L., White, S., Neilson, J. L., 2003. chapter 11. In: Birch, W. D. (Ed.), Geology of Victoria, 23rd Edition. Geological Society of Australia, Ch. 11.

De Rosa, R., Frazzetta, G., La Volpe, L., 1992. An approach for investigating the depositional mechanism of fine-grained surge deposits. The example of the dry surge deposits at "La Fossa di Vulcano". Journal of Volcanology and Geothermal Research 51, 305–321.

Dellino, P., Frazzetta, G., La Volpe, L., 1990. Wet surge deposits at La Fossa di Vulcano: depositional and eruptive mechanisms. Journal of Volcanology and Geothermal Research 43, 215–233.

Dellino, P., Isaia, R., La Volpe, L., Orsi, G., 2001. Statistical analysis of textural data from complex pyroclastic sequences: implications for fragmentation processes of the agnano-monte spina tephra (4.1ka), phlegraean fields, southern italy. Bulletin of Volcanology 63, 443–461.

Dellino, P., La Volpe, L., 1995. Fragmentation versus transportation mechanisms in the pyroclastic sequence of the Monte Pilato-Rocche Rosse (Lipari, Italy). Journal of Volcanology and Geothermal Research 64, 211–231.

Dellino, P., La Volpe, L., 1996. Image processing analysis in reconstructing fragmentation and transportation mechanisms of pyroclastic deposits. The case of Monte Pilato-Rocche Rosse eruptions, Lipari (Aeolian islands, Italy). Journal of Volcanology and Geothermal Research 71, 13–29.

Dürig, T., Dioguardi, F., Büttner, R., Dellino, P., Mele, D., Zimanowski, B., 2012a. A new method for the determination of the specific kinetic energy (SKE) released to pyroclastic particles at magmatic fragmentation: theory and first experimental results. Bulletin of Volcanology 74, 895–902.

Dürig, T., Mele, D., Dellino, P., Zimanowski, B., 2012b. Comparative analyses of glass fragments from brittle fracture experiments and volcanic ash. Bulletin of Volcanology 74, 691–704.

Dürig, T., Sonder, I., Zimanowski, B., Beyrichen, H., Büttner, R., 2012c. Generation of volcanic ash by basaltic volcanism. Journal of Geophysical Research 117, B01204.

Edmonds, P., 2008. Reconstruction of the volcanic architecture and evolution of the Purrumbete Basaltic Maar Complex, Newer Volcanics Province, Victoria, Australia. New evidence for multiple diatremes, honours thesis at the School of Geoscience, Monash University.

Edwards, J., Leonard, J. G., Peitifer, G. R., Mc Donald, P. A., 1996. Colac 1:250000 map. In: Geological Survey Report 98.

Finlayson, D. M., Johnstone, D. W., Owen, A. J., Wake-Dyster, K. D., 1996. Deep seismic images and the tectonic framework of early rifting in the Otway Basin, Australian southern margin. Tectonophysics 264, 137–152.

Fitton, J. G., 2007. The OIB paradox. Geological Society of America Special Papers 430, 387–412.

Fitton, J. G., Saunders, A. D., Norry, M. J., Hardarson, B. S., Taylor, R. N., 1997. Thermal and chemical structure of the Iceland plume. Earth and Planetary Science Letters 153, 197–208.

Francis, P. W., Glaze, L. S., Pieri, D., Oppenheimer, C. M. M., Rothery, D. A., 1990. Eruption terms. Nature 346, 519.

Frazzetta, G., La Volpe, L., Sheridan, M. F., 1989. Interpretation of emplacement units in recent surge deposits on Lipari, Italy. Journal of Volcanology and Geothermal Research 37, 339–350.

Freda, C., Gaeta, M., Karner, D. B., Marra, F., Renne, P. R., Taddeucci, J., Scarlato, P., Christiansen, J. N., Dallai, L., 2006. Eruptive history and petrologic evolution of the Albano multiple maar, (Alban Hills, Central Italy). Bulletin of Volcanology 68, 567–591.

Frey, F. A., Green, D. H., Roy, S. D., 1978. Integrated models of basalt petrogenesis: A study of quartz tholeiites and olivine melilitites from South Eastern Australia utilizing geochemical and experimental petrological data. Journal of Petrology 19, 463–513.

Gaonac'h, H., Lovejoy, S., Schertzer, D., 2005. Scaling vesicle distributions and volcanic eruptions. Bulletin of Volcanology 67, 350–357.

Gençalioğlu-Kuşcu, C., Atilla, C., Cas, R. A. F., Ilkay, K., 2007. Base surge deposits, eruption history, and depositional processes of a wet phreatomagmatic volcano in Central Anatolia (Cora Maar). Journal of Volcanology and Geothermal Research 159, 198–209.

Geoscience Australia, G., July 2012. Austalian stratigraphic names database. Accessed: 25/7/2012.
URL `http://www.ga.gov.au/products-services/data-applications/reference-databases /stratigraphic-units.html`

Ginibre, C., Wörner, G., Kronz, A., 2004. Structre and dynamics of the Lacher See Magma Chamber (Eifel, Germany) from major and trace element zoning in sanidine: a cathodoluminescence and electron microprobe study. Journal of Petrology 45, 2197–2223.

Graeber, F. M., Houseman, G. A., Greenhalgh, S. A., 2002. Regional teleseismic tomography of the western Lachlan Orogen and the Newer Volcanic Province, southeast Australia. Geophysical Journal International 149, 249–266.

Hammer, J. E., Rutherford, M. J., 2002. An experimental study of the kinetics of decompression-induced crystallization in silicic melt. Journal of Geophysical Research 107, 2021.

Hare, A. G., Cas, R. A. F., 2005. Volcanology and evolution of the Werribee Plains intraplate, basaltic lava flow-field, Newer Volcanics Province, southeast Australia. Australian Journal of Earth Sciences 52, 59–78.

Harms, E., Gardner, J. E., Schmincke, H.-U., 2004. Phase equilibria of the Lower Laacher See Tephra (East Eifel, Germany): constraints on the pre-eruptive strorage conditions of a phonolitic magma reservoir. Journal of Volcanology and Gethermal Research 134, 135–148.

Higgins, M. D., 2000. Measurement of crystal size distrbutions. American Mineralogist 85, 1105–1116.

Higgins, M. D., 2002. Closure in crystal size distributions (csd), verification of csd calculations, and the significance of csd fans. American Mineralogist 87, 171–175.

Higgins, M. D., 2006. Quantitative textural maeasurements in igneous and metamorphic petrology. Cambridge University Press.

Hill, K. A., Cooper, G. T., Richardson, M. J., Lavin, C. J., 1994. Structural framework of the Eastern Otway Basin: Inversion and interaction between two major structural provinces. Exploration Geophysics 25, 79–87.

Hill, K. A., Finlayson, D. M., Hill, K. C., Cooper, G. T., 1995. Mesozoic tectonics of the Otway Basin region: the legacy of Gondwana and the active pacific margin - a review and ongoing research. APEA Journal 35, 467–493.

Houghton, B. F., Nairn, I. A., 1991. The 1976-1982 Strombolian and phreatomagmatic eruptions of White Island, New Zealand: eruptive and depositional mechanisms at a 'wet' volcano. Bulletin of Volcanology 54, 25–49.

Houghton, B. F., Smith, R. T., 1993. Recycling of magmatic clasts during explosive eruptions: estimating the true juvenile content of phreatomagmatic volcanic deposits. Bulletin of Volcanology 55, 414–420.

Houghton, B. F., Wilson, C. J. N., Del Carlo, P., Coltelli, M., Sable, J. E., Carey, R., 2004. The influence of conduit processes on changes in style of basaltic Plinian eruptions: Tarawera 1886 and Etna 122 BC. Journal of Volcanology and Geothermal Research 137, 1–14.

Jensen-Schmidt, B., Cockshell, C., Boult, P. J., 2002. Structural and tectonic setting. In: Boult, P. J., Hibburt, J. E. (Eds.), Otway Basin, 2nd Edition. Vol. 1 of Petroleum Geology of South Australia Series. South Australia, Department of Primary Industries and Resources, Ch. 5.

Jones, R. N., McMahon, T. A., Bowler, J. M., 2001. Modelling historical lake levels and recent climate change at three closed lakes, Western Victoria, Australia (c. 1840 -1990). Journal of Hydrology 246, 159–180.

Jordan, S. C., Cas, R. A. F., Hayman, P. C., 2013a. The origin of a large (>3km) maar volcano by coalescence of multiple shallow craters: Lake Purrumbete maar, southeastern Australia. Journal of Volcanology and Geothermal Research 254, 5–22.

Jordan, S. C., Hayman, P. C., Cas, R. A. F., 2013b. Multi stage vesicle nucleation in the conduit system of a large maar volcano: Evidence from bubble number densities and bubble size distributions derived from pyroclasts of the lake purrumbete maar, southeastern australia. in submission.

Jordan, S. C., Jowitt, S. M., Cas, R. A. F., 2013c. Partial melting and channelised melt transport in the mantle underneath the Newer Volcanics Province, southeastern Australia: Geochemical evidence from the Lake Purrumbete maar. Bulletin of VolcanologyIn submission.

Joyce, E. B., 1975. Quarternary volcanism and tectonics in southeastern Australia. The Royal Society of New Zealand, 169–176.

Kokelaar, P., 1986. Magma-water interactions in subaqueous and emergent basaltic volcanism. Bulletin of Volcanology 48, 275–289.

Lautze, N. C., Houghton, B. F., 2007. Linking variable explosion style and magma textures during 2002 at Stromboli volcano, Italy. Bulletin of Volcanology 69, 445–460.

Le Bas, M. J., Le Maitre, R. W., Streckeisen, a., Zanettin, B., 1986. A chemical classification of the volcanic rocks based on the total alkali-silica diagram. Journal of Petrology 27, 745–750.

Lesti, C., Giordano, G., Salvini, F., Cas, R., 2008. Volcano tectonic setting of the intraplate, Pliocene-Holocene, Newer Volcanic Province (southeast Australia): Role of crustal fracture zones. Journal of Geophysical Research 113, B07407.

Lister, G. S., Etheridge, M. A., 1989. Detachment models for uplift and volcanism in the Eastern Highlands, and their application to the origin of passive margin mountains. In: Johnson, R. W. (Ed.), Intraplate Volcanism in Eastern Australia and New Zealand. Cambridge University Press, pp. 297–313.

Lorenz, V., 1986. On the growth of maars and diatremes and its relevance to the formation of tuff rings. Bulletin of Volcanology 48, 265–274.

Lorenz, V., 2007. Syn- and posteruptive hazards of maar-diatreme volcanoes. Journal of Volcanology and Geothermal Research 159, 285–312.

Love, A. J., Herczeg, A. L., Leaney, F. W., Stadter, M. F., Dighton, J. C., Armstrong, D., 1994. Groundwater residence time and palaeohydrology in the Otway Basin, South Australia: ^{2}H, ^{18}O, and ^{14}C data. Journal of Hydrology 153, 157–187.

Mangan, M. T., Cashman, K. V., 1996. The structure of basaltic scoria and reticulite and inferences for vesicularition, foam formation, and fragmentation in lava fountains. Journal of Volcanology and Geothermal Research 73, 1–18.

Massol, H., Koyaguchi, T., 2005. The effect of magma flow on nucleation of gas bubbles in a volcanic conduit. Journal of Volcanology and Geothermal Research 143, 69–88.

Mattsson, H. B., 2010. Textural variation in juvenile pyroclasts from an emergent, surtseyan-type, volcanic eruption: The Capelas tuff cone, Sao Miguel (Azores). Journal of Volcanology and Geothermal Research 189, 81–91.

Mazzarini, F., Ferrari, L., Isola, I., 2010. Self-similar clustering of cinder cones and crust thickness in the Michoacan-Guanajuato and Sierra de Chichinautzin volcanic fields, Trans-Mexican Volcanic Belt. Tectonophysics 486, 55–64.

McDonough, W. F., Sun, S.-s., 1995. The composition of the Earth. Chemical Geology 120, 223–253.

Mele, D., Dellino, P., Sulpizio, R., Braia, G., 2011. A systematic investigation on the aerodynamics of ash particles. Journal of Volcanology and Geothermal Research 203, 1–11.

Miller, J. M., Norvick, M. S., Wilson, C. J. L., 2002. Basement controls on rifting and the associated formation of ocean transform faults— Cretaceous continental extension of the southern margin of Australia. Tectonophysics 359, 131–155.

Morrissey, M., Zimanowski, B., Wohletz, K., Buettner, R., 2000. Phreatomagmatic fragmentation. In: Sigurdsson, H. (Ed.), Encyclopedia of Volcanoes. Academic Press, Ch. IV, pp. 431–445.

Murtagh, R. M., White, J. D. L., Sohn, Y. K., 2011. Pyroclast textures of the "ilchulbung" 'wet' tuff cone, "jeju island, south korea". Journal of Volcanology and Geothermal Research 201, 385–395.

Needham, A. J., Lindsay, J., Smith, I. E. M., Augustinus, P., Shane, P. A., 2011. Sequential eruption of alkaline and sub-alkaline magmas from a small monogenetic volcano in the Auckland Volcanic Field, New Zealand. Journal of Volcanology and Geothermal Research 201, 126–142.

Németh, K., 2010. Monogenetic volcanic fields: Origin, sedimentary record, and relationship with polygenetic volcanism. The Geological Society of America Special Paper 470, 43–66.

Németh, K., Martin, U., Harangi, S., 2001. Miocene phreatomagmatic volcanism at Tihany (Pannonian Basin, Hungary). Journal of Volcanology and Geothermal Research 111, 111–135.

Németh, K., White, J. D. L., Reay, A., Martin, U., 2003. Compositional variation during monogenetic volcano growth and its implications for magma supply to continental volcanic fields. Journal of the Geological Society, London 160, 523–530.

Pal, P., Das, J. K., Das, N., Bandyopadhyay, S., 2013. Synthesis of NaP zeolite at room temperature and short crystallization time by sonochemical method. Ultrasonics Sonochemistry 20, 314–321.

Papale, P., 1999. Strain-induced magma fragmentation in explosive eruptions. Nature 397, 425–428.

Parfitt, E. A., 2004. A discussion of the mechanisms of explosive basaltic eruptions. Journal of Volcanology and Geothermal Research 134, 77–107.

Pearce, J. A., Baker, P. E., Harvey, P. K., Luff, I. W., 1995. Geochemical evidence for subduction fluxes, mantle melting and fractional crystallization beneath the South Sandwich Island Arc. Journal of Petrology 36, 1073–1109.

Perincek, D., Cockshell, C. D., 1995. The Otway Basin: Early Cretaceous rifting to Neogene inversion. APEA Journal of Geophysical Research 35, 451–466.

Pirrung, M., Büchel, G., Lorenz, V., Treutler, H.-C., 2008. Post-eruptive development of the Ukinrek East Maar since its eruption in 1977 A.D. in the periglacial area of south-west Alaska. Sedimentology 55, 305–334.

Pittari, A., Cas, R. A. F., Edgar, C. J., Nichols, H. J., Wolff, J. A., Martí, J., 2006. The influence of palaeotopography on facies architecture and pyroclastic flow processes of a lithic-rich ignimbrite in a high gradient setting: The Abrigo Ignimbrite, Tenerife, Canary Islands. Journal of Volcanology and Geothermal Research 152, 273–315.

Polacci, M., Burton, M. R., La Spina, A., Mure', F.and Favretto, S., Zanini, F., 2009. The role of syn-eruptive vesiculation on explosive basaltic activity at mt. etna, italy. Journal of Volcanology and Geothermal Research 179, 265–269.

Porritt, L. A., Russell, J. K., Quane, S. L., 2012. Pele's tears and spheres: Examples from Kilauea Iki. Earth and Planetary Science Letters 333-334, 171–180.

Price, R. C., Gray, C. M., Frey, F. A., 1997. Strontium isotopic and trace element heterogeneity in the plains basalts of the Newer Volcanic Province, Victoria, Australia. Geochimica et Cosmochimica Acta 61 (1), 171–192.

Price, R. C., Nicholls, I. A., Gray, C. M., 2003. chapter. In: Birch, W. D. (Ed.), Geology of Victoria, 23rd Edition. Speciel Publications. Geological Society of Australia, Ch. 12.

Raue, H., 2004. A new model for the fracture energy budget of phreatomagmatic explosions. Journal of Volcanology and Geothermal Research 129, 99–108.

Reiners, P. W., 2002. Temporal-compositional trends in intraplate basalt eruptions: Implications for mantle heterogeneity and melting processes. Geochemistry, Geophysics, Geosystems 3.

Risso, C., N'emeth, K., Combina, A. M., Nullo, F., Drosina, M., 2008. The role of phreatomagmatism in a plio-pleistocene high-density scoria cone field: Llancanelo volcanic field (mendoza), argentina. Journal of Volcanology and Geothermal Research 169, 61–86.

Ross, P.-S., Delpit, S., Haller, M. J., Nemeth, K., Corbella, H., 2011. Influence of the substrate on maar-diatreme volcanoes - an example of a mixed setting from the Pali Aike volcanic field, Argentina. Journal of Volcanology and Geothermal Research 201, 253–271.

Ross, P.-S., White, J. D. L., 2012. Quantification of vesicle characteristics in some diatreme-filling deposits, and the explosivity levels of magma-water interactions within diatremes. Journal of Volcanology and Geothermal Research 245-246, 55–67.

Rust, A. C., Manga, M., 2002. Effects of bubble deformation on the viscosity of dilute suspensions. Journal of Non-Newtonian Fluid Mechanics 104, 53–63.

Sable, J. E., Houghton, B. F., Del Carlo, P., Coltelli, M., 2006. Changing conditions of magma ascent and fragmentation during the Etna 122BC basaltic Plinian eruption: Evidence from clast microtextures. Journal of Volcanology and Geothermal Research 158, 333–354.

Sandiford, M., 2003. Geomorphic constraints on the Late Neogene tectonics of the Otway Range, Victoria. Australian Journal of Earth Sciences 50, 69–80.

Sandiford, M., Wallace, M., Coblentz, D., 2004. Origin of the in situ stress field in south-eastern Australia. Basin Research 16, 325–338.

Self, S., Kienle, J., Huot, J.-P., 1980. Ukinrek maars, Alaska, II. deposits and formation of the 1977 craters. Journal of Volcanology and Geothermal Research 7, 39–65.

Self, S., Sparks, R. S. J., 1978. Characteristics of widespread pyroclastic deposits formed by the interaction of silicic magma and water. Bulletin of Volcanology 41, 196–212.

Shea, T., Houghton, B. F., Gurioli, L., Cashman, K. V., Hammer, J. E., Hobden, B. J., 2010. Textural studies of vesicles in volcanic rocks: An integrated methodology. Journal of Volcanology and Geothermal Research 190, 271–289.

Shimano, T., Nakada, S., 2006. Vesiculation path of ascending magma in the 1983 and the 2000 eruptions of Miyakejima volcano, Japan. Bulletin of Volcanology 68, 549–566.

Shimozuru, D., 1994. Physical parameters governing the formation of Pele's hair and tears. Bulletin of Volcanology 56, 217–219.

Slots, M., 1999. Basaltic phreatomagmatic volcanism at the Lake Purrumbete maar in the Newer Volcanics Province of southeastern Australia, honours thesis at the School of Geoscience, Monash University.

Smith, I. E. M., Blake, S., Wilson, C. J. N., Houghton, B. F., 2008. Deep-seated fractionation during the rise of a small-volume basalt magma batch: Crater Hill, Auckland, New Zealand. Contributions to Mineralogy and Petrology 155, 511–527.

Sohn, Y. K., Chough, S. K., 1989. Depositional processes of the Suwolbong tuff ring, Cheju Island (Korea). Sedimentology 36, 837–855.

Sohn, Y. K., Park, K. H., 2005. Composite tuff ring/cone complexes in Jeju Island, Korea: possible consequences of substrate collapse and vent migration. Journal of Volcanology and Geothermal Research 141, 157–175.

Son, M., Kim, J. S., Jung, S., Ki, J. S., Kim, M.-C., Sohn, Y. K., 2012. Tectonically controlled vent migration during maar-diatreme formation: An example from a Miocene half-graben basin in SE Korea. Journal of Volcanology and Geothermal Research 223-224, 29–46.

Spiegelman, M., Kelemen, P. B., 2003. Extreme chemical variability as a consequence of channelized melt transport. Geochemistry, Geophysics, Geosystems 4 (7).

Spieler, O., Kennedy, B., Kueppers, U., Dingwell, D. B., Scheu, B., Taddeucci, J., 2004. The fragmentation threshold of pyroclastic rocks. Earth and Planetary Science Letters 226, 139–148.

Stovall, W. K., Houghton, B. F., Gonnermann, H., Fagents, S. A., 2011. Eruption dynamics of Hawaiian-style fountains: the case study of episode 1 of the Kilauea Iki 1959 eruption. Bulletin of Volcanology 73, 511–529.

Stovall, W. K., Houghton, B. F., Hammer, J. E., Fagents, S. A., Swanson, D. A., 2012. Vesiculation of high fountaining Hawaiian eruptions: episodes 15 and 16 of 1959 Kilauea Iki. Bulletin of Volcanology 74, 441–455.

Strong, M., Wolff, J., 2003. Compositional variations within scoria cones. Geology 31, 143–146.

Sun, S.-s., McDonough, W. F., 1989. Chemical and isotopic systematics of oceanic basalts: implications for mantle composition and processes. Geological Society, London, Special Publications 42, 313–345.

Suzuki, Y., Fujii, T., 2010. Effect of syneruptive decompression path on shifting intensity in basaltic sub-Plinian eruption: Implication of microlites in Yufune-2 scoria from Fuji volcano, Japan. Journal of Volcanology and Geothermal Research 198, 158–176.

Szramek, L., Gardner, J. E., Hort, M., 2010. Cooling-induced crystallization of microlite crystals in two basaltic pumice clasts. American Mineralogist 95, 503–509.

Timms, B. V., 1976. A comparative study of the limnology of three maar lakes in western Victoria I. physiography and physicochemical features. Australian Journal of Marine and Freshwater Research 27, 35–60.

Toramaru, A., 1991. Model of nucleation and growth of crystals in cooling magmas. Contributions to Mineralogy and Petrology 108, 106–117.

Toramaru, A., 2006. Bnd (bubble number density) decompression rate meter for explosive volcanic eruptions. Journal of Volcanology and Geothermal Research 154, 303–316.

Toramaru, A., Noguchi, S., Oyoshihara, S., Tsune, A., 2008. Mnd (microlite number density) water exsolution rate meter. Journal of Volcanology and Geothermal Research 175, 156–167.

Tsukui, M., Suzuki, Y., 1995. Vesiculation of basaltic magma: magmatic versus phreatomagmatic eruptions in 1983 eruption of Miyakejima. Bulletin Volcanological Society Japan 40, 395–399.

Tweed, S., Leblanc, M., Cartwright, I., 2009. Groundwater - surface water interaction and the impact of multi - year drought on lakes conditions in South-East Australia. Journal of Hydrology 379, 41–53.

Valentine, G. A., 2012. Shallow plumbing systems for small-volume basaltic volcanoes, 2: Evidence from crustal xenoliths at scoria cones and maars. Journal of Volcanology and Geothermal Research 223-224, 47–63.

Valentine, G. A., Gregg, T. K. P., 2008. Continental basaltic volcanoes - processes and problems. Journal of Volcanology and Geothermal Research 177, 857–873.

van Otterloo, J., Cas, R. A. F., 2011. Mount gambier volcanic complex. IUGG field trip guide.

VanHook, A., 1969. Nucleation. Marcel Dekker, INC.

Vespermann, D., Schmincke, H.-U., 2000. Scoria cones and tuff rings. In: Sigurdsson, H. (Ed.), Encyclopedia of Volcanoes. Academic Press, Ch. IV, pp. 683–694.

Vogel, D. C., Keays, R. R., 1997. The petrogenesis and platinum-group element geochemistry of the Newer Volcanic Province, Victoria, Australia. Chemical Geology 136, 181–204.

Walker, G. P. L., 1984. Characteristics of dune-bedded pyroclastic surge bedsets. Journal of Volcanology and Geothermal Research 20, 281–296.

Walker, G. P. L., 1993. Basaltic-volcano systems. Geological Society, London, Special Publications 76, 3–38.

Walker, G. P. L., Wilson, C. J. N., Froggatt, P. C., 1981. An ignimbrite veneer deposit: the trail-marker of a pyroclastic flow. Journal of Volcanology and Geothermal Research 9, 409–421.

Wellman, P., McDougall, I., 1974. Cainozoic igneous activity in eastern Australia. Tectonophysics 23, 49–65.

White, J. D. L., 1996. Impure coolants and interaction dynamics of phreatomagmatic eruptions. Journal of Volcanology and Geothermal Research 74, 155–170.

White, J. D. L., McClintock, M. K., 2001. Immense vent complex marks flood-basalt eruption in a wet, failed rift: Coombs Hills, Antarctica. Geology 29, 935–938.

White, J. D. L., Ross, P.-S., 2011. Maar-diatreme volcanoes: A review. Journal of Volcanology and Geothermal Research 201, 1–29.

Wohletz, K. H., 1983. Mechanics of hydrovolcanic pyroclast formation: grain-size, scanning microscopy, and experimental studies. Journal of Volcanology and Geothermal Research 17, 31–63.

Wörner, G., Schmincke, H.-U., 1984. Petrogenesis of the Zoned Laacher See Tephra. Journal of Petrology 25, 836–851.

Zimanowski, B., 1998. Phreatomagmatic explosions. In: Freundt, A., Rosi, M. (Eds.), From Magma to Tephra. Elsevier, Ch. 2, pp. 25–53.

Zimanowski, B., Büttner, R., Koopmann, A., 2004. Experiments on magma mixing. Geophysical Research letters 31, L09612.

Zimanowski, B., Büttner, R., Lorenz, V., 1997a. Premixing of magma and water in MFCI experiments. Bulletin of Volcanology 58, 491–495.

Zimanowski, B., Büttner, R., Lorenz, V., Häfele, H.-G., 1997b. Fragmentation of basaltic melt in the course of explosive volcanism. Journal of Geophysical Research 102, 803–814.

Zimanowski, B., Froehlich, G., Lorenz, V., 1991. Quantitative experiments on phreatomagmatic explosions. Journal of Volcanology and Geothermal Research 48, 341–358.

Zimanowski, B., Wohletz, K., Dellino, P., Büttner, R., 2003. The volcanic ash problem. Journal of Volcanology and Geothermal Research 122, 1–5.

Zou, H., Zindler, A., 1996. Constraints on the degree of dynamic partial melting and source composition using concentration ratios in magmas. Geochimica et Cosmochimica Acta 60, 711–717.

Appendices: enclosed on CD

1. List of samples
2. Outcrop images of the Lake Purrumbete crater walls
3. Structural data
4. Grain size analysis data
5. Grain counting data
6. Vesicle analysis data
7. Experimental data
8. Image particle analysis (IPA) data